Characterisation of Alumina-Zirconia Composites Produced By Micron-Sized Powders

By

Abdelmuniem M. Alsebaie B.Sc. Eng

A Thesis Submitted in Fulfilment of the Requirements for the Degree of Master of Engineering (M.Eng)

Supervisor

Dr. Abdul-Ghani Olabi

School of Mechanical and Manufacturing Engineering

Dublin City University

December 2005

DECLARATION

I hereby certify that this material, which I now submit for assessment on the programme of study leading to the award of master of engineering is entirely my own work and has not been taken from the work of others save and to the extent that such work has been cited and acknowledged within the text of my work.

Signed:  ID: 53122241

Date: 18-01-2006

ACKNOWLEDGEMENTS

Finally, the acknowledgments. The first page to be seen by the reader, but the last one I wrote. The work is done, and now the only thing left is to put on record all that I owe to so many people. On the other hand, since I am not able of writing anything original about acknowledgments, I will not bother with trying to get a unique and interesting page. I will just try to transmit my own feelings towards all the people who have made possible the conclusion of this work. If I forget some body please forgive me, I thank you as well.

I am extremely thankful to my thesis advisor, Dr. Abdul Ghani Olabi, without his continuous help and advice this work would not be made possible.

Of course, I also feel in debt with my uncle Dr. Hassin Yunis for his effort, encouragement and cooperative support.

I am indebted to my father and my whole family, which have given me the chance of discovering what I like, and of devoting myself to it.

I also would like to take this opportunity to extend my thanks to Dr. Aran Rafferty and Dr. Tim Prescott for their assistance in technical support.

I would like to thank the technical staff of the School of Mechanical & Manufacturing Engineering, especially Mr. Liam Domican.

I also would like to gratefully acknowledge Libyan government for the financing of this research.

Last but not least I would like to take this opportunity to extend my thanks to each one of my friends, here in Ireland and back home, for their truthful and sincere concerns about my study and myself.

TABLE OF CONTENTS

LIST OF FIGURES

LIST OF TABLES

CHAPTER ONE

INTRODUCTION

CHAPTER ONE INTRODUCTION

1.0 Introduction

It is well known that additions of unstabilised-zirconia to alumina lead to an increase in fracture toughness. Claussen [1] was the first to discover this phenomenon in 1976. Reasons for the increase in fracture toughness include the interaction of the crack front with the second phase (crack blunting, crack deviation), and interaction of the crack front with pre-existing microcracks, formed during the tetragonal-monoclinic transformation of zirconia [1]. When very fine tetragonal zirconia grains are dispersed in a matrix, upon cooling from sintering they can be constrained from transforming by the surrounding matrix and thus retain in a metastable tetragonal phase. An approaching crack front is the catalyst, which triggers the transformation and the zone ahead of the crack tip is placed in compression [2]. In alumina-zirconia, very high tensile stresses are developed in the alumina matrix. However, the volume expansion of zirconia transformation is approximately 3-4%, which greatly exceeds the matrix stresses. This means that very small particles can become crack formers in this material combination. By retaining the tetragonal grains in the metastable state, the potential for transformation toughening is maximised. This can be achieved by using partially stabilised zirconia (PSZ), where additions of oxides (typically MgO, CaO, or Y_2O_3) lead to a tetragonal phase in a cubic zirconia matrix. The tetragonal precipitates must be kept small enough that they do not spontaneously transform within the cubic zirconia matrix, unless as a result of stress.

The colloidal processing route has the advantage of producing very fine and very homogeneous microstructures, with minimal aggregates of zirconia. Using the colloidal processing route (zirconium propoxide solution), narrower ZrO_2 grain size distributions (in the region of 200nm) is expected. According to Schehl et al. [3], this route also avoids the need for any stabilising oxide. This is due to the fact that all ZrO_2 grains have practically the same size and can be kept below the critical size for spontaneous transformation. These particles are also greater than the critical size needed for transformation during crack growth. Schehl et al. [3] used XRD to investigate a colloidally processed (95wt% Al_2O_3; 5wt% ZrO_2) sample. It was found that during cooling, the vast majority of particles (90.93 vol %) were retained below the critical size as tetragonal zirconia (t-ZrO_2) particles. A fracture toughness of 7.5

$MPa.m^{1/2}$ was recorded. Deville et al. [4] also highlights the difficulties associated with trying to avoid aggregate formation when using classical powder mixing. It was claimed that by using colloidal processing it should be possible to increase the zirconia content, but avoid aging phenomena related to the presence of aggregates. Also the monoclinic phase fraction could be much lower. In aging studies, it was found that colloidally processed samples (using unstabilised zirconia) showed no evidence of aging, and were thus preferred over yttria stabilised materials.

In a recent, comprehensive study, Moraes et al. [5] investigated a series of composites with yttria-tetragonal zirconia polycrystal (Y-TZP) constants ranging from 5-80 wt% prepared by conventional powder processing. It was found that the addition of Y-TZP promoted composites with higher densities, higher flexural strength and higher fracture toughness. An inverse dependence of K_{IC} on hardness was shown. Improvement in flexural strength as high as 93% and improvement in fracture toughness of 29% were obtained compared to pure alumina samples. Three different equations were used to measure fracture toughness, and found differences as high as 50% for K_{IC} values for the same composition. Tan et al. [6], investigated the Young's modulus of alumina-zirconia (unstabilised) ceramics and found that the Young's modulus value can be increased by additions of < 5wt% of unstabilised ZrO_2. It was also claimed that the modulus can be increased by increasing the compacting pressure of the green ceramics, which reduces the pore volume fraction and increases the bulk density.

1.1 Research objectives

Inert bioceramics, such as Al_2O_3 and ZrO_2, have inherently low levels of reactivity compared to other materials such as polymers and metals as well as surface active or resorbable ceramics. In a human body, they are expected to be non-toxic, non-allergenic, non-carcinogenic for a lifetime, and this leads to a corresponding range of engineering design philosophies for medical application [7]. Zirconia-toughened alumina ceramic can be found in orthopaedic femoral heads implants, mechanicaly fixed to their mating hip stems [8]. During the service this ceramic is subjected to wear resistence, fatigue, and flexural strength, fracture toughness and hardness, here its properties are high importance. Ceramic heads are harder than their metal counterparts and with proper polishing they can be smoother than metal heads.

Zirconia-toughened alumina ceramic femoral heads are designed to incorporate the wear properties and stability properties of current alumina ceramics with vastly improved strength and toughness.

In this study, alumina-zirconia (Al_2O_3-ZrO_2) has been used for the composites, produced using different techniques. The main objectives of this research are:

1. To study the alumina and zirconia ceramics made by the conventional powder processing, and the colloidal processing.
2. To compare the results of the colloidal process and conventional process.
3. To investigate the mechanical properties of alumina-zirconia composites.

1.2 Research Plan

There are several experimental aspects to be realised in order to achieve the research objectives.

1. Preparing the compositions using the two proposed methods; conventional powder processing and chemical colloidal process.
2. Measuring the particle size of the compositions.
3. Measuring the particle size during the colloidal suspension using stokes's law.
4. Densification measurements:
    a) Measuring the green density by vernier caliper method.
    b) Measuring the density after sintering using two methods; geometric method, helium Pycnometer.
5. Evaluation of the following mechanical properties: Vickers hardness, indentation, fracture toughness and Young's modulus.
6. Examining the microstructure and the surface fracture using SEM.

1.3 Structure of thesis

This chapter discusses the background of the research topic and the aims of the study. The literature review of related research topics are elaborated in Chapter 2. In Chapter 3, the experimental procedures are described. The results and discussion are detailed in Chapter 4. Finally, the conclusions and proposed further work are outlined in Chapter 5.

CHAPTER TWO
LITERATURE REVIEW

CHAPTER TWO
LITERATURE REVIEW

2.0 Introduction

Ceramic materials have been increasingly important for structural applications in modern industries as they exhibit exceptional properties such as hardness, toughness, densification and excellent ability to retain strength at elevated temperatures. A review of the literature pertaining to Al_2O_3-ZrO_2 composites is presented in this chapter. This review is divided into five main sections as follows:

2.2 Alumina-zirconia ceramics.

2.3 Applications of alumina-zirconia.

2.4 Toughening mechanisms in alumina-zirconia.

2.5 Alumina-zirconia: powder processing.

2.6 Alumina-zirconia: colloidal processing.

2.1 Alumina-zirconia ceramic

2.1.1 Alumina (Al_2O_3)

Alumina (Al_2O_3) is the most widely used engineering ceramic material due to its high hardness value, high melting point (2054 °C), low thermal expansion and high compressive strength leading to good thermal shock resistance [9]. Alumina also shows good electrical insulation at high temperatures, good wear resistance and high hardness, making it suitable for components such as ball valves, piston pumps and deep drawing tools. Diamond tools are needed to machine or grind alumina.

Alumina forms solid solutions with some oxides (for example Cr_2O_3) and low melting eutectics with silica and several other oxides. The Al^{3+} and O^{2-}/ions have relatively high mobility at high temperatures; therefore alumina can be sintered easily. Alumina is used both in a pure form and an alloying component in aluminium oxide based ceramics which contain more than 85% Al_2O_3.

Various methods are used in the preparation of alumina powders depending on the desired particle size and purity, for example thermal decomposition of aluminium containing salts, dehydration of aluminium hydroxide, mechanical grinding of fused alumina. Some other properties of Al_2O_3 are listed in Table 2.1. [9].

2.1.2 Zirconia (ZrO_2)

Zirconia is widely used in metallurgy and high temperature chemistry because of its refractory properties and chemical durability. More recently the advantageous properties of monolithic and composite ceramics fabricated from stabilised and partially stabilised zirconia have been recognised. The elimination of the damaging monoclinic/tetragonal phase transformation and the improved purity of modern synthetic zirconia powders have greatly enhanced the utilisation of this material for structural applications. In addition to high strength over a wide temperature range, partially stabilised zirconia has exceptional fracture toughness properties at low temperature. Unfortunately, this high fracture toughness is lost at high temperatures.

Zirconia (ZrO_2) has three crystalline modifications: cubic between the melting point 2700°C and 2370°C, tetragonal between 2370°C and 1000 °C, and monoclinic at lower temperatures. The phase transformations are accompanied by volume changes. However, the different phases and the phase transformations may be exploited to produce ceramics with enhanced mechanical properties [9].

Zirconia (monoclinic and partially stabilised) powder is used in refractory compositions to enhance thermal shock resistance and abrasion resistance. These materials are used in severe applications such as sliding gate plates for pouring steel, and in steel immersion applications such as stopper rods and as components in submerged entry nozzles. Typical mechanical properties of ZrO_2 are demonstrated in Table 2.1. [10].

Table 2.1 Mechanical properties of alumina (Al_2O_3) and zirconia (ZrO_2) [10, 11].

Properties	Unit	Alumina	Zirconia
Chemical formal	--	Al_2O_3	ZrO_2
Density	g/cm^3	3.98	5.8
Tensile strength	MPa	300-900	211-1400
Hardness	Hv	2200	1200
Young modulus	GPa	380	200
Fracture toughness	$MPa.m^{-1/2}$	4.40	1.54-4.07
Melting Point	°C	2054	2700

2.2 Applications of alumina-zirconia

Great progress in dental restoration techniques has been established by the use of ceramic materials since the 70's. Ceramic materials show relative advantages, like better esthetics, biocompatibility and chemical resistance. One problematic aspect of ceramic materials and of dental ceramics in particular is their low mechanical resistance and fracture toughness [12].

Osseointegrated dental implants have been used since 80's in the rehabilitation of partially and totally edentulous patients [13]. The metallic abutments used in prosthetic restorations with implants must compromise the esthetic in some cases. To minimise this problem, some implant systems developed ceramic abutments. The use of alumina and zirconia biomaterials has been proposed. Aluminas have shown excellent biocompatibility and wear resistance.

However zirconia exhibits low flexural strength and toughness. Pure zirconia cannot be used in the manufacture of parts without the addition of stabilisers [13]. The yttria-tetragonal zirconia polycrystal (Y-TZP) has become a popular alternative to alumina as a biomaterial and is used in dental applications such as endodontic posts, orthodontic brackets, crowns and bridges and in ceramic abutments. The ceramic has also been extensively used in orthopedics' implants [14] as shown in Figure 2.1.

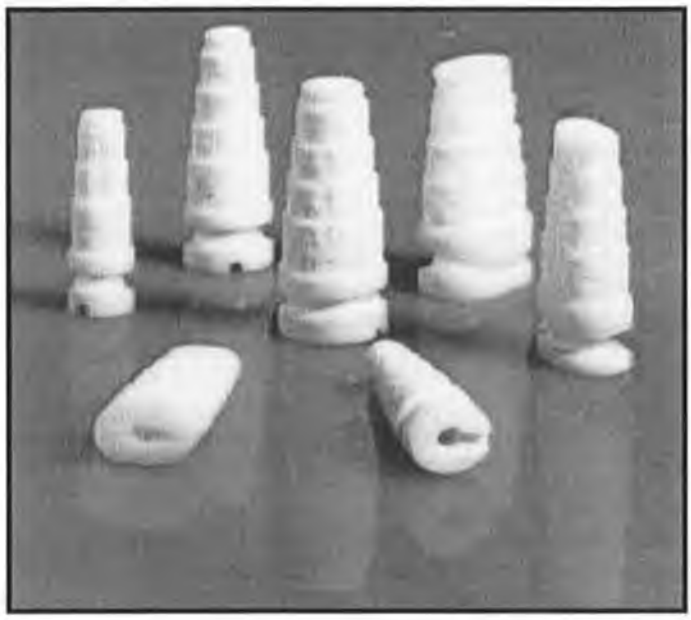

Figure 2.1: Alumina dental implants [14].

The ceramics that are commonly used in bone and joint replacement such as the ones shown in Figure 2.2 include: Alumina, which is used for the femoral head in many hip-joint prosthesis for its chemical stability, biological inertness, and excellent friction and wear resistance properties. However they are susceptible to overloading due to low fracture toughness.

Zirconia is used in the form of partially stabilized zirconia and has been promoted as an alternative to alumina due to its higher toughness as a result of transformation toughening.

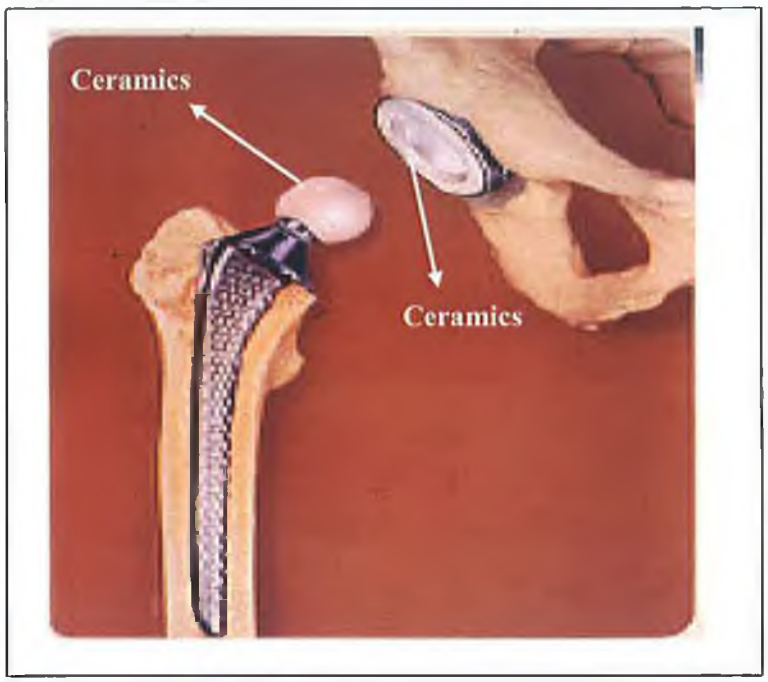

Figure 2.2: Hip joint prosthesis components [15].

Zirconia presents good esthetic aspects after polishing. It is inert in physiological environments and presents greater flexural resistance, toughness, and lower Young's modulus when compared with pure alumina [12]. The ability of Y-TZP to transform from a tetragonal crystalline structure to a more voluminous monoclinic structure, and thus obstruct crack propagation, gives the material its strength and toughness. The addition of zirconia to the alumina as a sintering additive has been used for a long time for the densification of the alumina based ceramic. However, the concept of toughening alumina ceramics by dispersion of zirconia particles in the matrix was only recognised in the last 20 years [13].

The microstructure of a composite material is formed from the addition of one second phase. A composite material is the way to improve the reliability and the lifetime of ceramic abutments by providing higher fracture toughness and mechanical strength. An additional advantage of Alumina-zirconia composites is its biocompatibility. Relatively little has been published in the literature on the use of alumina-zirconia composites as biomaterials [15].

2.3 Toughening mechanisms in alumina-zirconia

The essential idea behind all toughening mechanisms is to increase the energy needed to extend a crack. The basic mechanisms are crack deflection, crack bridging, and transformation toughening.

Transformation-toughening materials owe their very large toughness to the stress-induced transformation of a metastable phase in the vicinity of a propagating crack [17]. If these tetragonal particles are fine enough, then upon cooling from the processing temperature, it can be constrained from transforming by the surrounding matrix and consequently can be retained in a metastable tetragonal phase. Three classes of toughened zirconia ceramics have been identified:

1. *Partially stabilized zirconia* (PSZ): In this material the cubic phase is less than it exists in the totally stabilized as the results of adding MgO, CaO, or Y_2O_3. The cubic phase is then heat-treated to form coherent tetragonal precipitates. The heat treatment is such that it keeps the precipitates small enough so they do not spontaneously transform within the cubic zirconia matrix but only as a result of stress [18] as illustrated in Figure 2.3.

It was observed that tetragonal metastable precipitates dispersed within the cubic matrix were able to be transformed into the monoclinic phase when the constraint exerted on them by the matrix was relieved, for example by a crack advancing in the material. In that case, the stress field associated with expansion due to the phase transformation acts in opposition to the stress field that promotes the propagation of the crack. An enhancement in toughness is obtained, because the energy associated with crack propagation is dissipated both in the T-M transformation and in overcoming the compression stresses due to the volume expansion [14].

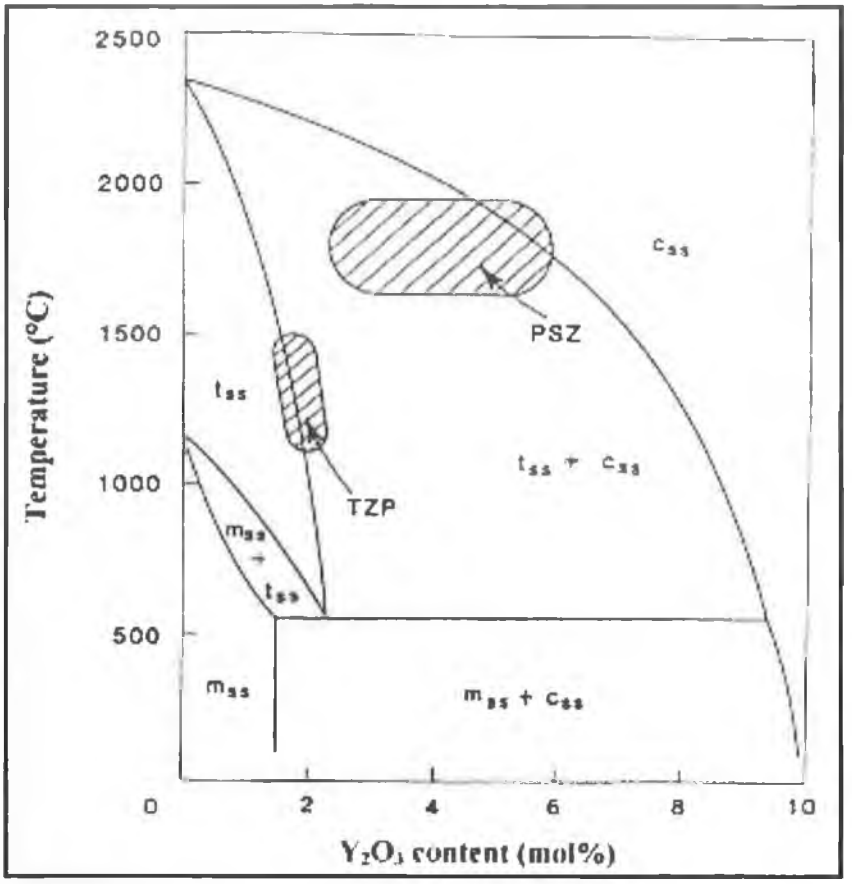

Figure 2.3 Part of ZrO_2-Y_2O_3 phase diagram. The capital letters refer to phases concerned: C- cubic, T-tetragonal, M-monoclinic [11].

2. *Tetragonal zirconia polycrystals* (TZPs): The TZP ceramics are fine grained, single phase, fully dense tetragonal ZrO_2 materials containing small amount (2-4%) of Y_2O_3 additives. The sintering is performed in the tetragonal field between 1300-1500 °C. The tetragonal phase may be retained at room temperature, provided that the grain size is maintained at a sufficiently fine level (0.1-1 μm) [9].

   The TZP materials are presently the strongest and toughest zirconia based ceramics. However, they lose these desirable properties at 150-300 °C due to the transformation of the metastable phases.

3. *Transformation toughened ceramics*: In transformation toughening, the volume expansion is exploited, which occurs at tetragonal to monoclinic transformation in ZrO_2 particles embedded into another oxide matrix, most frequently alumina. The mechanism of this transformation is rather complex. The mechanism is different for fine tetragonal particles whether present as

discrete grains or particles embedded into a matrix. In the last case, the transformation is also influenced by the matrix, too. Either way, the atomic rearrangement is fast, diffusionsless and shear like. It is similar to martensitic transformation observed in several metallic systems. The starting temperature of martensitic transformation depends on the pressure applied [19].

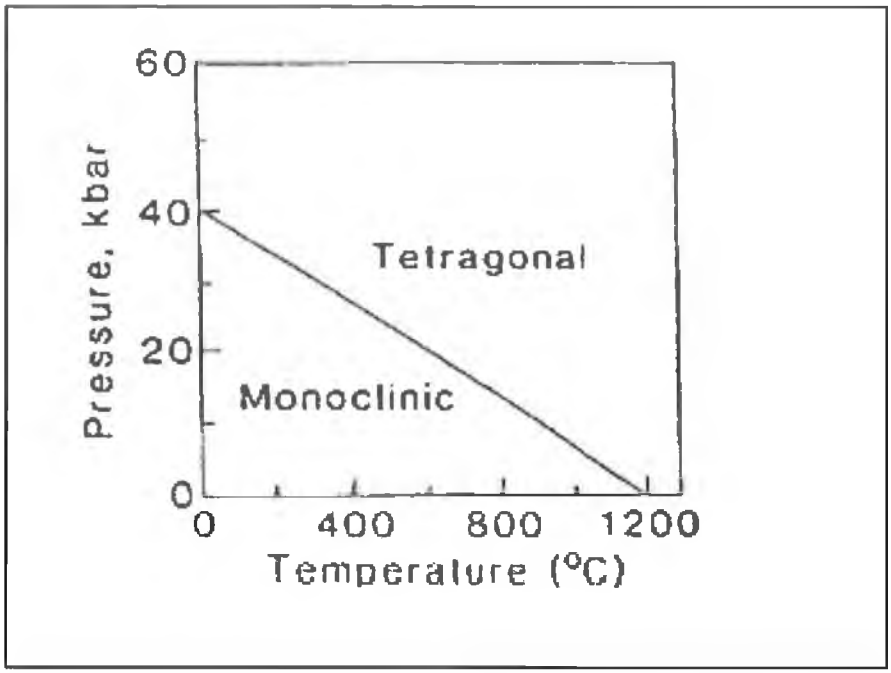

Figure 2.4 Dependence of temperature of martensitic transformation on pressure [19].

In the production process of ZrO_2 toughened aluminum oxide ceramics, ZrO_2 is added to alumina powder, in quantities of 10 to 20 vol %, in the form of fine ($\cong$ 0.8-1μm) particles. The mixture is then sintered in the tetragonal phase. When cooled, the ZrO_2 particles remain in tetrahedral phase even at room temperature. If a crack starts to propagate, the stresses around the tip initiate the tetragonal to monoclinic transformation which results in compressive stresses and a closure of the crack. Similar processes occur as a result of surface machining [20], these transformation principles are shown in Figure 2.5.

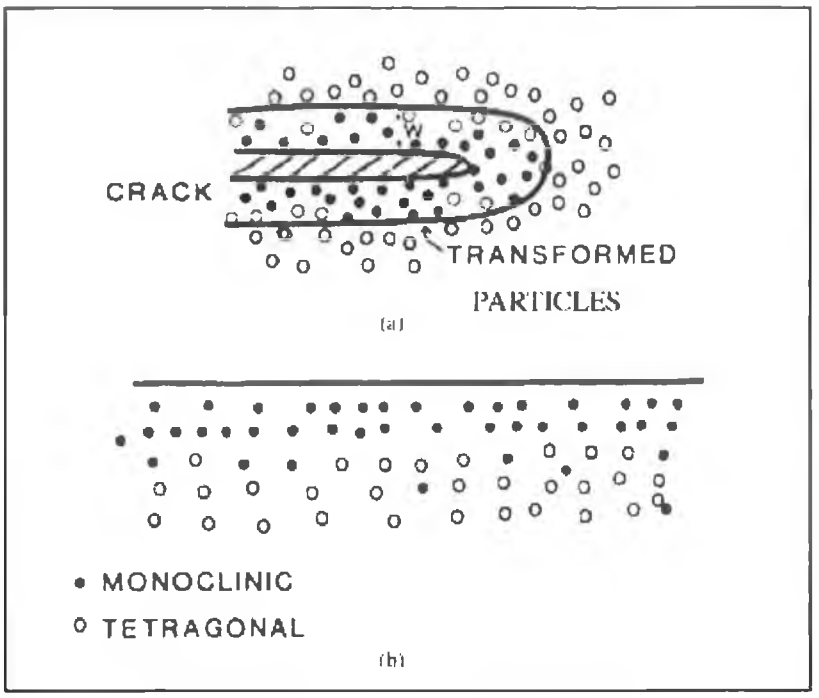

Figure 2.5 Principle of transformation toughening: a/ transformation around a crack tip b/ transformation at the surface due to grinding [16].

The fracture strength of sintered aluminium oxide materials is about 5 $MPa.m^{1/2}$. With the addition of 16 vol % ZrO_2 the fracture strength can be increased about three times. Transformation toughening has been successfully applied not only to alumina matrix but to other aluminium oxide ceramics such as mullite (3 $Al_2O_3.2SiO_2$) and spinell ($MgAl_2O_3$) [19, 20].

2.4 Alumina-Zirconia: Powder processing

There are many reports in the literature on the powder processing of alumina-zirconia ceramics. These studies cover a wide range of the powder's processing and properties aspects. This section attempts to summarise the main mechanical properties of alumina-zirconia ceramics.

Claussen [1] was one of the first to investigate the alumina-zirconia system. According to Claussen, the fracture toughness energy of a ceramic can be increased by a second phase dispersion, for example by SiC particles in Si_3N_4, Al_2O_3 spheres in glass, Mo particles in Al_2O_3, and Ni particles in MgO. This increase in fracture energy is usually attributed to the interaction of the crack front with the second phase; the energy-absorbing mechanisms are for example crack blunting, crack deviation, and crack front elongation.

Such" cracked" ceramics usually have low strengths. The same is true for many ceramic composites in which the fracture energy has been increased by second-phase dispersion. For instance, a 26% increase in fracture toughness resulting from the addition of 10 vol % 32-μm SiC particles to a Si_2O_4 matrix was accompanied by a 40% loss in strength. Thus, the necessary condition for applying this energy-absorbing mechanism to high-strength ceramics is the formation of very small evenly dispersed microcracks. The safest method of creating controlled microcracks in a ceramic matrix is the incorporation of second-phase particles with a considerably lower coefficient of expansion than that of the matrix. When such a composite is cooled from its fabrication temperature, highly localised tensile stresses arise which can cause cracking of the matrix [1].

Although the miximum tensile stress is independnt of particle size, cracks have been observed adjacent to the large particles only, not the small particles. In other words a critical particle size, D_c, must exist below which cracks are not formed. Based on an enrgy balance, Lange derived a relation for the critical particle size [1].

$$D_c \geq C/\sigma_t^2 \tag{2.1}$$

Where:

C: is a constant for a given particle-matrix pair.

σ_t^2: Tensile stress in the matrix. For alumina (with ZrO_2 particles) $\approx$ 2000MN/m^2 [1].

According to Claussen [1], a necessary condition for applying this energy-absorbing mechanism (intentionally induced micro-cracking) is the formation of very small, evenly dispersed microcracks. Safest way to do this is to use second-phase particles with a considerably lower coefficient of expansion than the matrix; on cooling from sintering, highly localised stress will lead to micro-cracking of the matrix.

If particles are too small cracks will not be formed at all. Particles will transform from tetragonal to monoclinic but will be too small to effect microcracking. This is due to the tensile stress generated around the particles being too small. In most material combinations (where the expansion coefficient of the matrix is larger than the second phase), relatively large second phase particles are needed to cause

microcracking. According to Claussen [1], ZrO_2 overcomes this problem due to the expansion caused by the T-M transformation; thus second phase particles can be kept much smaller.

A high density of microcracks is produced by tensile stresses caused by the expansion of the dispersed ZrO_2 particles during the tetragonal to monoclinic lattice transformation. It is assumed that the extent of the energy dissipation zone is markedly increased by the existence of the induced microcracks. Because of the extremely high tensile stresses developed in the matrix, very small ZrO_2 particles can become crack formers, thus limiting the internal flaws to small sizes. This behaviour is reflected in the modulus of rupture, which is lowered only slightly for volume fractions up to 15% [1]. Fracture toughness might be expected to increase when uniform, evenly dispersed ZrO_2 particles with a diameter slightly greater than D_c are used. Claussen [1] believed that fracture toughness increased up to 15% then fell off for higher volume. fraction. The concept of using unstabilised ZrO_2 inclusions could be applied to toughen most other ceramics. Further investigation showed that the fracture toughness of Al_2O_3 was increased considerably by the incorporation of a second-phase dispersion of unstabilised ZrO_2 particles [1]. Subcritical propagation and opening of microcracks in a large zone in front of the notch tip were believed to be responsible for this increase.

The most recent comprehensive study of alumina-zirconia was carried out by Cecilina et al. [13]. It was found that the fracture toughness ranges between 6.10 $MPa.m^{1/2}$ to 7.16 $MPa.m^{1/2}$. It was also found that the flexural strength ranges between 396.71 MPa to 736.55 MPa, those results are listed in Table 2.2.

Table 2.2 Materials properties of alumina-zirconia [13].

Materials	Hv (GPa)	E (GPa)	K_{IC} (MPa.m$^{1/2}$)	Flexural strength (MPa)
A	17.53 ± 0.52	380.00	610	396.71
5ZT	17.53 ± 0.76	365.22	6.38	441.40
10ZT	17.48 ±0.21	351.54	6.43	473.13
15ZT	17.41 ±0.23	338.85	6.65	491.14
21ZT	17.38 ± 0.38	324.79	6.85	510.79
80 ZT	15.44 ± 0.46	230.64	7.49	755.35
100ZT	13.20 ± 0.48	210.00	7.16	736.55

The zirconia addition had a large effect on increasing the fracture strength, but its influence on the fracture toughness was much smaller, as demonstrated by Claussen [1]. The reason for this behaviour can be referred to the absence of two of the main toughening mechanisms of ZTA: the crack bridging and the transformation toughening. The crack bridging is negligible because of the small grain size of alumina (only small bridges were detected in pure alumina). The transformation toughening is also absent because only 5% of ZrO_2 transforms on fracture surfaces [13]. The reason could be that the ZrO_2 average particle size is too small to activate the stress-induced phase transformation. In fact, the author had found greater values of fracture toughness when the grain size of alumina matrix and zirconia particles had been increased with thermal treatments of grain growth. The size of the tetragonal particle and the stabiliser content, have great influence in the tension required for the transformation of tetragonal particle. In terms of Young's modulus, the author found that the Young's modulus decreased with the increase of ZrO_2 content. The critical grain sizes increase with the Young's modulus of the composite, which is related to the restrictions imposed by the matrix. According to the rule of mixtures, the Young's modulus decreases as the zirconia content is increased in composites, while the critical grain sizes becomes smaller.

The ceramic strength values usually exhibit a large scattering (up to 100%) even for high performance ceramics. According to Claussen [1] this is a well known phenomenon, which arises from the scattering of the initial sizes of the defects responsible for failure. The first and most important step for improving the strength and reliability of ceramics is to reduce the size of cracks and defects. This can be

achieved by obtaining a fine-grained more uniform and dense structure by the use of improved powders (high purity, fine and narrow initial particle size distribution) as well as by adopting better processing techniques. The composites 80 ZT presented flexural strength of approximately 90% higher when compared to pure alumina, showing that the second phase addition provided the composite with a denser and a more refined microstructure, a reduced size of the crack population, and as expected that the strength of ceramics is inversely proportional to the square root of the grain size.

Cecilina et al. [13] analysed zirconia-alumina composites by controlling the amount of zirconia in order to achieve higher densities, higher flexural strength and fracture toughness. It was shown that there is an inverse dependence of K_{IC} on the hardness. The composites can achieve superior flexural strength approximately 90% and fracture toughness of 29% when compared to the pure alumina ceramics. Pure zirconia and the composite with 80% of zirconia addition exhibited Palmqvist crack system under an indentation load of 10 kgf. The other compositions exhibited median crack systems. The fracture toughness data generated by Claussen [1] showed differences of 50% for the same composition, the composites with higher zirconia content exhibited higher flexural strength and fracture toughness when compared with the pure alumina or even with the pure zirconia. These composites seem to be an adequate material to be used in the manufacture of implant abutments instead of the pure oxides.

Tan et al. [6] studied the Young's modulus of the green and sintered unstabilised Al_2O_3-ZrO_3 ceramics by measuring compression and shear velocities through the material. They found that the Young's modulus and sintered density of Al_2O_3–ZrO_2 ceramics can be enhanced by increasing the compacting pressure when forming the green ceramics and with the addition of < 5 wt% of unstabilised ZrO_2, defects such as microcracks, due to phase transformation of the ZrO_2, for a given green compacting pressure, the diametrical compressive fracture stress changes with wt% ZrO_2 with a maximum at 3 wt%. Above values of 3%, the modulus decreased. The fracture stress also increases with a higher green compacting pressure at a constant wt% ZrO_2. This behaviour is similar to that of the Young's modulus of the ceramics. A high number of grains per unit volume are believed to slow the propagation of cracks by deflecting their paths along the boundaries.

Deville et al. [4] studied the alumina-zirconia composites by using a classical powder mixing processing route. Different compositions ranging from 10 to 15 wt. % of zirconia added to a matrix of alumina were studied. It was found that the two different behaviour can be observed for the unstabilised materials: either ageing was occurring at quite a steady rate, or no ageing at all was observed, depending on the zirconia content. This behaviour might be related to the microstructure in a fairly simple manner. There is an increase of fracture toughness while increasing the zirconia content up to about 10 vol. % indeed, increasing the number of zirconia particles, this increases the number of microcracks created during cooling after sintering and when cracks are propagating within the material. The toughness was therefore increased, by microcracking toughening. However, beyond a certain level, those microcracks tend to percolate altogether, joining up between the particles and the toughness is abruptly decreasing. This microcracks percolation may also account here for the ageing behaviour. Microcracks present along the grain boundaries of the alumina matrix could act as preferential paths for the water diffusion inside the bulk of the material. The tensile stress accompanying the ($t \rightarrow m$) transformation upon cooling and the presence of water, cause microcracks to grow at subcritical stress levels. These microcracks change the transformation conditions of the adjacent tetragonal grains, such as strain energy and strain force between the grains, they consequently contribute to accelerate the transformation of tetragonal phase to monoclinic during ageing, generating additional microcracks. The microcracks on the transformed surface are a result of the volume expansion upon transformation, and lead to the severe degradation of the mechanical properties. When the zirconia content was above the mentioned maximum, 15 wt%, the microcracks percolation system provided the ceramic with preferential paths for water propagation within the material, increasing the ageing degradation. However, by keeping the zirconia content below this maximum, unstabilised zirconia particles transformed to monoclinic during cooling, without percolation of microcracks.

The alumina–zirconia composite has attracted material scientists' attention for decades due to its specific mechanical character, especially its toughening behaviour.

Green et al. [21] reported that alumina is commonly used as the matrix and zirconia is the dispersed phase. Alumina experiences grain growth during sintering which causes several disadvantages for single-phase applications porosity and

exaggerated (or abnormal) grain growth. The Introduction of a second phase may control the grain growth of alumina or promote sintering kinetics which leads to a fully-dense ceramic. Green et al. [21] it was found that MgO was the most effective additive to prevent the discontinuous grain growth of alumina. The addition of 0.25 wt% of MgO provided beneficial effects on the densification rate and full density, other effective sintering aids for alumina including NiO and TiO_2.

It was found that the addition of ZrO_2 was effective in inhibiting grain growth of alumina despite its inability to produce a ceramic with a satisfactory density. The addition of more than 5 vol % of ZrO_2 modified the grain growth of alumina from 6.9% μm in pure alumina to 2.82 μm. The grain growth of ZrO_2 was believed to occur by coalescence. This led to the location of the zirconia grains, mostly, at four-grain junctions.

It was also observed by Green et al. [21] that above 1550 °C some ZrO_2 grains were relocated to the interior of the alumina grains and became spherical. This occurrence was attributed to the growth of a number of alumina grains into a large grain which, during the process, swallowed up the small zirconia grains.

2.5 Alumina-zirconia: colloidal processing

Chemical methods are frequently used for the preparation of metals as well as ceramic powders. These methods have several advantages including the chemical homogeneity, uniformity of grain size, the reduction of contaminations, and possibility of making compounds.

There are many reports in the literature regarding colloidal processing of alumina-zirconia. The most recent comprehensive study of alumina-zirconia using colloidal processing was carried out by Schehl et al. [3]. It was found that colloidal processing has many advantages over other conventional processing methods: firstly, nanocomposites with a very small amount of secondary phases can be designed. Secondly, the formation of these phases can be predicted by referring to the information presented in phase equilibrium diagrams. Furthermore, new composites can be easily designed if one considers the phase evolution as a function of temperature.

The colloidal processing route also produces very homogeneous microstructures with a narrow particle size distribution of secondary phases and high final densities. Sintering behaviour studies of alumina-zirconia have revealed that densification starts at 1050 °C, whereas doped alumina start to densify at 1250 °C. Organic impurities might be a possible explanation to the delay in the formation of secondary phases at high temperatures from metal alkoxides coated on the surface of alumina particles, because it was located at the grain boundaries and act as diffusion barriers during sintering. As a consequence low energy grain boundaries cannot be formed and grains remain in the original position. At higher temperatures, when diffusion through grain boundaries is promoted, sintering is accelerated considerably. As a result, pores located at triple points between grains of different orientations are completely eliminated. Thus, higher final densities can be achieved compared to non-doped alumina. Moreover, secondary phase particles possess a nanoscaled uniform size and are distributed at the alumina grain boundaries and hence, increase the effectiveness of the reinforcement mechanisms that operate in these nanocomposites.

The mechanical properties of pure alumina and its composites, alumina-zirconia and alumina-yttria were investigated by Schehl et al.[3] Table 2.3 shows the percentage of the theoretical density, Young's modulus, bending strength and fracture toughness for alumina and alumina- based nanocomposites. The sintered samples listed in the Table are A which is (100 wt% alumina), AY (97.2 wt% alumina; 2.8 wt% yttria), and AZ (95 wt% alumina; 5 wt% zirconia).

The composites containing zirconia show a significant increase in K_{IC} values compared to pure alumina, A. For example the AZ and AY composites exhibit K_{IC} values of 7.5 and 5.8 $MPam^{1/2}$ respectively, whereas pure alumina, A, has only a value of 4.5 $MPam^{1/2}$. As for the bending strength, the AZ composite has the highest value of 343 MPa, followed by A, which has a value of 326 MPa. The AY composite has the lowest value 269 MPa.

Table 2.3 Density, Young's modulus, bending strength and fracture toughness of sintered samples [3].

Sample	density %TD	Young's modulus (GPa)	bending strength (MPa)	fracture toughness $MPam^{1/2}$
Alumina	99.04	400	326	4.5
Alumina-yttria	99.44	403	269	5.8
Alumina-zirconia	99.69	381	343	7.5

The densities of the alumina-zirconia and alumina-yttria composites are similar. The highest density was obtained for alumina-zirconia, followed by alumina-yttria. The lowest value of Young's modulus was observed in the case of the alumina-zirconia composite, which might be related to the low density value. Other differences cannot be observed. Nevertheless, the considerable increase in the fracture toughness of doped alumina composites, mainly in those composites containing zirconia as a secondary phase. The high fracture toughness is attributed to the stress induced transformation of metastable tetragonal grains towards monoclinic symmetry ahead of a propagating crack, with a consequent increase in the work of fracture toughness. The microstructures of the alumina, alumina-zirconia, and alumina-yttria nanocomposites after sintering at 1600 °C for 2 hours are shown in Figure 2.6.

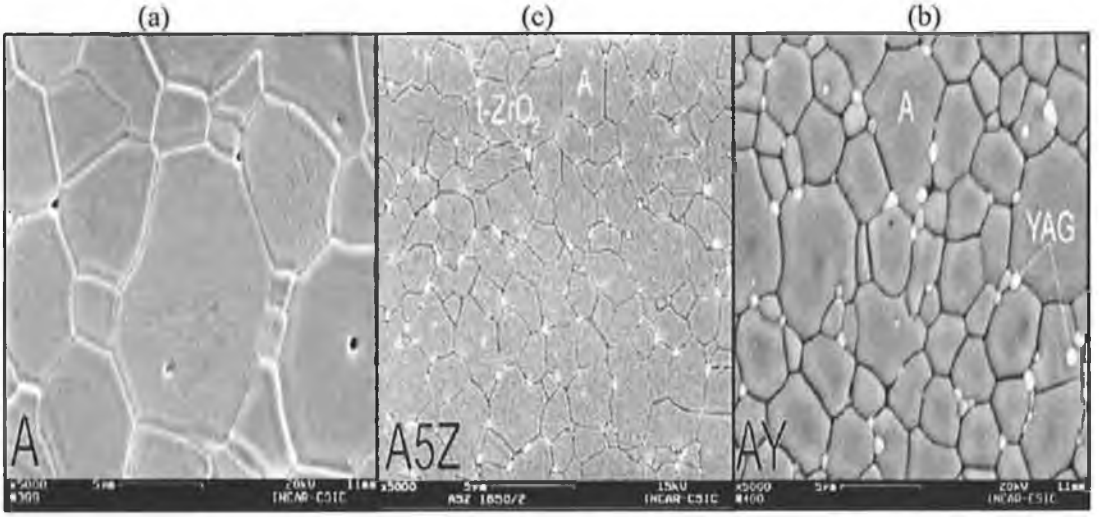

Figure 2.6 SEM micrograph of (a) pure alumina A, (b) alumina-zirconia AZ, and (c) alumina-yttria AY nanocomposites after sintering at 1600 °C for 2 hours [3].

The pure alumina, A, sample shows a dense and a homogenous equiaxed microstructure that has a mean grain size of 5.9 μm. Intragranular pores are clearly visible in Figure 2.6(a). The microstructure of the alumina-zirconia AZ showed a matrix formed by alumina grains with a mean grain size of 1.63 μm and a homogeneous distribution of zirconia grains of 200 nm grain sizes. The zirconia grains are located in 50% of the triple points, as shown in Figure 2.6(b). The microstructure of the AY sample is composed of alumina grains having a mean grain size of 3.56 μm and YAG grains at triple points that are homogeneously distributed throughout the alumina matrix in Figure 2.6(c). It can be seen that only about 25% of the triple points are occupied by YAG particles with a mean particle size of about 200 nm. However a polished cross-section shows interfaces between grains that do not correspond to the real triple points.

As a consequence of these microstructural features, alumina grain boundaries present a homogeneous stress field distribution that will affect the mechanical behavior and properties.

Several investigations have been carried out to understand the difference between the classical powder mixing processing route and colloidal processing route.

Deville et al. [4] processed alumina-zirconia composites using a classical powder mixing processing route and a new modified colloidal processing route. Using classical powder mixing processing route to reach a very fine and homogeneous microstructure has been proved to be almost an impossible target. Avoiding aggregates formation during the process is a difficult task, when considering all the processes developed so far. On the other hand, the (SEM) study of the microstructure of samples obtained by the colloidal processing route, done by Deville et al. [4], clearly showed a very fine and also a very homogeneous microstructure, with no evidence of the presence of aggregates.

According to Deville et al. [4], with such a processing route, it should be possible to increase the zirconia content up to values that will lead to better mechanical properties, but avoiding the ageing phenomena related to the presence of aggregates. The advantages of such a microstructure is two-fold: by keeping a nanometer grain size, the important residual strains after cooling will improve the resistance to crack propagation and thus toughness. By avoiding zirconia grains aggregates, it would be possible to increase the zirconia volume fraction so that the

transformation toughening becomes effective in the material and therefore increases the toughness again. Compared to the unstabilised materials fabricated by the powder mixing route, the starting monoclinic phase fraction could be much lower, therefore keeping all the potential for transformation toughening. The Al_2O_3-10wt%ZrO_2 and Al_2O_3-15wt%ZrO_2 samples start with monoclinic volume fraction as high as 60 or 66 vol. %, which limits the potential for transformation toughening.

Caldero et al. [22]. have studied Alumina composites with 5 to 20 wt% zirconia obtained by alumina powder–zirconium alkoxide mixtures without any dopant and with a matrix grain size in the range 1–2 μm are superplastic at 1350 °C and strain rates ~10^{-4}, exhibiting stable microstructure during sintering and mechanical testing, without significant cavitations or crack growth.

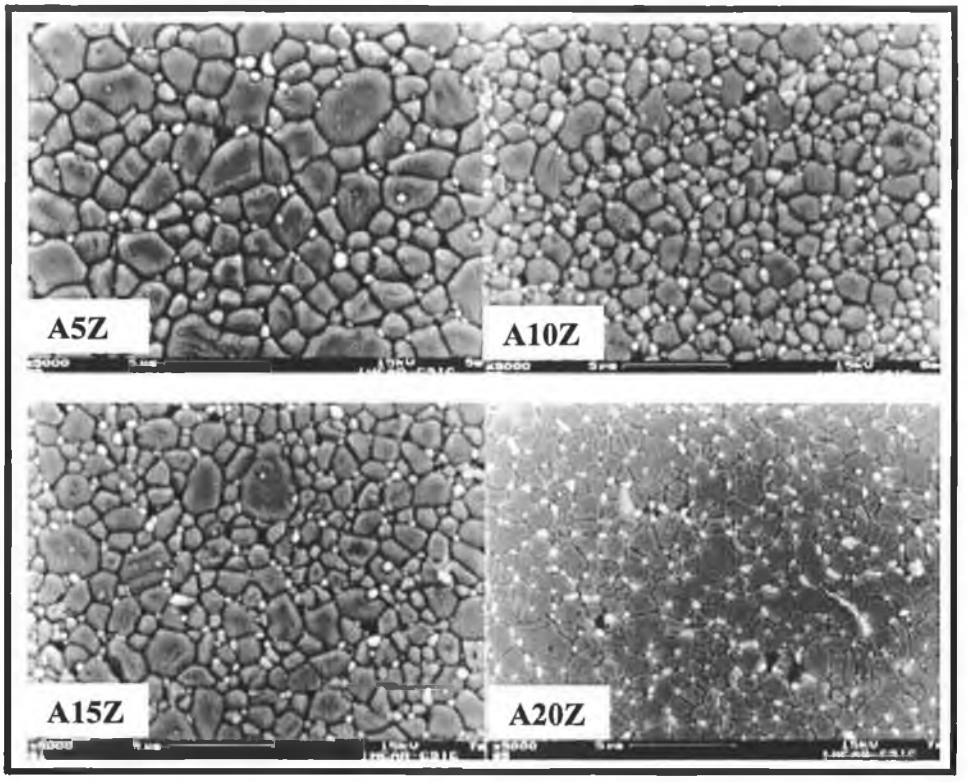

Figure 2.7 SEM micrographs showing polished and etched composites containing zirconia (clockwise A5Z, A10Z, A15Z, and A20Z) [22].

The composites obtained by the powder–alkoxide mixture route have homogeneous grain sizes and phase distribution. it can be seen in Figure 2.7 that the zirconia particles are located at grain boundaries between bigger alumina grains, with at least six pinning zirconia particles at each alumina grain boundary, using this route

it is possible to obtain composites achieving effective stress relaxation against growth of critical flaws and the propagation of grain boundary opening with very low percentage of zirconia particles. These results support the suitability of alumina/zirconia interphases for achieving high ductility at high temperature. The pinning effect and relaxation knetics of dispersed alumina–zirconia interphases, with higher cohesive strength and faster diffusion kinetics than alumina interfaces, is considered to be responsible for the observed superplastic behaviour.

Fegley et al. [23] have developed several ways for designing transformation-toughened ceramics such as zirconia–toughened alumina, mullite, and spinel. The following methods has been used, mechanical mixing of powders, attrition milling of zirconia grinding media, sol gel syntheses, reactive sintering, and evaporation decomposition of slurries. These methods attempt to control the chemistry and microstructure of sintered ceramics and thereby their mechanical properties.
Specifically, toughened mechanisms of samples resulting form stress-induced transformation or microcrack nucleation may be optimised by minimizing the zirconia particle size and size distribution. Also, maintaining tetragonal zirconia is essential for stress-induced transformation toughening, where a uniform zirconia particle distribution is important for optimizing microcrack nucleation-induced toughening.

It was described a new zirconia-alumina powder preparation method, such as single-phase and doped oxide powders of controlled size, size range, shape, and composition [23]. This technique involves hydrolysis of a zirconium oxide in an α-alumina dispersion. If the alumina particles are small and have a narrow size distribution, the resulting zirconia-alumina particles are also small and narrow. The techniques described herein are advantageous over conventional techniques such as mechanical mixing because they yield powders that are small, narrow in size, and of controlled chemical composition. Such "ideal" powders, which arguably assess processing advantages over commercial powders, may permit better design of zirconia toughened ceramics.

Wang et al. [24] has studied the influence of acidity on the electrostatic stability of alumina suspension in ethanol during colloidal processing. The ethanolic solution was determined using ion-transfer functions. The operational pH meter reading in ethanolic solution was converted using glass and calomel electrode pairs

connected by a concentrated aqueous KCI salt bridge. Because of the lack of standard buffer solutions in EtOH, two aqueous standards of pH values of 4 and 7 were used during standardization. Because of the slow response of pH electrodes in EtOH, generally 0.5-1 hours of processing time was required to obtain stable operational pH readings versus time, those readings are shown in Figure 2.8.

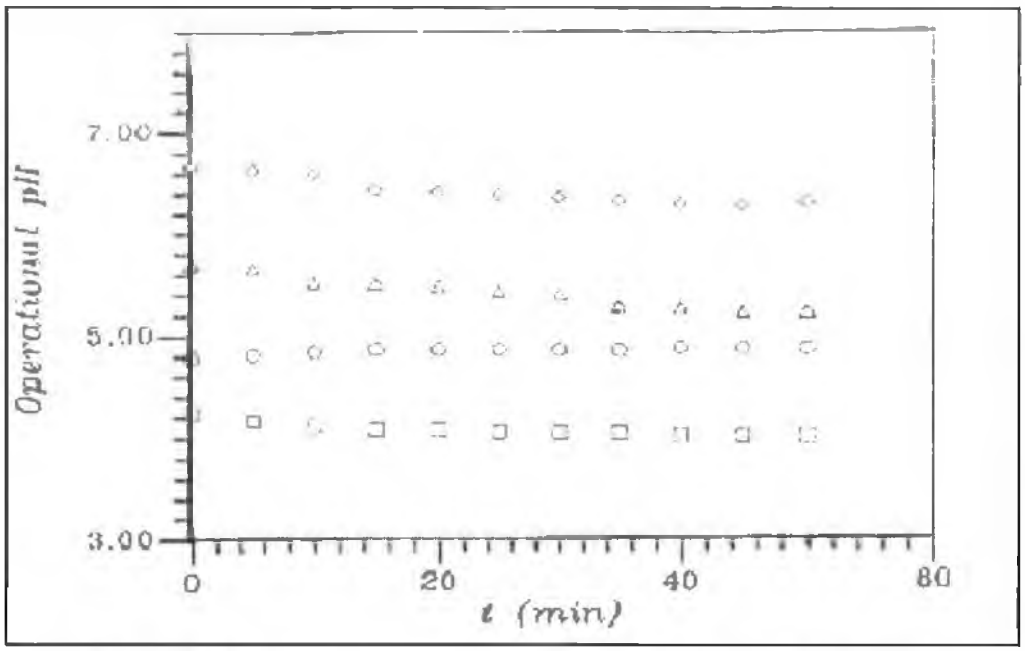

Figure 2.8 measurement of operational pH as a function of time [24].

When alumina powders are dispersed in EtOH, there is an acidity-dependent electrical charge on the particle surface. In this case, the charging mechanism is the absorption of protons or hydroxyls onto the surface sites of alumina (AlOH).

At lower operational pH values, alumina powders were observed to be positively charged. The surface charge changed from positive to negative as the operational pH increased. These results identify the isoelectric point of alumina particles in EtOH. The electrophoretic mobility of alumina as a function of the operational pH is shown in Figure 2.9.

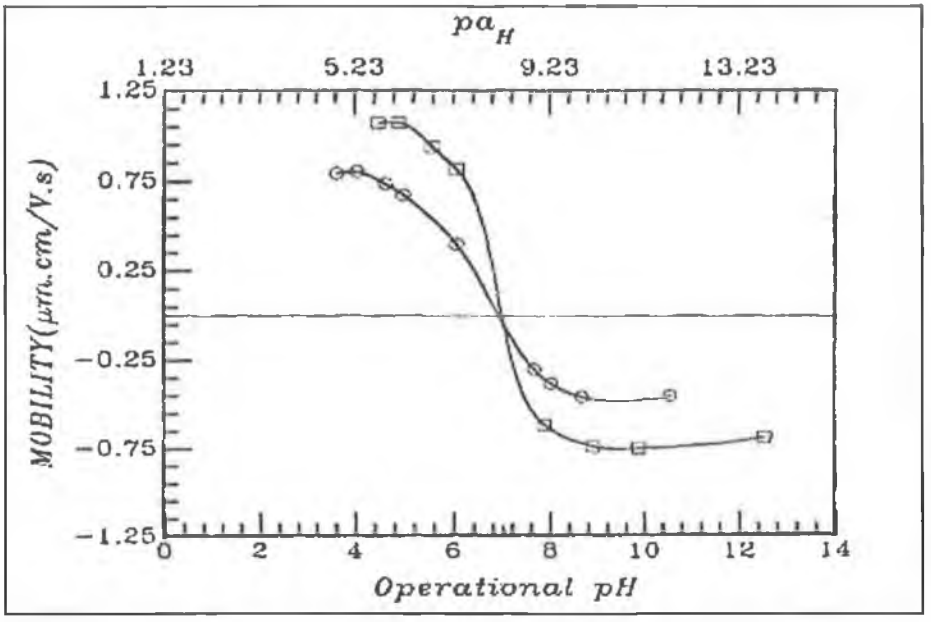

Figure 2.9 Electrophoretic mobility of Al_2O_3 particles in EtOH as a function of operational pH [24].

Schehl el at. [3], studied alumina-zirconia powders prepared by controlled hydrolysis zirconium propoxide in a dispersion of alumina powders in 100% ethanol. When alumina particles are dispersed in ethanol, protons or hydroxyls are adsorbed on the surface of the alumina particles. The addition of metal alkoxides to this dispersion causes a substitution reaction between the metal alkoxide and the OH groups on the surface of the alumina. As a consequence, the surface of the oxide particle is coated with metal alkoxide, as illustrated in Figure 2.10.

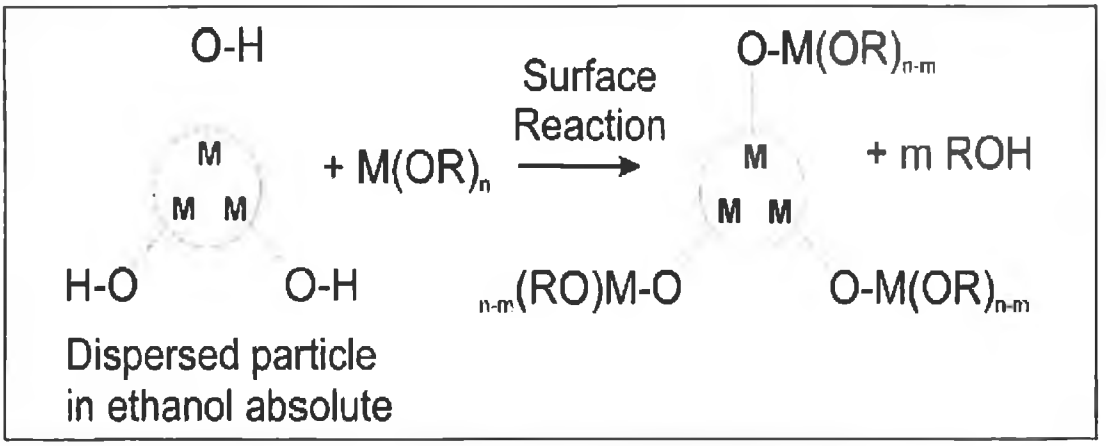

Figure 2.10 Substitution reactions between the metal alkoxide and the OH groups on the surface of alumina [3].

Figure 2.11 represents the TG curve of alumina-zirconia in air. This curve shows a weight loss of about 2 wt% as a result of the decomposition of organic groups (M (OR_{n-m} to M_xO_y). After 400 °C no more weight loss is observed and apparently all organic groups have been eliminated

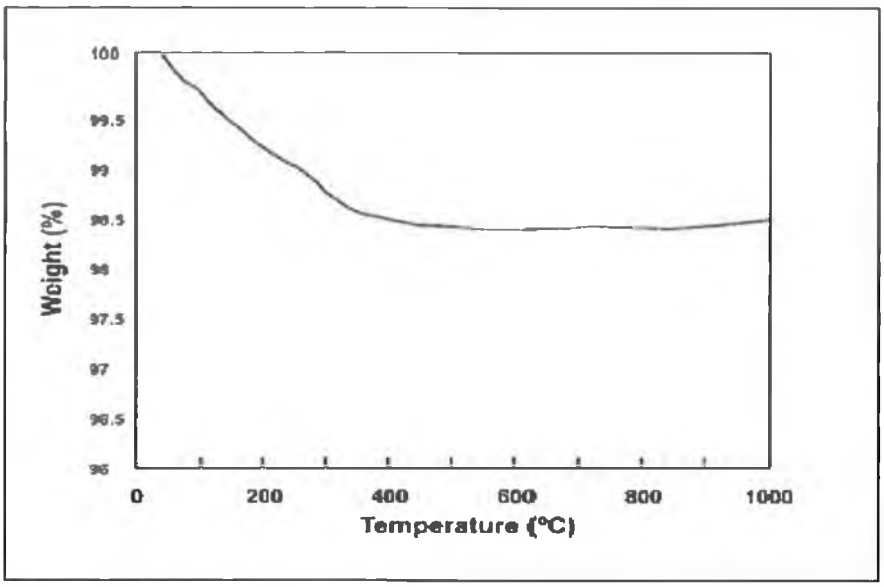

Figure 2.11 TG curve in air of the AZ sample [3].

Cortesi et al. [25] investigated the effectiveness of the ZrO_2 and Al_2O_3 particles. High purity, narrow size-distribution, submicrometer Al_2O_3 particles were coated with zirconium alkoxide, then the alkoxide was hydrolyzed in a continuous-flow reactor. Alumina-zirconia composites were obtained by aggregating the composite after hydrolysis.

A multistep hydrolysis batch process was also tested, but the results revealed the same coating quality of the hydrolysis method, but had a lower yield.

It was found in alumina-zirconia composite powders containing more than 16 wt% that ZrO_2 was obtained by flocculating powder synthesized in a continuous-flow reactor from commercial alumina powder and zirconium *n*-propoxide. This alumina powder and zirconium *n*-propoxide had a narrow size-distribution. The sintered samples had a fine grained, homogeneous microstructure, and it was also found that as the ZrO_2 content decreased, the grain size and the microstructure density decreased.

CHAPTER THREE
EXPERIMENTAL TECHNIQUES

CHAPTER THREE
EXPERIMENTAL TECHNIQUES

3.0 Introduction

This chapter describes the materials and the equipment which were used to prepare alumina and zirconia ceramics using two methods; the conventional powder processing, and the colloidal processing, in order to investigate the mechanical properties of alumina-zirconia composites in this research study.

3.1 Materials

The raw materials used consisted of:

1. High-purity alumina (Al_2O_3) powder, (American Premalox Ceramic of purity 99.25 %) and the average particle size is 2.16 μm.
2. High-purity Unstabilised Zirconia (ZrO_2) powder, pure zirconia (American Premalox Ceramic of purity 99.8 %) and the average particle size is 3.58 μm.
3. Zirconium (IV) propoxide, 70 wt% solution in 1-propanol (Steinheim, Germany).
4. Propan-2-ol $CH_3CH\ (OH)\ CH_3$, (VWR International Ltd, England).
5. Absolute ethanol (99.97% ethanol) C_2H_5OH (Merck KGaA, Darmstadt, Germany).
6. Acetic Acid, 99.7 % (CH_3CO_2H) (Sigma-Aldrich Chemie GmbH, Riedstr. Germany).

3.2 Powder preparation

3.2.1 Ball milling

Alumina powder was mixed with different amounts (5, 10, 20 wt %) of unstabilised zirconia. The powders were mixed and grinded in conventional ball milling as shown in Figure 3.1. The milling media were alumina balls of 24 mm diameter, the milling time was 24 hours, and the milling turning speed was 300 rpm. These parameters

were selected based on the works done by Sherif et al. [26]. Ball-milled powders were sieved though a 125 μm sieve.

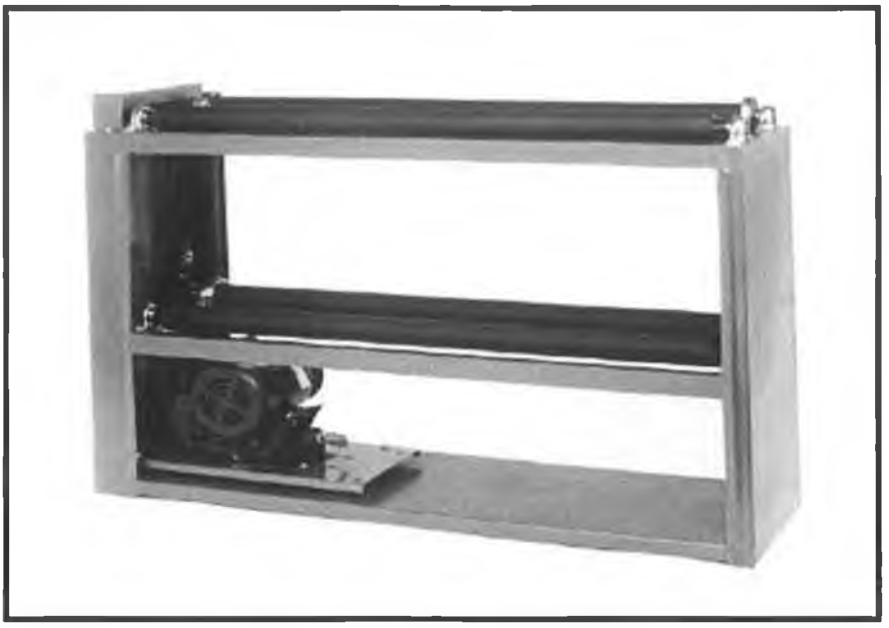

Figure 3.1 Conventional ball milling [27].

3.2.2 Jar mills

A 120 g of the formulated alumina powder was processed in a cylindrical jar with a capacity of 2.0 liters. Powder processing was accomplished using 480 g alumina balls (24 mm diameter) at a ball-to powder weight ratio of approximately 1:4. As shown in Figure 3.2, these mills have an alumina content of 85-90% with the remainder being silica.

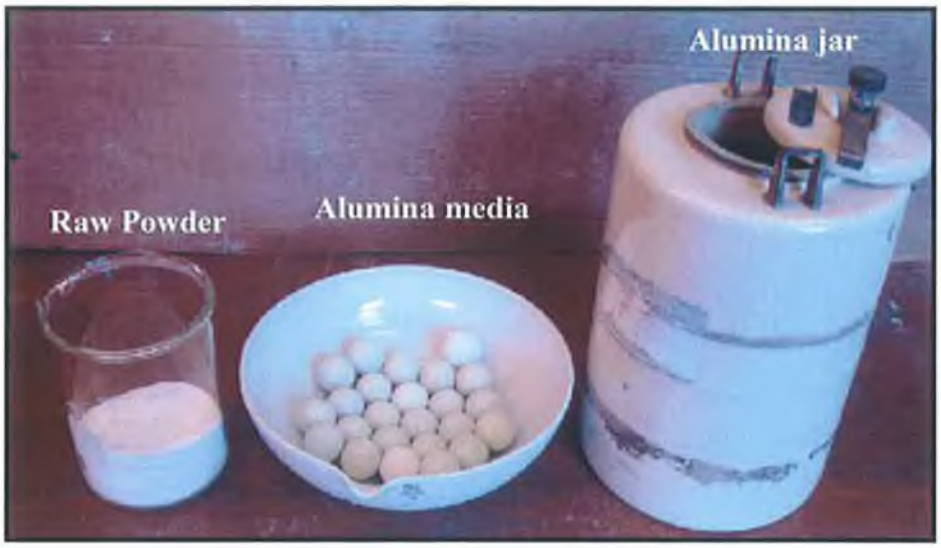

Figure 3.2 The alumina jar mill.

After ball milling, the alumina-zirconia powder was milled using a Netzsch attrition mill (Netzsch Ltd. Germany.) as shown in Figure 3.3. The mill contained an alumina grinding tank. The 120g of alumina powder was dispersed in 180 ml of propan-2-ol, and 360 g of 0.5 mm MgO-stabilised ZrO_2 media was added to the mixture, at a ball-to powder weight ratio of approximately 3:1. The milling speed was 2300 rpm for 1 hour. After attrition milling, the samples were dried in a drying oven for 30 minutes at 120 °C. The flowchart of this process is shown in Figure 3.4.

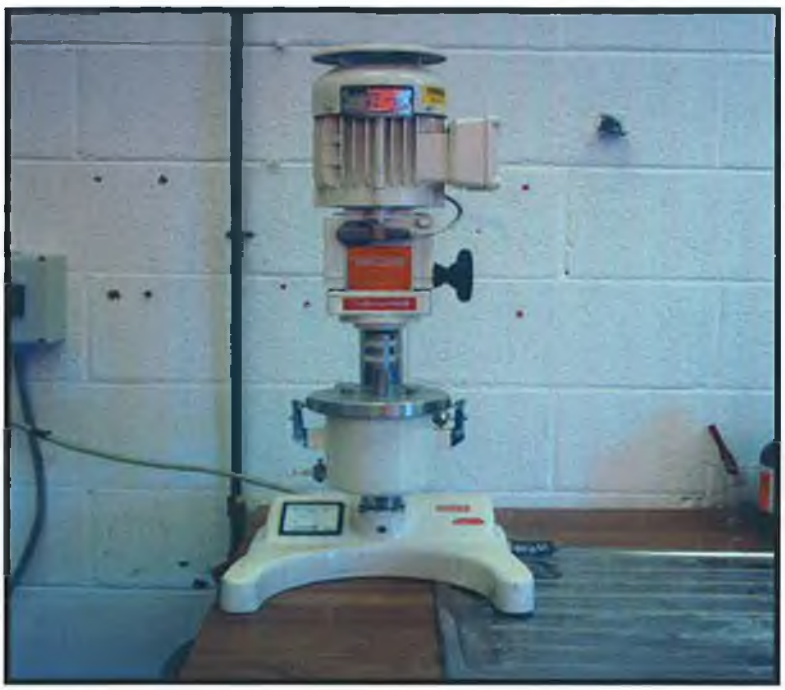

Figure 3.3 The Netzsch attrition milling equipment.

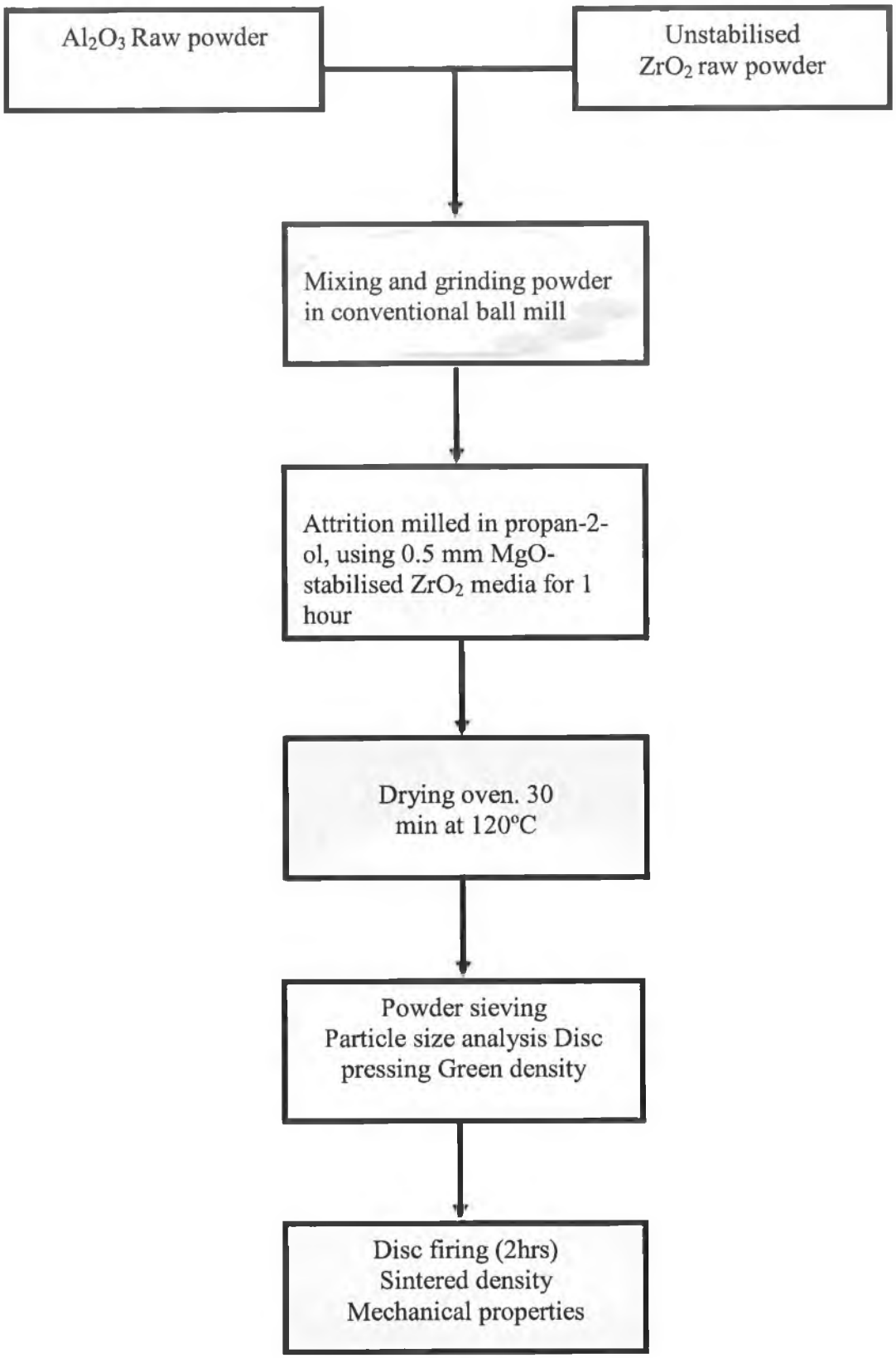

Figure 3.4 Powder processing diagram for preparing (Al_2O_3-ZrO_2).

3.2.3 Colloidal method

A 120 g amount of alumina powder was added to 300 ml of absolute ethyl alcohol (EtOH). Zirconium propoxide solution (Sigma-Aldrich) was added, to the mixture, dropwise from a pipette. The suspension was heated to 60 °C on a hotplate and magnetically stirred for 30 minutes as shown in Figure 3.4.

The acidity of the suspension was monitored using a pH meter (Hanna-Italia) and the acidity adjusted by additions of approximately 25 ml of glacial acetic acid. The suspension was transferred to evaporating dishes and dried for 30 minutes at 120 °C. The resultant powder was subjected to a thermal treatment at 850 °C for 2 hours, in order to eliminate most of the organic components [28], using a muffle furnace (Lenton, Ltd, England). The powder was then attrition milled using the same conditions as for the conventionally processed powders. Finally the powder was sieved through a 45 μm sieve. The flowchart describing this method is shown in Figure 3.6.

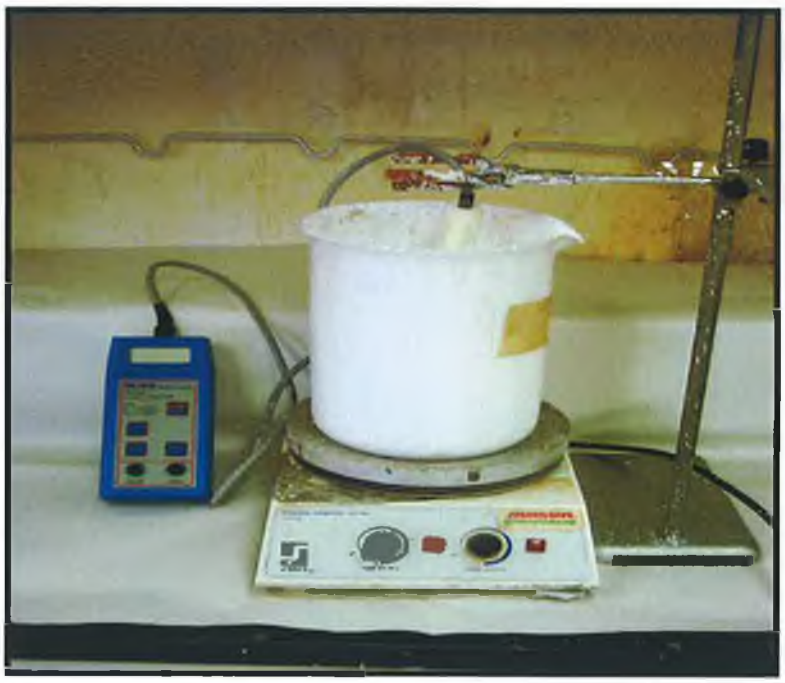

Figure 3.5: The colloidal process setup.

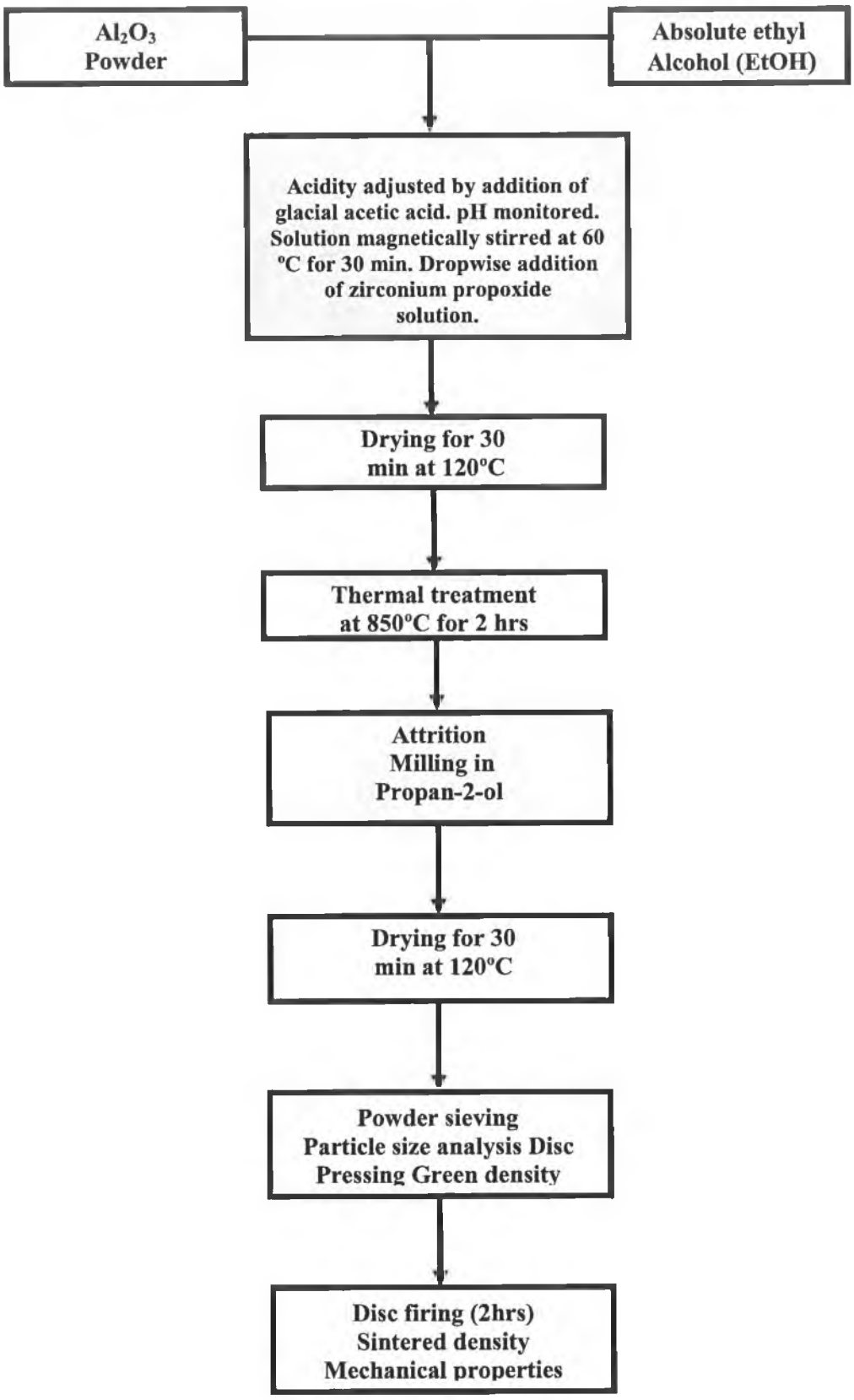

Figure 3.6 Colloidal processing diagrams for preparing (Al_2O_3-ZrO_2).

3.2.4 Sedimentation measurement

The stability of the suspension was reflected in its sedimentation behaviour. A graduated cylinder was filled with suspension and the settling speed of the particles was measured (in seconds). A ruler was used for measuring the distance traveled by the settling particles (in mm) as shown in Figure 3.7.

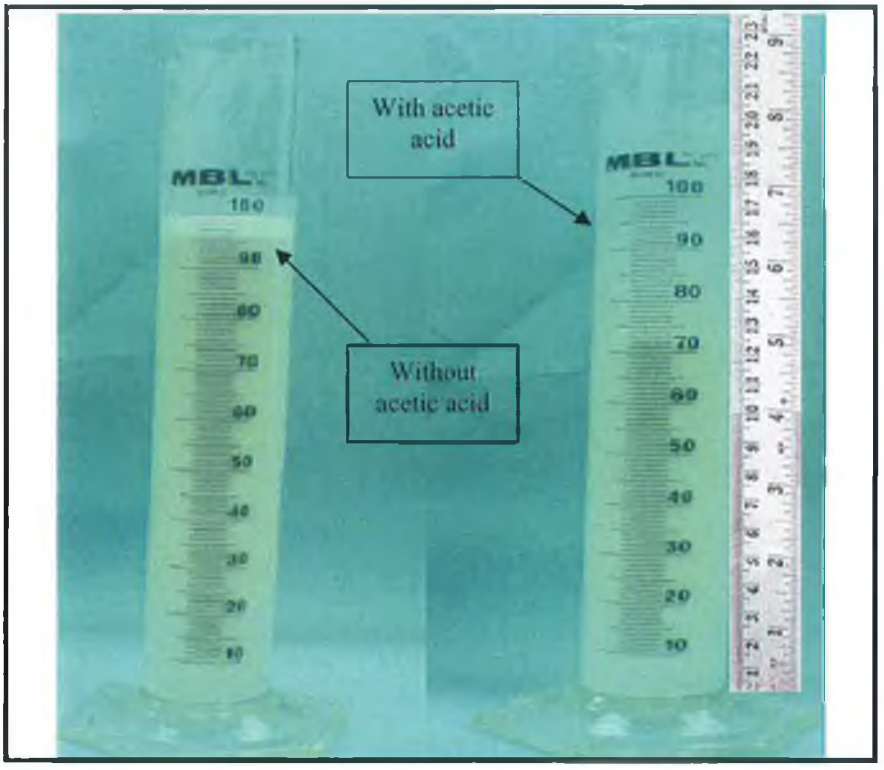

Figure 3.7 Sedimentation measurement of the settling speed of the colloidal suspension.

3.3 Powder compaction tool

A steel die set was used to produce discs of 26 mm in diameter with different thicknesses. Figure 3.8 shows an assembly of the die and the punch.

To facilitate compaction, graphite powder was used to lubricate the die walls in between processing time.

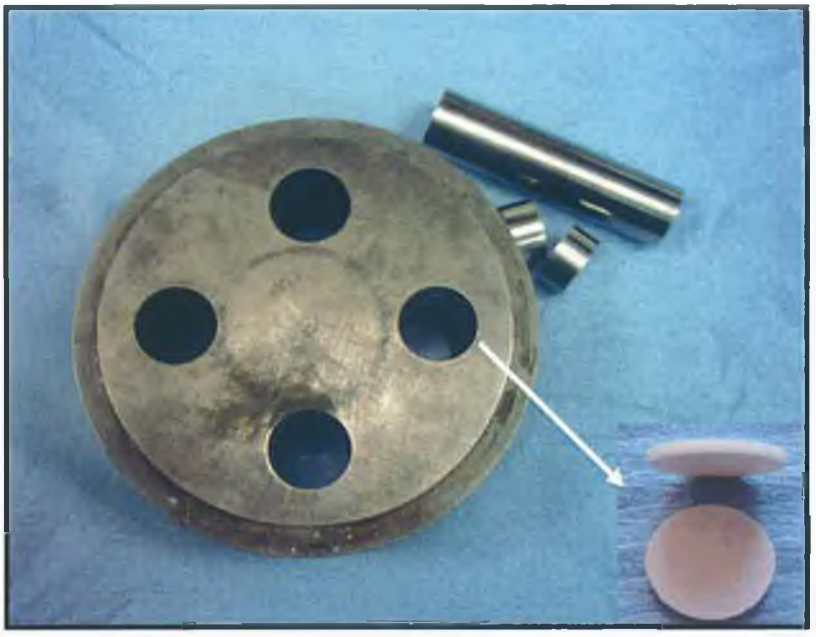

Figure 3.8 The compaction steel die and punch.

3.4 Powder pressing

A uniaxial press (Moore & Son, Birmingham, UK) with a maximum load of 50 tonnes was used to press the discs. A powder quantity of approximately 3 g was added to a 26 mm diameter steel die to make individual discs. A load of 20 $kg.cm^{-2}$ was applied for 20 s. Graphite powder was routinely used to lubricate the die in between pressing. The powder press is shown in Figure 3.9.

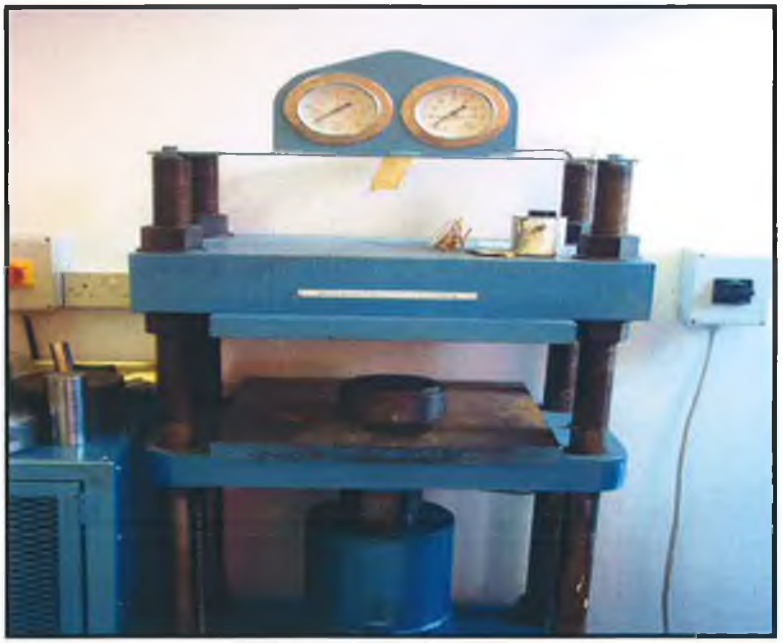

Figure 3.9 Uniaxial press (Moore & Son, Birmingham, UK)

3.5 Sintering furnace

The pressed powder discs were then sintered in a horizontal tube furnace (Carbolite, Sheffield, UK) shown in Figure 3.10. The maximum operation temperature of this furnace is 1600 °C. The furnace was calibrated before performing the sintering operations, see Table of Appendix A for the calibration data.

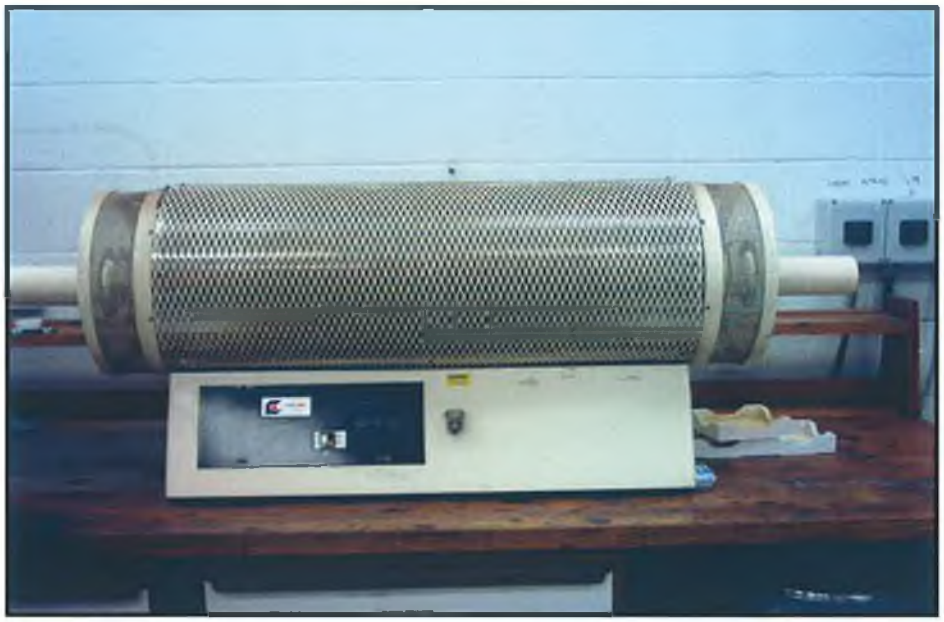

Figure 3.10 Horizontal Tube furnaces (Carbolite, Sheffield, UK)

From Figure 3.11 the samples' temperature was ramped from room temperature to 1550°C in air, using a ramp rate of 10°C per min. The temperature was held at 1550°C for 2 hours and then ramped down to room temperature using a ramp rate of 20°C per min. The sintering temperature was selected based on the works done by Liu et al. [29].

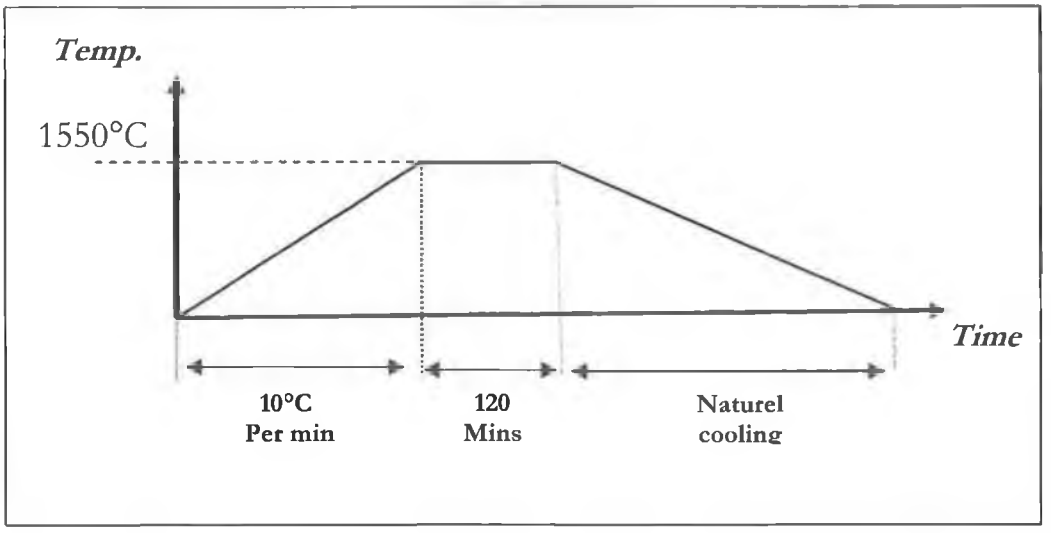

Figure 3.11 The temperature sintering profile of the powder samples.

3.6 Density measurement

The geometry of the discs was measured using vernier callipers. The thickness and the diameter were measured to an accuracy of 0.01mm. The mass was measured to an accuracy of 0.1 mg. The sample density, for example the ratio mass/volume, was thus calculated. The same approach was employed for the sintered samples. To increase the accuracy of measurements, the average values of two diameter measurements and four thickness measurements were used to calculate the densities.

The density of each disc was also measured using a large volume helium Pycnometer (Accupyc 1330, Micromeritics, UK). Since helium, which can enter even the smallest voids or pores, is used to measure the volume per unit weight, the final result is often referred to as skeletal density. The instrument determines the skeletal density and volume of a sample by measuring the pressure change of helium in a calibrated volume. The equipment is shown in Figure 3.12. The mean value and the standard deviation were determined from five successive density measurements.

Figure 3.12 The Micromeritics helium pycnometry equipment.

3.7 Particle size analysis

Particle size was investigated using laser diffraction based particle size analysis (Mastersizer S, Malvern Ltd. UK). Mastersizer S is a modular instrument designed for the measurement of the particle size distribution of wet and dry samples.

Small quantities, around (3-5 g), of the powder were added to a solution of (50 ml) water and (5 ml) of Calgon dispersant. The beaker, containing the mixture, was placed in an ultrasonic bath for 15 minutes. This suspension was then added, dropwise, to the sample dispersion unit. The sample dispersion unit pumped the sample through the sample cell. The particle size analyzer is shown in Figure 3.13.

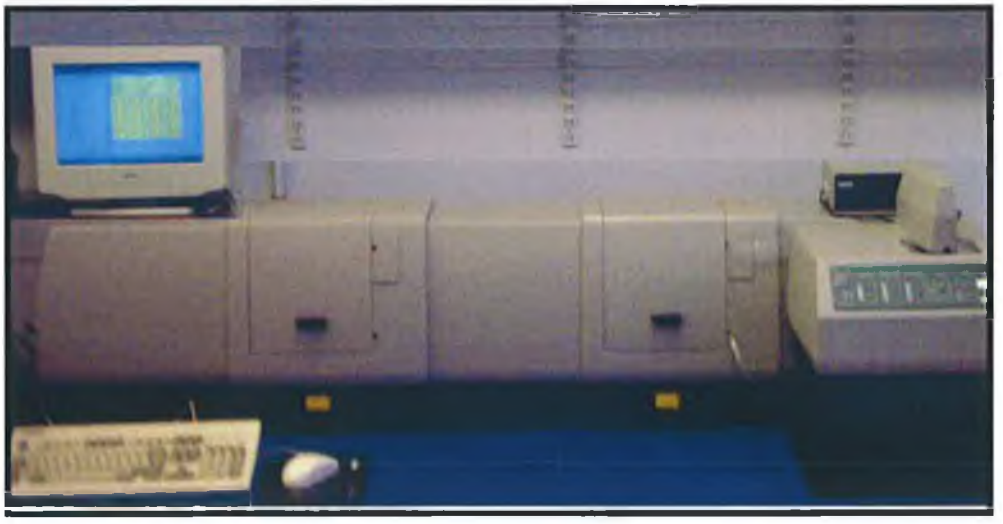

Figure 3.13 The particle size analyzer (Malvern mastersizer).

3.8 Grinding and polishing

The samples were mounted in bakelite, using a hot-compression mounting procedure A Buehler Simplimet 2000. Hot-compression mounting involves setting a sample in a thermoplastic or thermosetting resin, subjected to an elevated temperature (from 140 to 200°C) and high pressures (from 20 to 40MPa) for 7 to 10 minutes. As shown in Figure 3.14. The operating parameters used are listed in Table 3.1.

Figure 3.14 The Mounting Press (Buehler Simplimet 2000) [33].

Table 3.1 The operating parameters used in the mounting process.

Equipment	Buehler Simplimet 2000 Mounting Press
Resin	Brown Bakelite Thermosetting Resin
Temperature	Hot 150°C and Cold 15°C
Time	11 minutes hot followed by 4 minutes cold
Pressure	290lbs psi

In this stage of the metallographic preparation process, automation of the grinding and polishing techniques is essential. Automation of the grinding cycle eliminates operation errors such as; applied force, rotation per minute and dosing (delivery of liquid abrasive solution).The grinding and polishing were performed using a grinding and polishing wheel (Buehler, Motopol 2000) see figure 3.15.

Silicon carbide paper of 600 grit was used for 1 minute, and then another silicon carbide paper of 1200 grit was for 1 minute. The samples were then polished using a napless paper (DP-Cloth, Struers, Denmark) with water-based diamond suspensions, in successive grades, of 30 μm, 9 μm, 6 μm, 3 μm and 1 μm for 1 minute. Fine polishing was performed using a napped cloth (Mastertex) with 0.05μm colloidal silica slurry for 3 minutes [30, 31, and 32]. The grinding wheel speed was 200 rpm and the platen pressure was 20 N in each step.

Figure 3.15 The Buehler Motopol 2000 Semi-Automatic Specimen Preparation unit. [33]

3.9 Hardness measurement

Vickers hardness tests were carried out at University College Dublin (UCD). Figure 3.16 shows the Vickers tester used for the hardness measurements. The tester is equipped with a standard diamond indenter [34]. Hardness measurements were taken under two different loads of 10 kg and 20 kg. To increase the accuracy, five measurements were taken for each load and the average was calculated.

Figure 3.16 The Vickers hardness tester.

Figure 3.17 shows the schematic of the indentation, the two diagonals, d_1 and d_2 of the indentation left in the surface of the material after the removal of the load were measured using the ocular on the hardness tester and their means calculated [35].

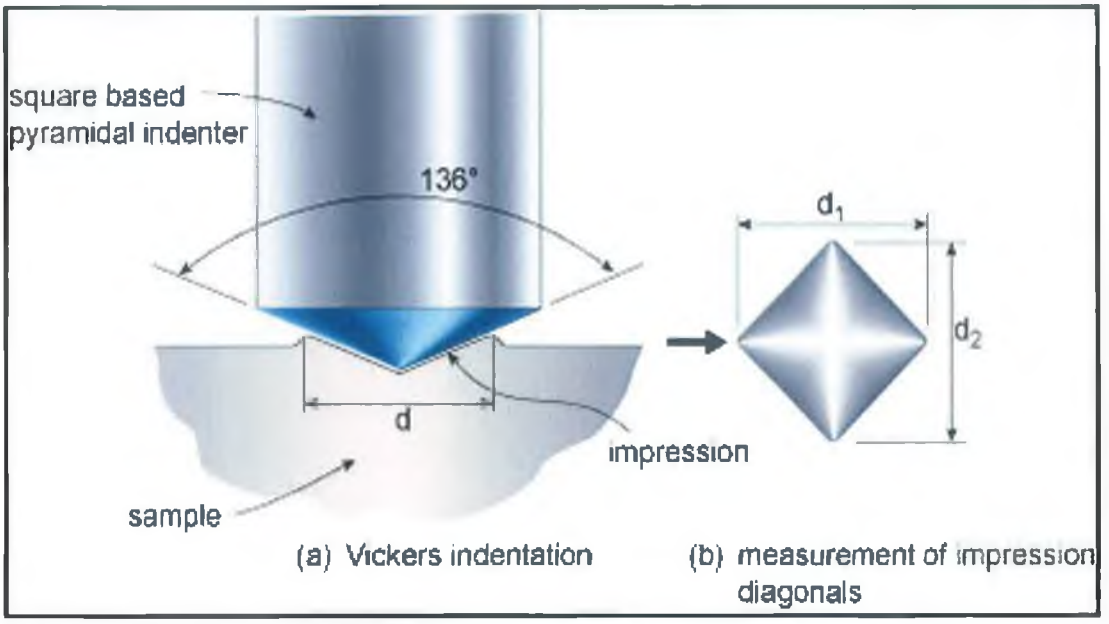

Figure 3.17 the schematic of the indentation [36].

The Vickers hardness was measured using the following formula.

$$Hv = \frac{2F\sin\frac{136^{\circ}}{2}}{d^2} \approx 1.854\frac{F}{d^2} \tag{3.1}$$

Where:

H_V: is the Vickers hardness in ($kgf.mm^{-2}$)

F: is the load in (kg-force)

d: is the arithmetic mean of two diagonals, d_1 and d_2 in (mm)

The utilisation of equation 3.1 to calculate the hardness was performed in the Microsoft Excel™ software. The spreadsheets containing all the measurements and the calculated values are listed in the Appendix B.

3.10 Fracture toughness

The fracture toughness was determined by two methods. The first method was performed by measuring the radial crack length and substituting its value into the Lawn and Wilshaw equation [37]. This gave the fracture toughness value according to this formula [35].

$$K_{c,idt} = \psi_b \left(\frac{P}{C_0^{\frac{3}{2}}} \right) \tag{3.2}$$

Where:

$K_{c,idt}$: is the fracture toughness (GPa)

ψ_b : is the half angle of Vickers indenter (68°)

P: is the indentation load in (MN)

C_O: is the radial crack length (m)

The second method was performed by calculating $K_{c,\ idt}$, using the hardness and the Young's modulus values, following equation 3.3, as done in the works of Anstis et al. [38]. The $K_{c,\ idt}$ values obtained from this equation was compared to the values derived from equation 3.2.

$$K_{c,idt} = 0.016 \left(\frac{E}{H} \right)^{\frac{1}{2}} \frac{P}{c_0^{\frac{3}{2}}} \tag{3.3}$$

Where:

E: is the Young's modulus in (GPa)

H: is the hardness in (GPA)

The calculated fracture toughness values obtained from the above mentioned methods were performed in the Microsoft Excel™ software. The spreadsheets containing all the measurements and the calculated values are listed in the Appendix C. Some sample fracture toughness calculations are listed in Table 4.2.

3.11 Young's modulus testing

A steel die was designed for making rectangular ceramic bars of (45×19×2.5 mm) dimensions that were then uniaxially pressed and sintered. The design of the die components is shown in Appendix E. In order to calibrate the measuring method, aluminium and steel bars of (60×19×3 mm) were tested as reference materials. The average Young's modului of these metals were calculated and found to be 66.4 GPa and 196 GPa for aluminum and steel, respectively. These calculated values were compared with the standrad Young's modulus values for these matels, which are 70 GPa and 200 GPa for aluminum and steel, repectively [39]. Two modes of vibration were used in this test, flexural and torsional. Flexural tests were conducted with the sample resting on a foam mat as shown in Figure 3.18. These samples were situated at 0.224L from both ends. The piezoelectric detector was held in contact with the sample at the centre of the side face. The top of each bar was struck at its central point using a thin plastic rod [40].

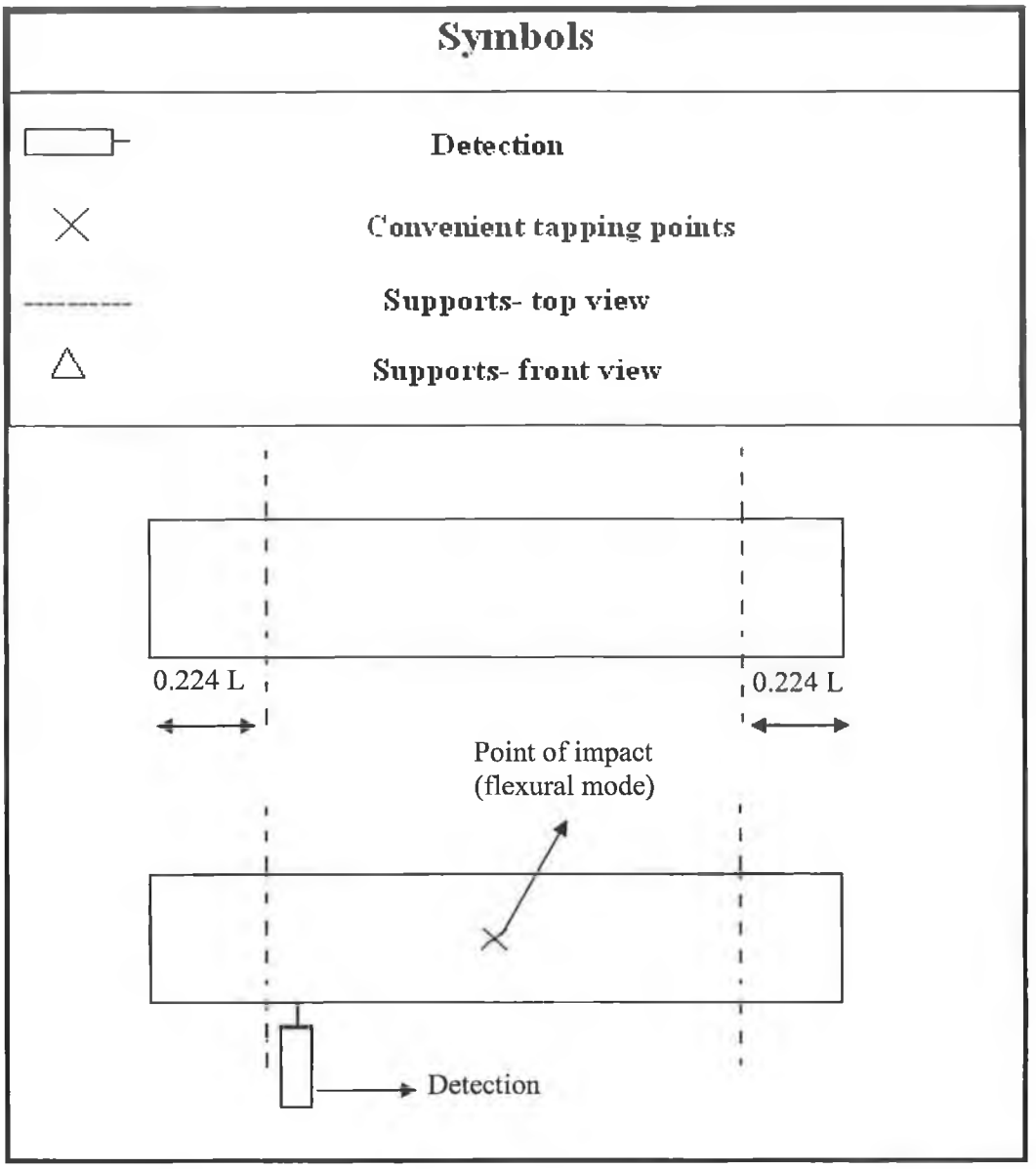

Figure 3.18 The sample arrangements for Young's modulus testing.

Figure 3.19 shows the torsional testing configuration used. By tapping the corner of the sample with a small mallet and sensing the vibration with the probe, the readings were obtained quickly. Changing the probe placement, operator and tapping strength caused extremely low variations in readout [41].

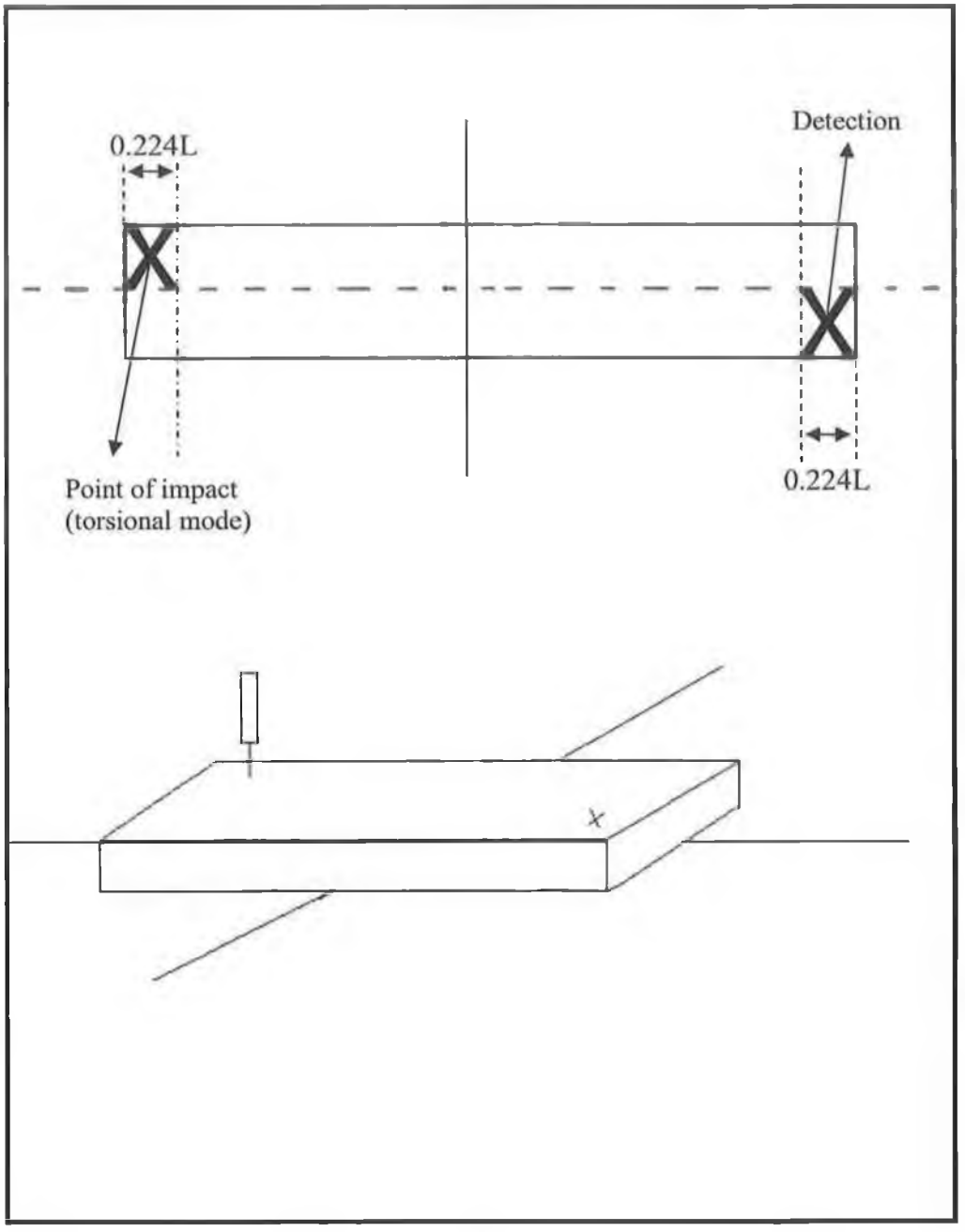

Figure 3.19 The configuration of torsional vibration measurements.

The impulse excitation frequency tester (Lemmens Electronika Grindosonic) used to measure the resonant frequency via a microphone is shown in Figure 3.20.

Figure 3.20 The impulse excitation frequency tester (Grindosonic Modulus Tester).

The measured frequency, along with the length, the thickness, and the density of the sample were used in equation 3.4 to calculate Young's modulus [41].

$$E = \frac{0.94642 \quad \rho L^4 f^2 T}{t^2} \tag{3.4}$$

Where:

ρ: is the density in (kg/m^3)

L: is the specimen length in (m)

***f*:** is the frequency in (Hz)

T: is the shape factor (dependent on Poisson's ratio)

t: is the specimen thickness in (m)

Theoretical values of Young's modulus were also determined for comparison purposes using a rule of mixtures [6], and described by the following relation.

$$E = E_1 f_1 + E_2 f_2 \tag{3.5}$$

Where:

E_1 and E_2 are the Young's modulus values of material 1and material 2 respectively

f_1 and f_2 are the volume fractions of material 1 and material 2 respectively

$$f_1 = \frac{m_a}{\rho_a} \Bigg/ \left(\frac{m_a}{\rho_a} + \frac{m_b}{\rho_b} \right) \tag{3.6}$$

Where:

m: is the mass in (g)

ρ: is the density in (g/cm^3)

m_a and m_b are the mass values of material 1 and material 2 respectively (g)

p_a and p_b are the density values of material 1 and material 2 respectively in (g/cm^3)

Young's modulus values described in the above mentioned equations were calculated in the Microsoft Excel™ software. The spreadsheets containing all the measurements and the calculated values are listed in Appendix D.

3.12 Dilatometer test

A steel die set was used to produce bars of (10×5×3 mm) dimensions. Figure 3.21 shows an assembly of the die and the punch. (Die lubrication was carried out at regular intervals by cleaning with graphite powder).

Firgure3.21 The steel die set used for the dilatometer test.

A high temperature dilatometer was used to measure the sintering shrinkage properties of the ceramics. The dilatometer used was a Dil 402 PC (Netzsch) horizontal pushrod type with a temperature range of 25 to 1600°C, see figure 3.22. Bars measuring (10×5× 3 mm) were pressed using a pressure of 20 kg/cm^2 for 20 s. These were then sintered using a constant heating rate of 3 °C/min , when the temperature reached 1600 °C, the sample were held for 2 hours. Then the samples were naturally cooled in air to room temperature [42].

Figure 3.22 The dilatometer system used for thermal treatment.

3.13 Scanning electronic microscopy (SEM)

Polished samples were preliminarily thermally etched in air atmosphere at 1450°C for 30 min, with heating rates of 10 °C/min. A scanning electron microscope (JEOL Ltd) was used to observe the polished and the fracture surfaces of the sintered samples (in backscatter mode). The SEM system used is shown in Figure 3.23.

Figure 3.23 Scanning electronic microscopy system.

CHAPTER FOUR
RESULTS AND DISCUSSION

CHAPTER FOUR
RESULTS AND DISCUSSION

4.0 Introduction

In this chapter, the densification and the mechanical properties of the alumina-zirconia composites prepared by colloidal process and conventional mixing process are discussed. The results were obtained from experiments following the procedures which have been described in Chapter 3.

4.1 Particle size distribution

Traditionally, the addition of zirconia to alumina has been carried out via conventional powder processing. Recently, attention has shifted towards the use of chemical precursors to achieve fine grained microstructures and inhibit the potential for aggregate formation.

The first stage of this work involved powder processing. Particle size analysis of raw alumina and zirconia powders showed bi-modal distributions for both powders. It can be seen from Figure 4.1 that the average particle size of alumina was approximately 1μm whereas the average particle size of zirconia was 2-3 μm. Zirconia showed a prominent broad peak at 2 μm, with evidence of particles sizes >10 μm. The alumina raw powder also showed a peak for particles sizes of about 10 μm.

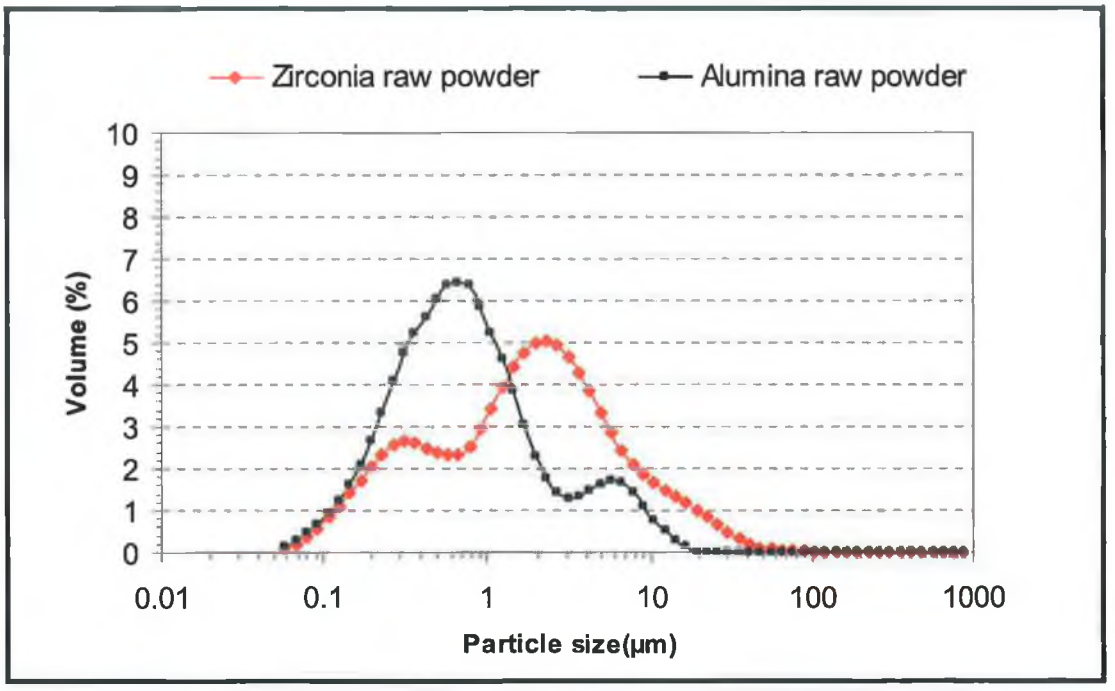

Figure 4.1 The particle sizes of the raw alumina and zirconia powders used.

Ball milling was effective in breaking down the largest particles. However, for further particle size reduction, attrition milling proved to be effective using 0.5 mm diameter MgO-stabilized ZrO_2 ball media was used. More experiments were carried out using different quantities of solution, grinding media, powder and milling speeds to establish optimum conditions. It was found that a high mill speed (in excess of 1050 rpm) and a media/powder ratio ≥ 3 were necessary to achieve efficient milling of 120 g quantities of the powder. These conditions and their effects are illustrated in Figure 4.2.

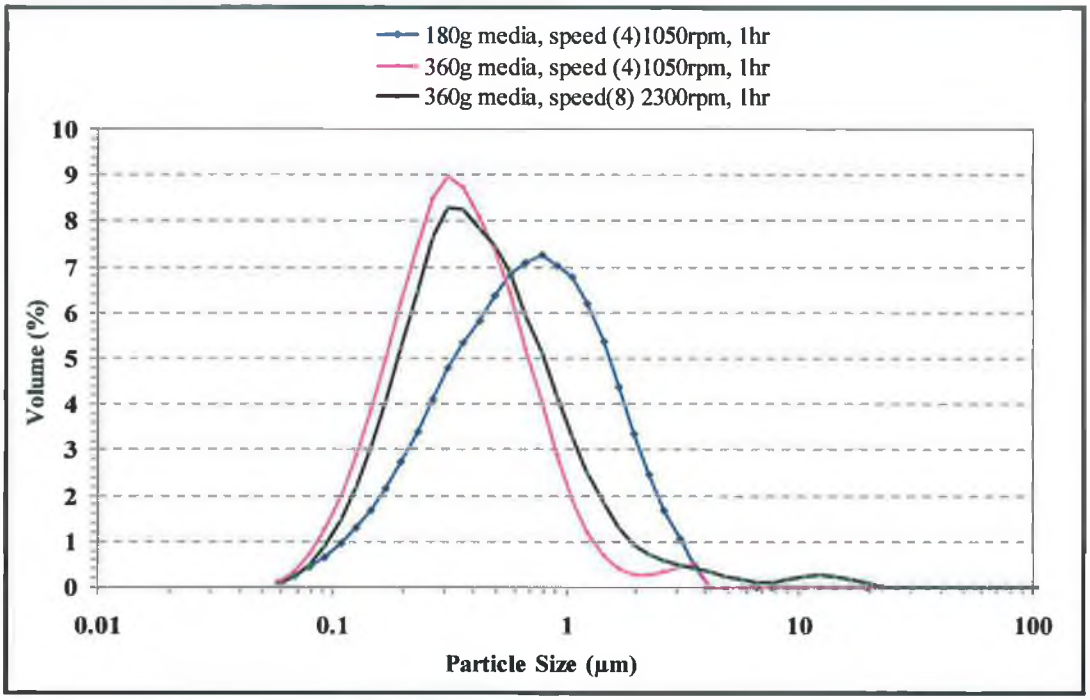

Figure 4.2 The effect of attrition milling conditions on particle size.

Using the milling conditions established in the previous trials, it was possible to reduce the particle size for both methods.

Figure 4.3 shows the particle sizes of both powder, processed and colloidally processed Al_2O_3-20% ZrO_2. It can be seen that no particles greater than 10um exist after attrition milling. The distributions of the powder processed and colloidal processed Al_2O_3-ZrO_2 are similar, see Figure 4.3. An explanation for this is that the zirconia propoxide is coating the Al_2O_3 particles, as opposed to forming individual nm-scale particles of ZrO_2.

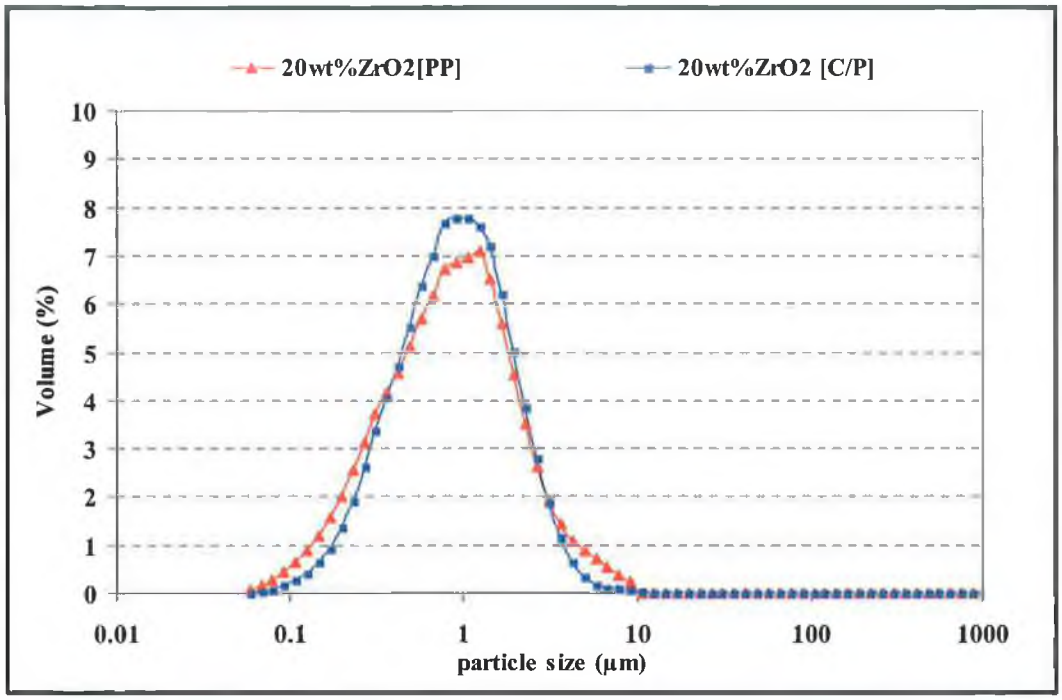

Figure 4.3 Comparison of the particle size distributions of Al_2O_3-20wt%ZrO_2 powder produced by colloidal and traditional powder processing.

4.2 Zirconium propoxide

To make colloidally processed samples, zirconium (IV) propoxide, $Zr(OCH_2CH_2CH_3)_4$ was added as a solution to alumina powder dispersed in EtOH. From the information supplied by the manufacturer, it was known that the zirconium propoxide contained 70wt% solution in 1-propanol, or that 100 ml of zirconium propoxide contained 70 g of $Zr(OCH_2CH_2CH_3)_4$. Through calculation, it was found the relationship between the quantity of the solution and the resulting quantity of pure ZrO_2 on removal of the organics by heating.

This was calculated by considering the atomic masses of the individual elements as follows:

$Zr\ (OCH_2\ CH_2\ CH_3)_4$

Can be also expressed as:

$Zr\ O_4\ C_{12}\ H_{28}$

In terms of the atomic mass, this can be expressed as:

$$91.11 + (15.999 \times 4) + (12.01115 \times 12) + (1.00797 \times 28)$$

$= 327.57456\ g = 327.58\ g$ (4.1)

Upon heating, the solution was decomposing and gives off CO_2 and H_2O. The following is the balanced equation for this reaction.

$$Zr\ (O\ CH_2\ CH_2\ CH_3)_4 + 18O_2 \longrightarrow ZrO_2 + 12CO_2 + 14H_2O \quad (4.2)$$

On the right hand side of this equation, only ZrO_2 will remain as a solid. In terms of the atomic mass, this can be expressed as:

$$327.58\ g \longrightarrow 123.22\ g \quad (4.3)$$

As it was stated above, 100 ml of the solution contains 70 g of $Zr(OCH_2CH_2CH_3)_4$. Therefore, 100 ml of the solution contains:

$70 \times (123.22/327.58)$ g of solid ZrO_2

$= 26.33$ g of solid ZrO_2

Based on the previous result, it can be calculated that a compound made up of 100 g of alumina and 5% ZrO_2 will require:

$5 \times 100/26.33 = 18.98$ ml of zirconium propoxide solution

Similarly, a compound made up of 100 g of alumina and 10% ZrO_2 was requiring:

$10 \times 100/26.33 = 37.97$ ml of zirconium propoxide solution

And, a compound made up of 100 g of alumina and 20% ZrO_2 was required

$20 \times 100/26.33 = 75.95$ ml of zirconium propoxide solution

In order to verify these calculations, 37.97 ml of zirconium propoxide was heated in a furnace in 850 °C. It was anticipated that the 37.97 ml of zirconium propoxide would yield approximately 10g of ZrO_2. To verify this, the 37.97 ml of zirconium propoxide was heat-treated at 850°C and the yielded ZrO_2 powder mass measured 10.50 g. This was deemed satisfactory in terms of validating the calculations outlined above.

No nanometer size powder resulted from the ZrO_2 powder extracted in this exercise. From Figure 4.4 it can be seen that the zirconia powder extracted from the zirconium propoxide after the heat-treatment at 850°C had an average particle size of approximately 25 μm. This is large compared to the particle size of attrition milled

zirconia which was 1-3 μm. Zirconia showed a prominent broad peak at 12 μm, with evidence of particle sizes 10 μm.

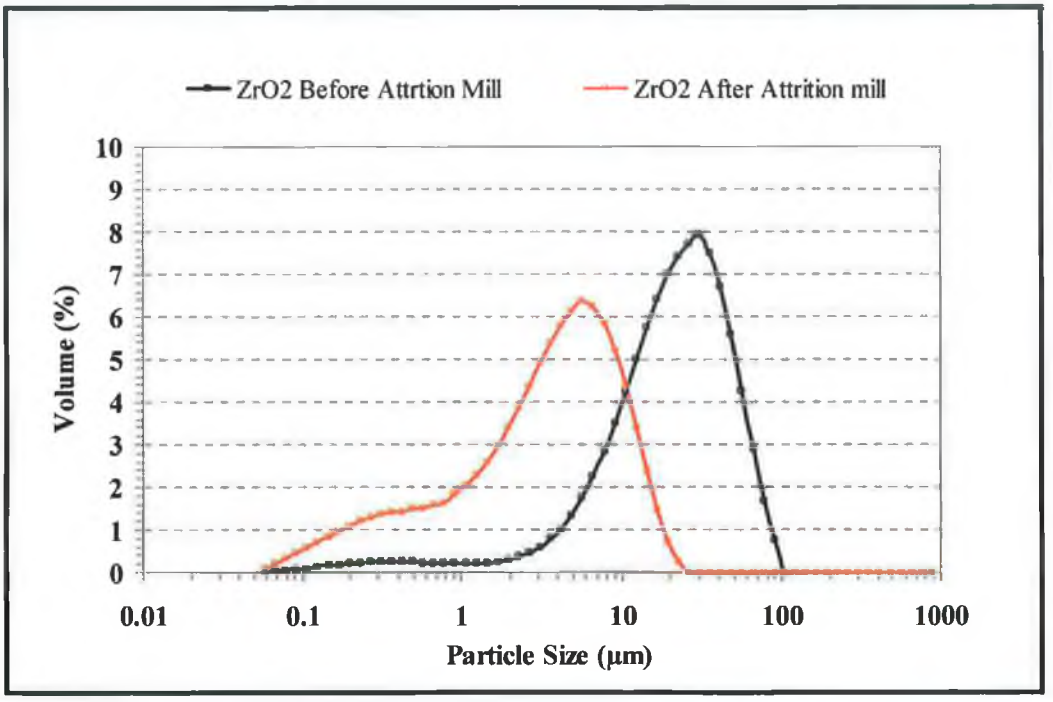

Figure 4.4 The particle size vs. volume (%) of pure zirconia propoxide before and after attrition milling.

4.3 Stability of suspension

During the colloidal suspension, it was necessary to add glacial acetic acid to the alumina and EtOH in order to create a stable alumina suspension [24]. By adding the acetic acid, a repulsive force was set up between the alumina particles. This stabilised the pH of the alumina suspension and allowed the ZrO_2 solution to enter between the alumina particles, resulting in a homogeneous mixture. Figure 4.5 shows the operational pH recorded as a function of time. After 90 minutes, the pH of the suspension containing the CH_3COOH had become stable whereas the pH of the suspension without CH_3COOH had remained fluctuating.

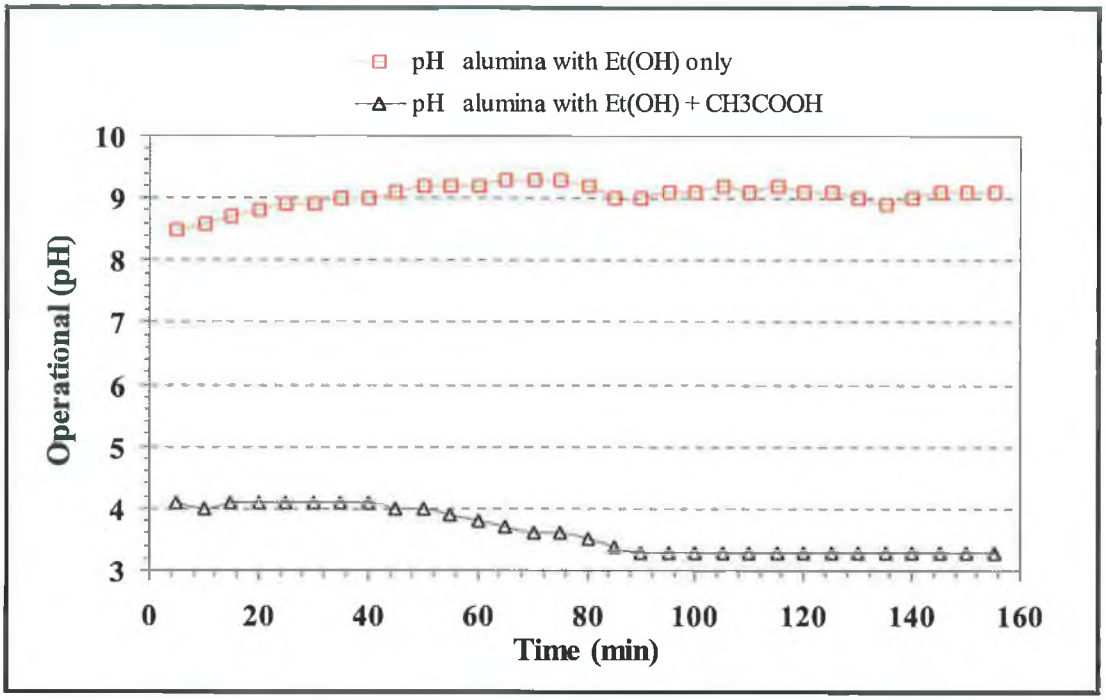

Figure 4.5 Colloidal process: pH stability of solution after addition of ZrO_2 propoxide (non-aqueous).

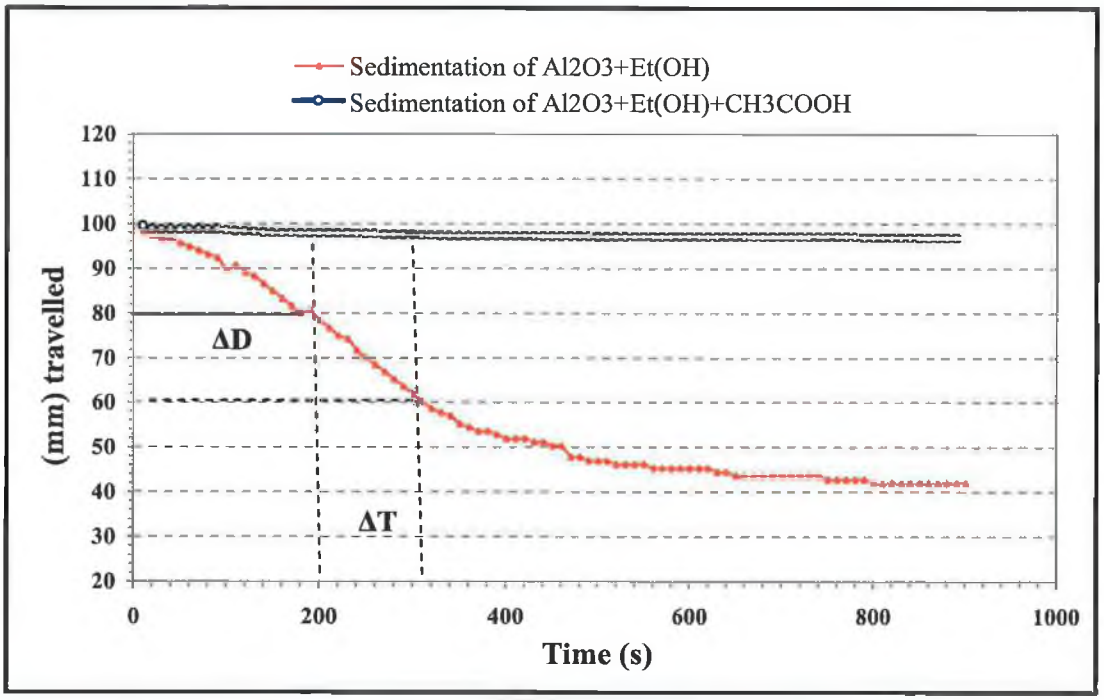

Figure 4.6 Sedimentation rates (in a graduated cylinder) of Al_2O_3+Et (OH) suspensions.

In previous study, Wang et al. [24] investigated EtOH solutions modified with glacial acetic acid, as shown previously in Figure 2.8. It has been found that measured operational pH as a function of time for four solutions of varying pH. In general the results obtained by Wang et al. [24] are in good agreement with those obtained in this work. In Wang's study, a processing time of 0.5-1 hour was required to obtain stable pH readings. This time period is slightly shorter then the time which was found to be required in the work undertake in this study, in which a stable solution was only observed after 1.5 hours. Wang et al. [24] attribute this long processing time to the slow response of pH electrodes, and it is likely that a similar phenomenon is occurring here. This possibility is strengthened by the almost immediate stability observed in Figure 4.6 where there is no depending on pH electrodes. In Wang study identified an isoelectric point for alumina particle suspended in EtOH at pH= 7.1. These results suggest there is an acidity dependent surface charge on the alumina particles that are suspended in EtOH.
According to Wang et al. [24] from the figures of Figure 4.5, Figure 4.6 it is clear that this is indeed the case.

The stability of the suspension was reflected in its sedimentation behaviour. Two graduated cylinders were filled separately with the same suspensions described above and the settling behaviour of the particles was monitored. The observation is shown in Figure 4.6. As can be seen, the suspension containing CH_3COOH additions remained stable, over time where as the sedimentation rate of the suspension without CH_3COOH was much faster, illustrating the instability of this solution. It is important that the suspension be stable when making the addition of ZrO_2 propoxide, otherwise it will not mix properly resulting in a non-homogeneous distribution of ZrO_2 particles, and aggregate formation.

4.4 Stokes's law

During the colloidal process, the particle size of the suspension was calculated using Stokes's law [43]. This law expresses the particle size distribution of the powder in terms of its speed of sedimentation in a liquid. Generally in liquids the larger the particles size the faster the sedimentation. By investigating Figure 4.6, the free-settling velocity of the particles can be calculated from the following equation:

$$Vt\ (m/s) = (\Delta d / \Delta t) \quad (4.4)$$

Where:

Δd: is the linear region of (Y) travelling distance.

Δt: is the linear region of (X) time.

With reference to Figure 4.6, a method of velocity calculation for both alumina-ethanol and alumina-ethanol-acetic acid was applied. The linear section selected covered the range of 200 up to 310 seconds which corresponds to a particle travelling distance of 78.375 to 60.225 mm for the alumina-ethanol suspension. The same range of time is used in the case of alumina-ethanol-acetic acid corresponding to a particle travelling distance of 97.85 to 97.355 mm.

The free-settling velocity calculation of the suspension without acetic acid in the selected linear region:

$$Vt = (78.375 - 60.225) / (310 - 200) = 0.165\ mm/s \quad (4.5)$$
$$= 0.000165\ m/s$$

The free-settling velocity calculation of the suspension with acetic acid in the selected linear region:

$$Vt = (97.85 - 97.355) / (310 - 200) = 0.0045\ mm/s \quad (4.6)$$
$$= 0.0000045\ m/s$$

From the previous calculations, the partial free-settling velocity Vt of the suspensions, alumina-ethanol and alumina-ethanol-acetic acid has been obtained.
Particle diameter can be calculated by rearranging Stokes's law [41] to solve for ***d***, as follows:

$$d = \sqrt{\frac{18\ \mu v_t}{g\ (\rho_p - \rho_m)}} \qquad (4.7)$$

Where:

μ: is the fluid viscosity of 100% ethanol = 1.22 g/m.s

g: is the local acceleration due to gravity = 9.81 m/s^2

ρ_p: is the density of alumina particle = 3989000 g/m^3

ρ_m**:** is the density of the surrounding fluid in, for ethanol = 789000 g/m^3

The particle diameter calculation for the suspension of alumina-ethanol without acetic acid, using the density of surrounding fluid of ethanol:

$$d = \sqrt{\frac{18 \times 1.22 \times 0.000165}{9.81(3989000 - 789000)}} \times 10^6\ \mu m / m = 10.74 \mu m$$

therefor the suspension with no acetic acid shows a particle size of 10.74 μm. The particle diameter calculation during the suspension of alumina-ethanol with acetic acid, using a rule of mixtures to calculate the density of a solution of ethanol and acetic acid:

μ: is the fluid viscosity of 90% ethanol and 10% acetic = 1.217 g/m.s

ρ_m**:** is the density of the surrounding fluid in, for ethanol and acitic acid = 815000 g/m^3.

$$d = \sqrt{\frac{18 \times 1.217 \times 0.0000045}{9.81(3989000 - 815000)}} \times 10^6\ \mu m / m = 1.77 \mu m$$

It has been found that the suspension with acetic acid shows a particle size of 1.77 μm.

Obscuration of the (Alumina\absolute ethanol\acetic acid), using laser diffraction based on particle size analysis (Mastersizer S, Malvern Ltd. UK), as shown in Figure 4.7. From Figure 4.8, it can be observed that the process of obscuration of Alumina-absolute ethanol and CH_3COOH with time was slow compared with alumina-H_3COOH suspension; the obscuration rate was much faster. Result of graduated cylinders coincides with the results obtained by obscuration.

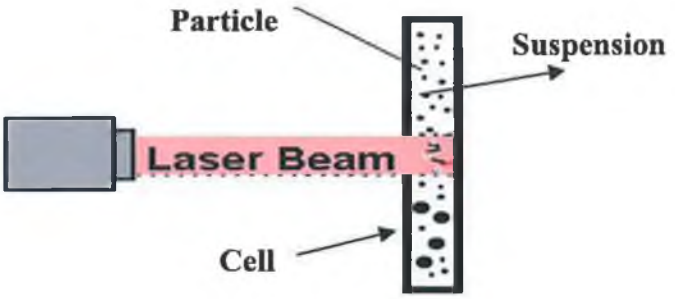

Figure 4.7 Obscuration diagram

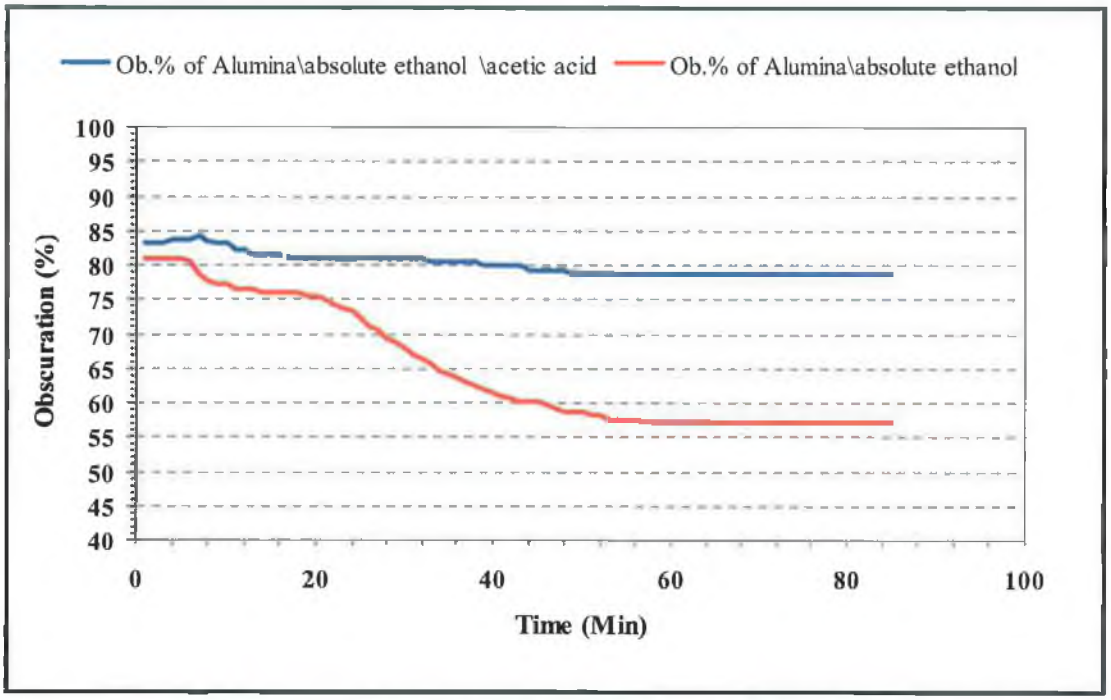

Figure 4.8 Time vs. obscuration of (Alumina\absolute ethanol\acetic acid).

4.5 Density

The sintering and the densification behaviour of the composite powders prepared by powder and colloidal methods were investigated. Disc samples have been prepared by pressing and sintering. The sintering temperature of 1550 °C was chosen according to work done by Dorey et al. [44].

From Figure 4.9, it can be seen that there are dramatic differences in the sintering shrinkage behaviour of the alumina-5wt%zirconia and alumina-10wt%zirconia composites. The alumina-10wt%zirconia begins to densify at a lower temperature, sinters gradually and finishes up with a linear shrinkage of approximately 22%. The alumina-5wt%zirconia begins to shrink after the alumina-10wt%zirconia and then the gradient is very sharp with a final linear shrinkage of approximately 24%. Many sintering additives have been used to induce the secondary-phase sintering [3]; this could explain the homogeneity of the microstructures obtained in the present work as well as the small diameter and narrow size distribution of secondary phases like YAG, tetragonal zirconia and mullite.

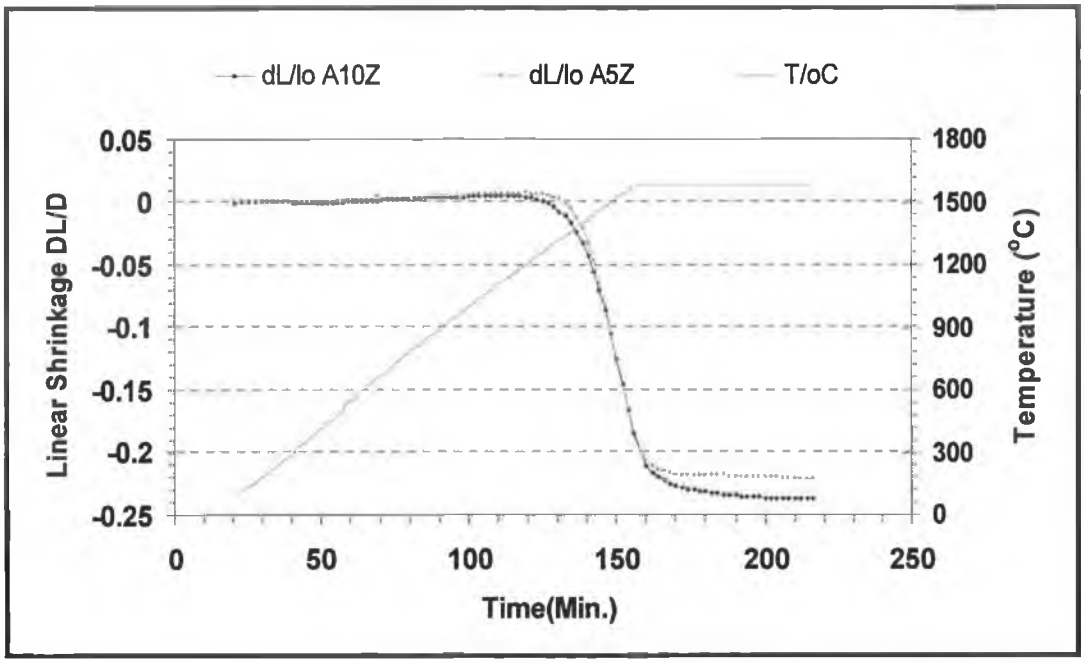

Figure 4.9 Shrinkage rate of Al_2O_3-5wt%ZrO_2 and Al_2O_3-10wt% ZrO_2 up to 1600 °C.

The green, sintered and true density have been measured for both powder processing and colloidal processing after sintering at 1550 °C for different Alumina-zirconia composites. A summary of the main properties are shown in Table 4.1.

Table 4.1 Designation, compositions, and properties of the alumina-zirconia samples.

Composition	Green Density %TD	Processing route	Sintering Temp.	True density[b]	Sintering density[a]
Al_2O_3-5wt% ZrO_2	48.6	Mixing powder	1550°C	93.8	97.6
Al_2O_3-10wt% ZrO_2	49.3	Mixing powder	1550°C	94.9	96.6
Al_2O_3-20wt% ZrO_2	51.2	Mixing powder	1550°C	95.8	94.2
Al_2O_3-5wt% ZrO_2	49.0	Colloidal	1550°C	92.6	97.5
Al_2O_3-10wt% ZrO_2	48.4	Colloidal	1550°C	95.3	96.4
Al_2O_3-20wt% ZrO_2	46.5	Colloidal	1550°C	96.6	95.2

- Sintering time: 2 hours
- TD: Theoretical density
- a: measured using geometric method (accuracy 0.01 mm) and Mettler precision balance (accuracy 0.1 mg)
- b: measured using helium pycnometry

From Table 4.1, it can be seen that the green density ranged from 46.5% to 51.2% for all the samples as measured using geometric method. The volume of sintered discs was also measured using geometric method and densities ranging from 92.6% to 96.6% were calculated. The rule of mixtures was used to calculate the densities. Helium pycnometry was also used to measure the density of the sintered samples and these values were generally higher than those obtained using the geometric approach. These points to the presence of some open porosities in the samples. Helium gas will penetrate the open pores and give a value for skeletal density. The lack of complete 100% theoretical density can be related to the presence of closed pores.

4.6 Vickers hardness

The hardness testing was carried out on the samples shown in Table 4.1 using loads of 10 kg and 20 kg. The hardness results are illustrated in Figure 4.10.

From Figure 4.9, it can be noticed that the hardness decreases by increasing the zirconia percentage. It is evident that the hardness of the sample, with 20% of zirconia, made with powder processing has decreased by 4.5% and 16 % with loads of 10 and 20 kg respectively. For the colloidally processed samples, the addition of 5% ZrO_2 causes a fall in the hardness but there is no further decrease, in hardness, for samples containing >5wt% ZrO_2. In fact, for additions > 8wt% of ZrO_2, the hardness is seen to increase slightly. It is known that additions of unstabilised zirconia lead to microcracking upon cooling from sintering. This leads to higher fracture toughness but a lower strength.

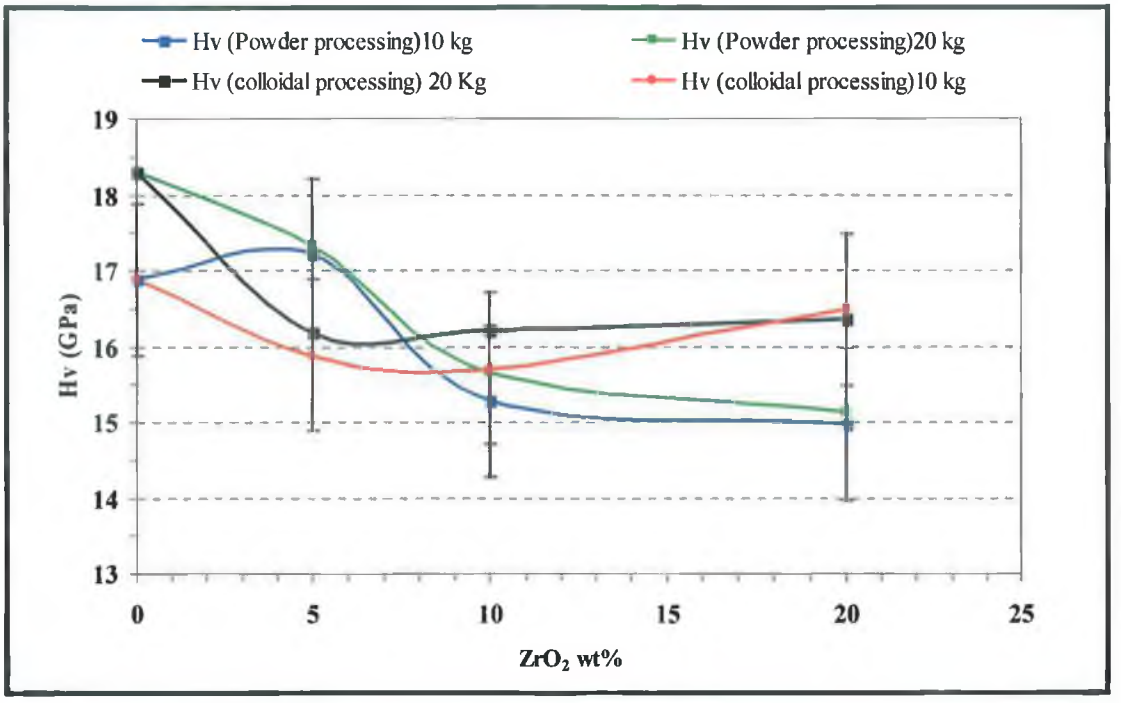

Figure 4.10 Vickers hardness vs. wt% ZrO_2 in Al_2O_3.

4.7 Fracture toughness

In terms of the fracture toughness, additions of up to 10% ZrO_2 led to an increase in the fracture toughness but this value fell off for >10wt% ZrO_2. Figure 4.11 shows the fracture toughness as determined by the method of Lawn & Wilshaw [1]. It is believed that the main toughening mechanism taking place here is micro-cracking. For >10 wt% ZrO_2, the microcracks are percolating, leading to a reduction in the fracture toughness. It is worth noting that the colloidally processed samples tested under 20 kg do not show a dramatic fall-off in the fracture toughness. It can be observed that in this case, there is retention of the tetragonal phase taking place and a spontaneous transformation when the load is applied, due to ZrO_2 particles are fine enough to be constrained by the alumina matrix. It was not possible to generate cracks for the 20wt% ZrO_2, colloidal processed, samples under 10 kg. It can be mentioned from reference [1] that the fracture toughness of alumina was increased considerably by the incorporation of a second-phase dispersion of unstablilised zirconia particles. Subcritical propagation and opening of microcracks in a large zone in front of the notch tip are thought to be responsible for this increase.

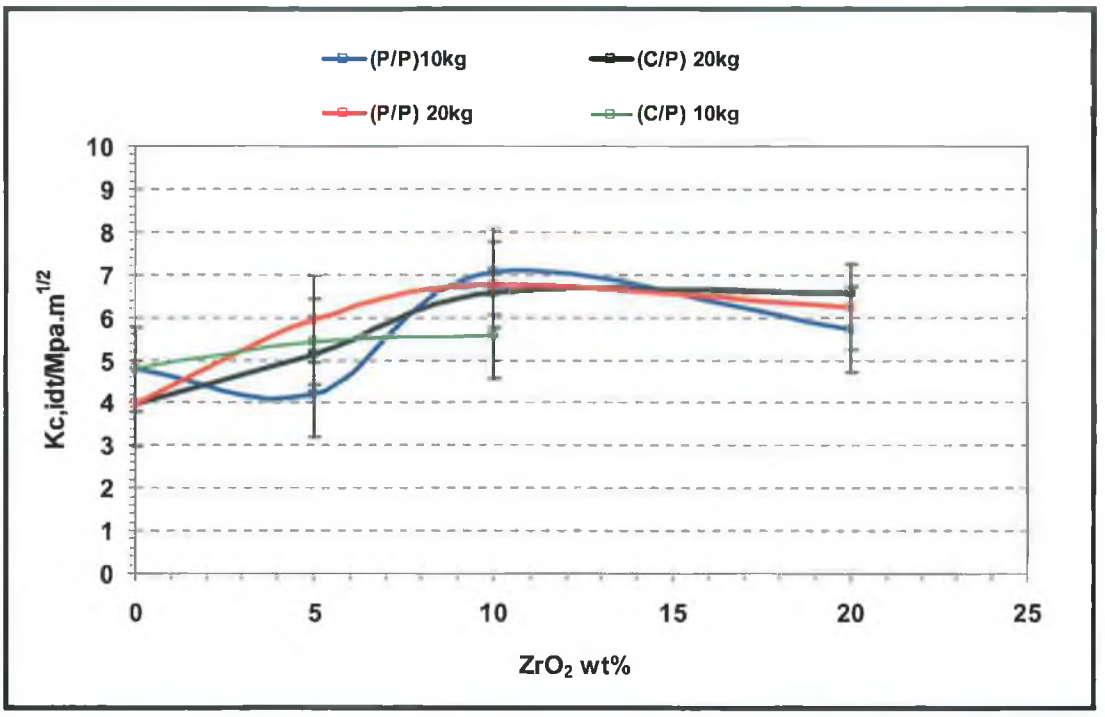

Figure 4.11 The wt% of ZrO_2 vs. fracture toughness, based on (Lawn & Wilshaw)

For the Anstis approach, similar trends were observed, as can be seen in Figure 4.12. However, toughness values of almost 9 MPa.m$^{1/2}$ were generated, which were higher than the toughness value 7 MPa.m$^{1/2}$ determined using Lawn and Wilshaw formula (3.2). As indicated in reference [37], the reason for this behaviour can be related to the absence of the main two toughening mechanisms of ATZ: crack bridging and transformation toughening. The crack bridging is negligible because of the small grain size of alumina (only small bridging was detected in pure alumina). The transformation toughening is also absent because only 5% of zirconia transformation was present on the fracture surfaces. The reason for this can be the fact that the ZrO_2 average particle size is too small such that it can activate the stress induced phase transformation. It can be noticed that greater values of fracture toughness are evident when the grain size of the alumina matrix and the zirconia particles had been increased due to thermal treatments and grain growth. The size of the tetragonal particle and the stabiliser content, have great influence on the tension required for the transformation of tetragonal particle [45]

Also it was confirmed in reference [46], using the method of Lawn [1], that the alumina–10 wt% zirconia composites with unstabilised zirconia indicated the highest values of fracture toughness. For this composite, the wt% of zirconia ranged between 10–20% for each tested method.

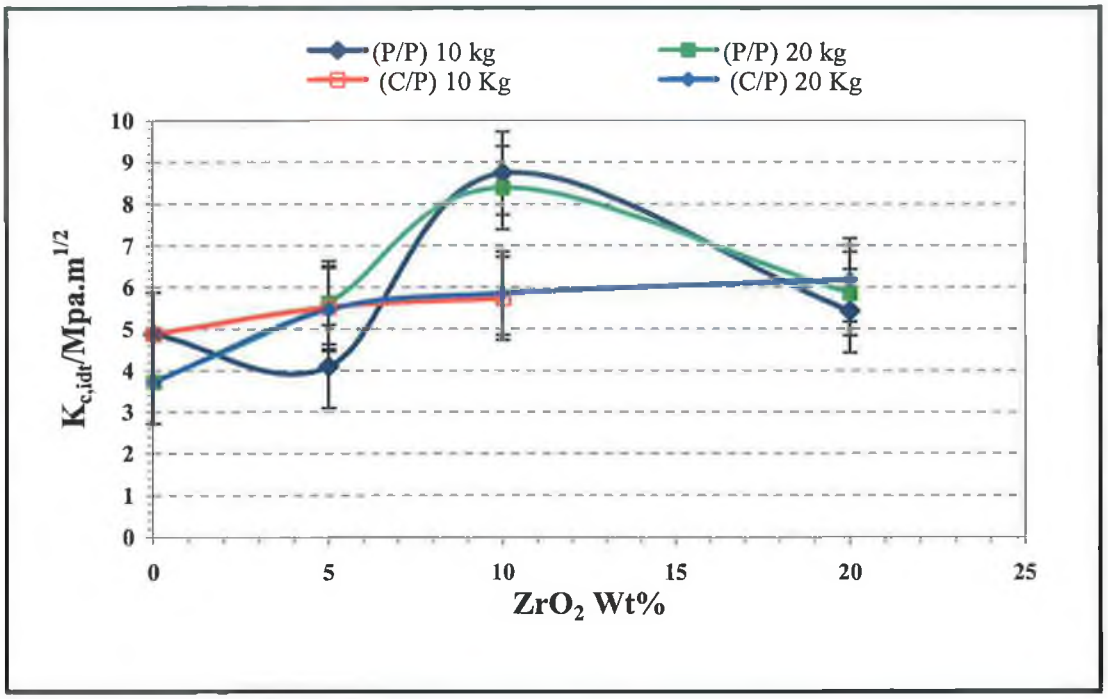

Figure 4.12 The wt% of ZrO_2 vs. fracture toughness, based on (Anstis)

The current results coincide with the results obtained in reference [47]. It was found that there is an increase of the fracture toughness by increasing the zirconia content up to about 10 vol. %. It can be noticed that increasing the number of zirconia particles, would increase the number of microcracks created during cooling after sintering and when cracks are propagating within the material.

The data obtained from the two previous figures are summarised in Table 4.2.

Table 4.2 The comparison between Lawn & Wilishaw and Anstis methods.

Composites	$K_{c,idt}$/MPa.m$^{1/2}$ Lawn &Wilshaw Load (10 kg)	$K_{c,idt}$/MPa.m$^{1/2}$ Anstis Load (10 kg)	$K_{c,idt}$/MPa.m$^{1/2}$ Lawn&Wilshaw Load (20 kg)	$K_{c,idt}$/MPa.m$^{1/2}$ Anstis Load (20 kg)
Al_2O_3	4.778	4.881	3.969	3.722
Al_2O_3-5wt%ZrO_2 (p/p)	4.187	4.102	5.940	5.636
Al_2O_3-10wt%ZrO_2 (p/p)	7.076	8.740	6.771	8.388
Al_2O_3-20wt%ZrO_2 (p/p)	5.730	5.429	6.260	5.846
Al_2O_3-5wt%ZrO_2 (c/p)	5.422	5.524	5.120	5.468
Al_2O_3-10wt%ZrO_2 (c/p)	5.572	5.732	6.576	5.857
Al_2O_3-20wt%ZrO_2 (c/p)	No crack	No crack	6.575	6.175

4.8 Young's Modulus

Young's modulus was measured using an excitation frequency technique. Al_2O_3 bars were made and used as a standard. The technique was adjusted to have an accuracy of ± 0.85%. An average value of the modulus, 363.9 GPa, was measured for Al_2O_3.

Table 4.3 Young's modulus results.

Composites	**Rule of Mixtures E (GPa)**	**Powder Processed E (GPa)**	**Colloidal Process E (GPa)**
Al_2O_3	363.9	363.9	363.9
5% ZrO_2	358.3	340.3	350.3
10% ZrO_2	352.6	338.1	333.6
20% ZrO_2	340.46	276.1	326.8

The rule of mixtures was employed to calculate the expected modulus variation. A Young's modulus value of 200 GPa was used as the theoretical value for unstabilised ZrO_2 [1]. A Young's modulus value of 380 GPa was considered for Al_2O_3, [11]. Pycnometry was used to measure the density and values of 4.14 g/cm^3 and 6.20 g/cm^3 were measured for the raw Al_2O_3 and ZrO_2 powders respectively. From the rule of mixtures, a drop off in the modulus was expected upon increasing the ZrO_2 content. This theory can be confirmed from the obtained results displayed

in Table 4.3 for, both, the powder processed and colloidally processed samples. Results were obtained by Moraes et al. [5] in their investigations of alumina-Y-TZP composites.

In Table 4.3, there is a significantly high deviation of the modulus of the 20% ZrO_2 powder processed sample as compared to the value obtained from colloidal processing. This is most likely due to the presence of uncontained, catastrophic microcracking in the powder processed sample, as the zirconia transforms from tetragonal to monoclinic. For the colloidally processed samples, there is less microcracking (as the particles are more finely dispersed), and thus there is no dramatic reduction in the Young's modulus.

This result, therefore, agrees with that of Moraes et al. [5]. It was found that the critical grain sizes increases with the Young's modulus of the composite, which is related with the restrictions imposed on the matrix. At the time that the Young's modulus decreases with the zirconia content, in accordance with the rule of mixtures, the critical grain sizes decreases with higher zirconia.

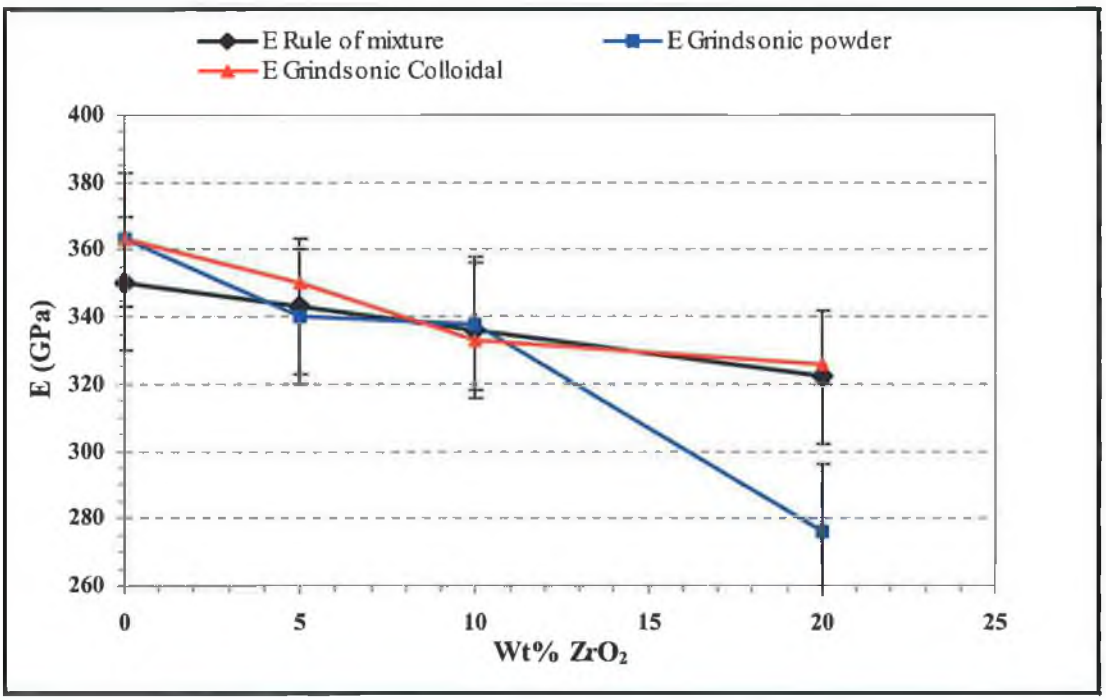

Figure 4.13 Young's modulus vs. ZrO_2 %, measured using Grindosonic.

According to Tan et al. [6], changes in the acoustic impedance can be brought about by porosities, microcracks and different phases in the composite. In their study

of Al_2O_3-unstabilised ZrO_2 composites, it was found that the modulus of sintered Al_2O_3-ZrO_2 ceramics could be increased by the additions of <5wt% of unstabilised ZrO_2, which has resulted a maximum modulus record for 3wt %. While the modulus values were decreased with the addition of unstabilised zirconia of quantities above 3wt%.

4.9 Microstructural analyses

The microstructure of the alumina-zirconia samples that have been sintered at 1550°C for 2 hours were examined using backscattered scanning electron microscopy (SEM). A standard ceramographic procedure was followed, by taking a cross-section of the specimen then polishing it to a 1 μm finish. After polishing, the samples were thermally etched at 1400°C for 30 minutes to reveal the grain definitions.

Backscattered electrons are defined as the electrons emitted the specimen with energies of 90 to 99% of the energy, the incoming beam electron. These electrons arise from elastic collisions between the beam electron and atoms in the sample. Backscattered electrons can escape from deep within the specimen and are generally emitted over an area much greater than the focused beam diameter striking the sample surface. Collection and amplification of these backscattered electrons gives rise to two imaging modes distinctly different from each other or emissive images [48].

The scanning electron micrographs have been used in backscatter mode to gives a strong atomic number contrast between the zirconia (bright phase) and the alumina (dark phase). It can be noted that the alumina and the zirconia are well dispersed for both materials.

The zirconia grains are well-distributed in the material, as it can be seen in Figure 4.14 and 4.15, and they are mostly surrounded by alumina grains. Many of these grains are located at triple points between grains.

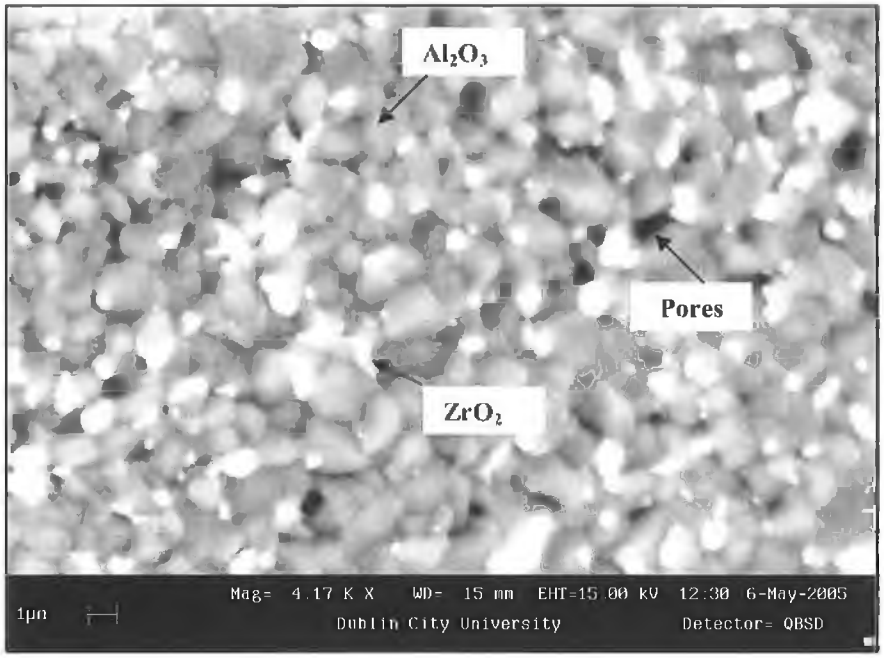

Figure 4.14 SEM (backscatter mode) image of a polished A10Z (colloidally processed). The dark grains are alumina and the bright grains are zirconia.

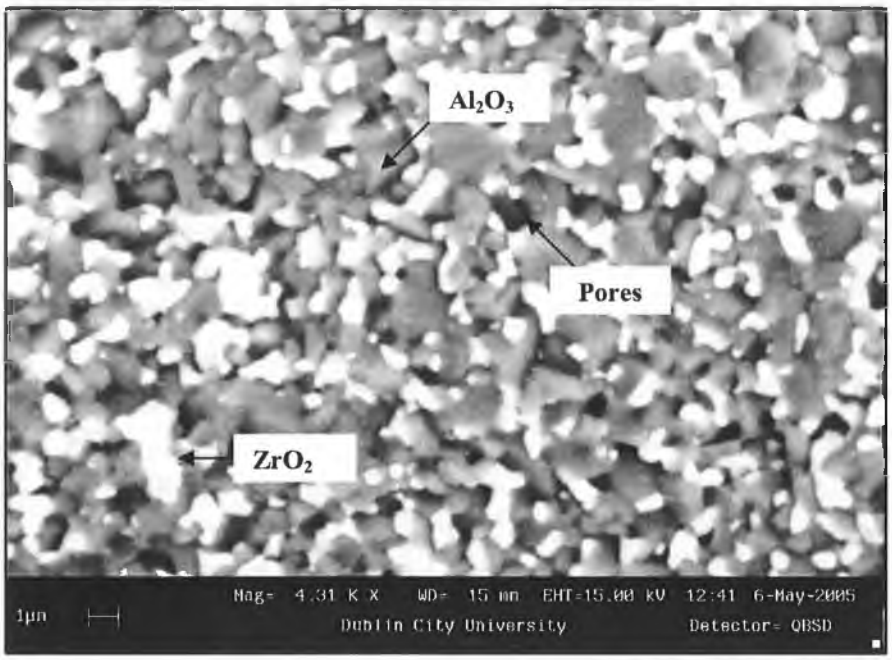

Figure 4.15 SEM image of a polished A10Z (Powder processed). The dark grains are alumina and the bright white grains are zirconia.

Figures 4.16 and 4.17 show the micrographs of A20Z obtained by colloidal and powder processing methods respectively. From figure 4.16, it appears that the zirconia grains are reasonably well dispersed in the alumina with a maximum grain size of 1-2 μm.

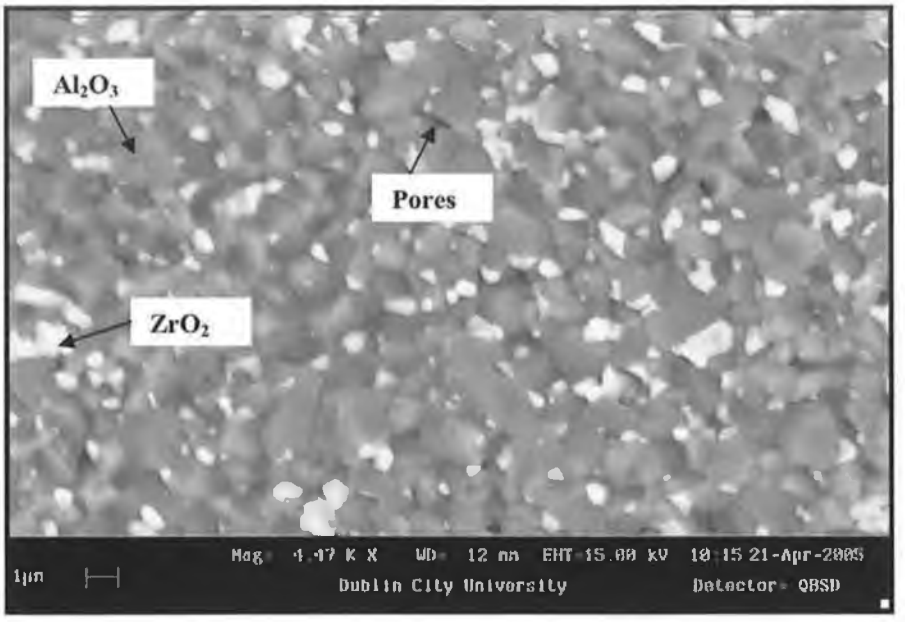

Figure 4.16 SEM image of a polished A20Z (Colloidally processed). The dark grains are alumina and the bright grains are zirconia.

Figure 4.17 shows the powder processed A20Z sample. The aim was to obtain very fine ZrO_2 particles that are homogeneously distributed, and to avoid agglomerates at the alumina grain boundaries, and therefore minimise the microstructural flaws. It may be noted as it was discussed before that the colloidal processing route is similar to the conventional powder mixing technique in terms of the zirconia particle size. (See Figure 4.16 and 4.17).

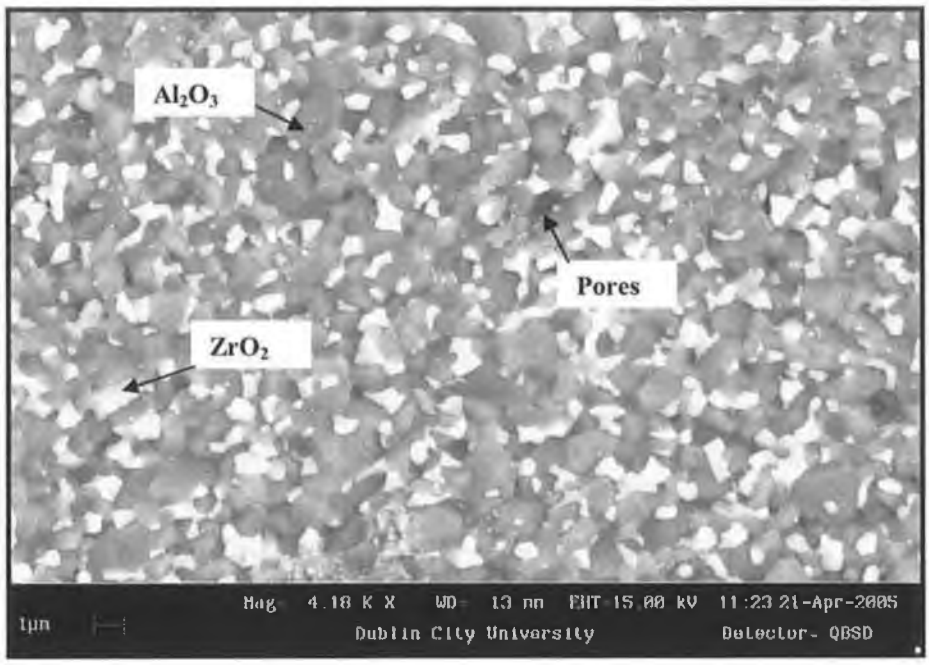

Figure 4.17 SEM image of a polished A20Z (Powder processed), ZrO_2 grains (the brighter phase) homogeneously distributed in a fine grain Al_2O_3 matrix (the darker phase).

It can be seen from Figure 4.14 to 4.17 that the zirconia particles appear as a bright phase, according to the higher atomic number of zirconia with respect to alumina, while alumina particles appear as a dark phase. Note the uniform and homogeneous distribution of zirconia throughout the alumina matrix as well as the typical intergranular location of the zirconia at the grain boundaries of the alumina. The current results coincide with reference [49].

The microstructure of the alumina–zirconia composites obtained by the colloidal processing synthesis technique was very fine with submicrometer alumina grains and, mainly intergranular. They also found that the zirconia particles have a narrow grain size distribution. This enabled a high portion of the tetragonal phase, retained at room temperature (after sintering), to transform under applied stresses. This indicated that the dominant toughening mechanism in these composites is transformation toughening. This is in agreement with reference [47].

Zirconia toughened alumina [50] (ZTA) is a two–phase binary ceramic formed by adding zirconia powder to alumina powder and sintering it to form a dense product with an improved toughness over the conventional alumina ceramics. Toughening arises mainly from the tetragonal to the monoclinic zirconia transformation. Zirconia has also been added to many other ceramic matrices in an attempt to improve their

toughness, notably mulllite and cordierite. The zirconia mixed with the fine alumina powder may either be pure, unstabilised, zirconia particles, or TZP particles, usually using yttria to stabilise the tetragonal phase. Since both phases are present as particles, conventional powder processing is used.

Alumina-zirconia can be hot pressed or pressureless sintered to, nearly, the theoretical density at 1600 °C. The starting zirconia particle size essentially stays as the zirconia grain size in the sintered microstructure and has a strong effect on its toughness and strength. The zirconia is retained in the tetragonal form, provided the particle size remains below the critical size for the transformation to monoclinic zirconia. This particle size is larger for single phase zirconia as a result of the alumina having a higher elastic modulus; the stiff alumina particles constrain the t-ZrO_2 preventing the transformation which requires a volume fraction zirconia. For example, with 5vol. % the critical particle size is > 2 μm but with 20 vol. % it is 0.7 μm [51, 52]. This is partly due to the decreased elastic modulus with higher zirconia content. However, thermal mismatch stresses between the two phases are also important, as are the tensile strains promoted by monoclinic transformation, present when additions of above 10vol.% are made. The mean zirconia grain spacing is also important [53].

The addition of zirconia has a marked effect on the microstructure of the alumina. For a composition and treatment which would contain elongated grains from abnormal grain growth without zirconia present, adding >3vol.% leads to a predominantly equiaxed microstructure. Small additions of up to 1vol.% dramatically refine the alumina grain size. Additions of more than 3vol.% zirconia distributes intergranular zirconia particles at every four grain junctions, which prevents abnormal grain growth can still occur.

The zirconia is present either as: angular grains on the alumina grain boundaries, typically at grain junctions, or as fine spherical, intragranular grains. The intragranular grains are invariably smaller than the intragranular grains and are believed to be zirconia starting powder particles incorporated into the alumina during grain boundary migration [54]. The smaller particles are usually tetragonal while the larger ones are either monoclinic or tetragonal.

CHAPTER FIVE
CONCLUSIONS

CHAPTER FIVE

CONCLUSIONS AND FUTURE WORK

5.1 Conclusions

The aim of this thesis was to study the alumina and zirconia ceramics made by the conventional powder processing, and the colloidal processing. To compare the results of the colloidal process and conventional process by investigating the mechanical properties of alumina-zirconia composites. The conclusions to be drawn from this investigation are as follows.

- Attrition milling was an effective technique in achieving powder particle sizes as low as 0.4 μm.
- High attrition milling speed and media/powder ratios higher than 3 were needed for efficient milling.
- Sintered densities values of between 92.6% and 97.6% were recorded using either the geometric method or the helium pycnometry.
- Additions of glacial acetic acid were needed to form stable suspensions of the alumina powder and the zirconium propoxide.
- The powder processed samples, experienced a decrease in the hardness as the zirconia content increased. Additions of up to 10wt% ZrO_2 led to an increase in the fracture, but this increase fell off for additions >10wt% ZrO_2.
- The colloidal samples' initial tests showed a fall off in the hardness for 5wt% ZrO_2 but no further decrease with >5wt% ZrO_2 additions. A slight increase in hardness is seen for additions of between 5wt% and 20wt% ZrO_2.
- The fracture toughness of the colloidally processed samples has increased for additions of up to 20wt% ZrO_2. No dramatic fall off was recorded for 20wt% additions, as was the case for the powder processed samples.
- Young's modulus dropped off as a result of increasing the ZrO_2 content. A dramatic fall off for 20wt% ZrO_2 for the powder processed samples is

believed to be due to the uncontained cracking. This was not observed for the colloidally processed samples.

- The microstructure samples revealed that the zirconia grains were uniformly distributed in the alumina matrix. Most of the grains were located at the junctions of the alumina grains and the grain boundaries, which revealed the intergranular nature of the zirconia grains. Very few grains were located within the alumina grains, possessing the intragranular type. As most of the zirconia grains were placed at the grain junctions, the zirconia grains pinned down the motion of the alumina grains.

5.2 Recommendation for future work

1. Design and procurement of a die set to measure the fracture toughness using a fracture strength method.
2. Brunauer, Emmett and Teller (BET), surface area measurement of 20% zirconia (powder method) vs. 20% zirconia (colloidal method).
3. Use of yttria solution and zirconium propoxide to make yttria-stabilised zirconia solution, and alumina-yttria-stabilised zirconia composites.

REFERENCES

REFERENCES

[1] N. Claussen. Fracture toughness of Al_2O_3 with an unstabilised ZrO_2 dispersed phase, J. Am. Ceram. Soc. Vol. 59, 1-2 (1976)pp 49-51

[2] M. W. Barsoum, Fundamentals of Ceramics, Institute of Physics Publishing, Bristol, (2003) pp 381-378

[3] M. Schehl, L.A. Dı´az, R. Torrecillas, Alumina nanocomposites from powder–alkoxide mixtures, Acta Materialia 50 (2002) pp1125–1139

[4] S. Deville, J. Chevalier, G. Fantozzi, J. F. Bartolome, J. Requena, J. Moya, R. Torrecillas, L. A. Dıaz, Low-temperature ageing of zirconia-toughened alumina ceramics and its implication in biomedical implants Journal of the European Ceramic Society, 23 (2003) pp 2975–2982

[5] D. B. Maria, N. E. Carlos, D. F. Jamil, G. O. Leandra., Mechanical properties of alumina-zirconia composites for ceramic abutments, Materials Research, Vol. 7, No.4, (2004) pp 643-649

[6] K. S Tan, P. Hing, and P. Ramalingam, The elastic moduli and diametrical compressive fracture stress of Al_2O_3–ZrO_2 ceramics J. Phys. D: Appl. Phys. 30 (1997) pp1029–1037.

[7] http://www.fda.gov/cdrh/pdf4/K042600.pdf, 510(k) Premarket notification DePuy, Feb 11 2005, 20-12-2005

[8] A. Marti, Inert bioceramics (Al_2O_3, ZrO_2) for medical application, Injury, Int. J. Care Injured 31 (2000) pp S-D33-36

[9] http://surphy.fat.bme.hu/pub/MaterSci/T10.DOC.pdf 04-07-2005 (pp171)

[10] L. Richard, Lehman Said K. El-Rahaiby john B. Wachhtman, Jr. Handbook on continuous fiber-Reinforced ceramic matrix composites, (1999) pp 119-122

[11] C. Piconi, G. Maccauro, Zirconia as a ceramic biomaterial. Biomaterials, 20 (1999) pp 1 –25

[12] R. C. Fries, Handbook of materials for medical devices ASM international, 1998 Chapter (1)

[13] M. Cecilia, C. Nelson, J. Filho, L. Guimarães, Mechanical properties of alumina-zirconia composites for ceramic abutments, Vol. 7, No. 4, (2004) pp 643-649

[14] C. Piconl, G. Maccauro, F. Muratori, E. Brachdel Prever, Alumina and zirconia ceramics in joint replacements, Journal of Applied Biomaterials & Biomechanics, 1 (2003) pp 19-32

[15] T, Burg , O. Standard, http://www.materials.unsw.edu.au/news/biomed-s.pdf, Materials for Biomedical Engineering, , 2001 Materials Science and Engineering, Student Notes,05-07-2005

[16] J. Hevalier, Leading Opinion what future for zirconia as a biomaterial, Biomaterials, 27 (2006) pp 535–543

[17] D. Zeng, N. Katsube and W. O. Soboyejo, Discrete modeling of transformation toughening in heterogeneous materials Mechanics of Materials, 36 (2004) pp 1057-1071

[18] G. Ying, R. Lederich, and W. Soboyejo, Residual stresses and transformation toughening in $MoSi_2$ composites reinforced with partially stabilized Materials Science and Engineerin, 210 (1996) pp 25-41

[19] M. Barsoum, Fundamental of ceramics. (2003) pp 381-385

[20] http://surphy.fat.bme.hu/pub/MaterSci/T10.DOC.pdf 05-07-2005 pp (173-174)

[21] D. Green, J., Hannink, R. H. J. and Swain, M. V., Transformation toughening of ceramics. LRC Press, Boca Raton (Florida). (1989)

[22] C. Moreno, M. Sehehl, M. Popa, Superplastic behavior of zirconia-reinforced alumina nanocomposites from powder alcoxide mixtures, Acta Materialia ,50 (2002) pp3973–3983

[23] B. fegley, R. White, H. Kent Bowen, Preparation of Zirconia-Alumina powders by Zirconium Alkoxide Hydrolysis, J. Am. Ceram. Soc. 68 [2] (1985) ppC-60-C-62

[24] G. Wang, P. Sarkar, P. S. Nicholson, Influence of acidity on the electrostatic stability of alumina suspension in ethanol, J. Am. Ceram. Soc. 80 [4] (1997) pp965-72

[25] P. Cortesi, H. Bowen, Continuous Coating of Alumina Particles with Alkoxide-derived Zirconia Particles, ceramics international 15 (1989) pp 173-177

[26] M. Sherif el-Eskandarany, K. Aoki, K. Sumiyama, and K. Suzuki, Cyclic solid-state transformations during ball milling of alumina-zirconia powder and the effect of milling speed, metallurgical and materials transactions a, 30A, (1999) pp1877

[27] R. Joanna, Groza, Ceramic technology and processing, chapter 3 milling and equipment, (1998) pp 20-54

[28] D. Jayaseelan, T. Nishikawa, H. Awaji, E. D. Gnanam, pressureless sintering of sol-gel derived alumina-zirconia composites, materials scin. And Eng. 256(1998) pp 265-270

[29] G. J. Liu, H. B. Qiu, R. J. Brook, and J. K. Guo, Processing and mechanical behavior of Alumina-Zirconia nanocomposites, materials research bulletin, vol. 33 No.2, (1998) pp.281-288,

[30] R.E. Chinn, Preparation of Microstructures of Alumina Ceramics, Structure, Vol 33, (1998) pp 16–20

[31] F. Leander, Douslas L., powder metal technologies and applications ASM, Vol. 7 (1998) pp 722-723

[32] ASM International, Preparation and analysis of ceramic microstructures, grinding and polishing chapter 4, ASM International Materials Park, Ohio, USA, www.asminternational.org/bookstore 17-05-2005

[33] http://webpages.dcu.ie/~stokesjt/ThermalSpraying/Book/Chapter10.pdf, J. Stokes, Coating Characterisation equipment, Chapter 10, (2003) pp 155-156

[34] Standard test method for Vickers indentation hardness of advanced ceramic, ASTM: C-1327-99, (1999) pp1-8

[35] S. Pratapa. 1997 MSc. Thesis, Synthesis and character of aluminium titanate/zirconia-alumina composite, Curtin university of technology, (1997) pp52

[36] http://www.twi.co.uk/j32k/protected/band_3/jk74.html, 16-05-2005

[37] B. Lawn, Fracture of brittle solids, (2nd Ed.) Cambridge University Press, (1993) pp3-7

[38] G. R. Anstis, P. Chantikul, B. R. Lawn, D. B. Marshall, critical evaluation of indentation techniques for measuring fracture toughness: I direct crack measurements, Journal of the American Ceramic Society, 64 (1981) pp533-538

[39] J. M. Antunes, A. Cavaleir, L. F. Menezes, M. I. Sim, J. V. Fernand, Ultra-microhardness testing procedure with Vickers indenter, Surface and Coatings Technology 149 (2002) pp 27–35

[40] J. W. Lemmens N. V., operating instructions for the Grindosonic MK5 "Industrial" instrument, (1994) pp 14-16

[41] K. Heritage, C. Frisby, A. Wolfenden, iimpulse excitation technique for dynamic flexural measurements at moderate temperature, Review of Scientific Instruments, 59 (6), (1998) pp 973-974

[42] A. Rafferty, Y. Gun'ko, R. Raghavendra, An investigation of co-fired varistor-ferrite materials, Journal of the European Ceramic Society 24 (2004) pp 2005–2013

[43] H. Robert, P. Dongreen, Perry's chemical engineering handbook, international edition, sixth edition 1984, pp 63-65

[44] R. A. Dorey, J. A. Yeomans, P. A. Smith and J. Pan, In situ optical dilatometric measurements of the initial stages of sintering of alumina, Acta mater. 49 (2001) pp 519-527

[45] T.K., Gupta, Lange, F.F.; Bechtold, J.H., Effect of stressinduced phase transformation on properties of polycrystalline zirconia containing metastable tetragonal phase, J. Mater. Sci., 13(1978) pp 1464-1470

[46] M. Szutkowska, Fracture resistance behaviour of alumina–zirconia composites, Journal of Materials Processing Technology 153–154 (2004) pp 868–874

[47] A.H. De Azaa, J. Chevalier, G. Fantozzi, M. Schehl, R. Torrecillas, Crack growth resistance of alumina, zirconia and zirconia toughened alumina ceramics for joint prostheses, Biomaterials, Volume 23, Issue 3, February 2002, pp 937-945

[48] L. Perry, M. electronic failure analysis handbook, (1999) pp (11)

[49] S. Biamino, P. Fino, M. Pavese, C. Badini, Alumina–zirconia yttria nanocomposites prepared by solution combustion synthesis, Ceramics International available on line 31st May 2005

[50] M. Glendenning, PhD thesis, university of Sheffield, Sheffield, UK, (1994) pp 45-48

[51] Green, D. J., critical microstructures for microcracking in alumina-zirconia composites, Am. Ceram. Soc., 65 (1982) pp 610-14

[52] S. Hori, Kurita, R., Yoshimura, M. and Somiya, S., influence of small zirconia additions on the microstructure and mechanical properties of alumina, Am. Ceram. Soc., vol. 24 (1988) pp 423-9

[53] S. Hori, Kurita, R., Yoshimura, M. and Somiya, S., influence of small zirconia additions on the microstructure and mechanical properties of alumina, Am. Ceram. Soc., vol. 24 (1988) pp 423-9

[54] K. B. Heuer, A. H., Exaggerated grain growth in zirconia toughened alumina. J. Am. Ceram. Soc., vol. 69 (1986) pp 23

APPENDICES

APPENDIX A

Temperature Equivalence of the horizontal furnace

Cooling down °C	Furnace Temp. °C	Furnace Temp. °C	Thermocouple °C
1536	1550	50	33
1496	1500	100	55
1446	1450	150	149
1396	1400	200	166
1352	1350	250	236
1304	1300	300	302
1354	1250	350	328
1210	1200	400	383
1165	1150	450	440
1119	1100	500	492
1075	1050	550	540
1030	1000	600	609
984	950	650	651
938	900	700	691
891	850	750	749
844	800	800	801
794	750	850	841
745	700	900	887
696	650	950	936
648	600	1000	1001
598	550	1050	1038
544	500	1100	1084
491	450	1150	1140
445	400	1200	1185
398	350	1250	1234
348	300	1300	1285
291	250	1350	1333
245	200	1400	1382
145	150	1450	1431
138	100	1500	1478
96	50	1550	1530

APPENDIX B

Excel sheet of Vickers Hardness Test

1. Hardness test data sheet (load 10 kg)

Sample	10kg d1/mm	d2/mm	d(avg)/mm	d(avg)/mm	Hv_10kgf	H (GPa)
Al2O3 (1)	105	101	103	0.103		
Al2O3 (2)	102	108	105	0.105		
Al2O3 (3)	103	104	103.5	0.1035		
Al2O3 (4)	104	108	106	0.106		
Al2O3 (5)	103	103	103	0.103		
Al2O3 (6)	103	101	102	0.102		
Average Al2O3			**103.75**	**0.10375**	**1722.398026**	**16.891**
5% ZrO2	107	104	105.5	0.1055		
5% ZrO2	103	103	103	0.103		
5% ZrO2	103	104	103.5	0.1035		
5% ZrO2	104	101	102.5	0.1025		
5% ZrO2	98	101	99.5	0.0995		
Average 5% ZrO2			**102.8**	**0.1028**	**1754.379324**	**17.205**
10% ZrO2	109	117	113	0.113		
10% ZrO2	112	111	111.5	0.1115		
10% ZrO2	108	110	109	0.109		
10% ZrO2	109	105	107	0.107		
10% ZrO2	108	102	105	0.105		
Average 10% ZrO2			**109.1**	**0.1091**	**1557.615387**	**15.275**
20% ZrO2	113	110	111.5	0.1115		
20% ZrO2	108	111	109.5	0.1095		
20% ZrO2	109	115	112	0.112		
20% ZrO2	112	110	111	0.111		
20% ZrO2	109	105	107	0.107		
Average 20% ZrO2			**110.2**	**0.1102**	**1526.674813**	**14.972**
5% ZrO2 c/p	108	104	106	0.106		
5% ZrO2 c/p	107	108	107.5	0.1075		
5% ZrO2 c/p	105	109	107	0.107		
5% ZrO2 c/p	107	108	107.5	0.1075		
5% ZrO2 c/p	105	110	107.5	0.1075		
5% ZrO2 c/p	104	108	106	0.106		
5% ZrO2 c/p	104	111	107.5	0.1075		
Average 5% ZrO2			**107**	**0.107**	**1619.355402**	**15.880**
10% ZrO2 c/p	108	112	110	0.11		
10% ZrO2 c/p	108	106	107	0.107		
10% ZrO2 c/p	106	105	105.5	0.1055		
10% ZrO2 c/p	108	108	108	0.108		
10% ZrO2 c/p	109	109	109	0.109		
10% ZrO2 c/p	106	106	106	0.106		
Average 10% ZrO2			**107.5833333**	**0.107583333**	**1601.842224**	**15.709**
20% ZrO2 c/p			105	106		
Average 20% ZrO2			**105**	**0.105**	**1681.632653**	**16.491**

2. Hardness test data sheet (load 10 kg)

		20kg				
Sample	d_1/μm	d_2/μm	d(avg)/μm	d(avg)/mm	Hv	H (GPa)
Al2O3	145	141	143	0.143		
Al2O3	145	141	143	0.143		
Al2O3	140	141	140.5	0.1405		
Al2O3	137	144	140.5	0.1405		
Al2O3	142	139	140.5	0.1405		
Al2O3	140	137	138.5	0.1385		
Al2O3	138	146	142	0.142		
Al2O3	136	143	139.5	0.1395		
Average Al2O3			140.9375	0.141	1865.097329	18.290
5% ZrO2	145	142	143.5	0.1435		
5% ZrO2	152	147	149.5	0.1495		
5% ZrO2	145	144	144.5	0.1445		
5% ZrO2	147	144	145.5	0.1455		
5% ZrO2	148	146	147	0.147		
5% ZrO2	147	150	148.5	0.1485		
5% ZrO2	146	144	145	0.145		
5% ZrO2	150	149	149.5	0.1495		
Average 5% ZrO2			146.625	0.1448	1768.489973	17.343
10% ZrO2	159	149	154	0.154		
10% ZrO2	154	152	153	0.153		
10% ZrO2	154	155	154.5	0.1545		
10% ZrO2	156	155	155.5	0.1555		
10% ZrO2	154	152	153	0.153		
10% ZrO2	156	152	154	0.154		
10% ZrO2	160	155	157.5	0.1575		
10% ZrO2	156	152	154	0.154		
Average 10% ZrO2			154.4375	0.15236	1597.341582	15.665
20% ZrO2	143	151	147	0.147		
20% ZrO2	155	155	155	0.155		
20% ZrO2	154	155	154.5	0.1545		
20% ZrO2	155	153	154	0.154		
20% ZrO2	162	153	157.5	0.1575		
20% ZrO2	155	153	154	0.154		
20% ZrO2	154	160	157	0.157		
20% ZrO2	162	153	157.5	0.1575		
20% ZrO2	155	154	154.5	0.1545		
Average 20% ZrO2			154.5555556	0.1536	1571.655273	15.413
5% ZrO2 C/P	149	147	148	0.148		
5% ZrO2 C/P	152	154	153	0.153		
5% ZrO2 C/P	146	152	149	0.149		
5% ZrO2 C/P	147	153	150	0.15		
5% ZrO2 C/P	150	149	149.5	0.1495		
5% ZrO2 C/P	146	149	147.5	0.1475		
5% ZrO2 C/P	148	148	148	0.148		
5% ZrO2 C/P	148	145	146.5	0.1465		
5% ZrO2 C/P	151	152	151.5	0.1515		
Average 5% ZrO2 C/P			149.2222222	0.1499	1650.199533	16.183
10% ZrO2 C/P	150	152	151	0.151		
10% ZrO2 C/P	151	153	152	0.152		
10% ZrO2 C/P	149	150	149.5	0.1495		
10% ZrO2 C/P	147	146	146.5	0.1465		
10% ZrO2 C/P	149	147	148	0.148		
10% ZrO2 C/P	150	146	148	0.148		
10% ZrO2 C/P	144	148	146	0.146		
Average 10% ZrO2 C/P			148.7142857	0.14978	1652.844789	16.209
20% ZrO2 C/P	147	151	149	0.149		
20% ZrO2 C/P	148	146	147	0.147		
20% ZrO2 C/P	147	148	147.5	0.1475		
20% ZrO2 C/P	151	152	151.5	0.1515		
20% ZrO2 C/P	153	148	150.5	0.1505		
20% ZrO2 C/P	147	150	148.5	0.1485		
20% ZrO2 C/P	154	151	152.5	0.1525		
20% ZrO2 C/P	147	147	147	0.147		
20% ZrO2 C/P	150	149	149.5	0.1495		
Average 20% ZrO2 C/P			149.2222222	0.1491	1667.955419	16.357

APPENDIX C

Excel sheet of Fracture toughness data

1. Lawn and Wilshaw method (load 10kg)

	10kg		Lawn & Wilshaw 1975		
Sample	Crack 1	Crack 2	Avg/2Co mm	2Co/m	Kc,idt/MPa.m2
Al2O3 (1)	235	285	260	0.00026	
Al2O3 (2)	238	243	240.5	0.0002405	
Al2O3 (3)	249	294	271.5	0.0002715	
Al2O3 (4)	262	296	279	0.000279	
Al2O3 (5)	250	258	254	0.000254	
Average Al2O3			261	0.000261	4.778244014
5% ZrO2	284	298	291	0.000291	
5% ZrO2	265	304	284.5	0.0002845	
5% ZrO2	268	330	299	0.000299	
5% ZrO2	285	293	289	0.000289	
5% ZrO2	241	282	261.5	0.0002615	
Average 5% ZrO2			285	0.000285	4.187567257
10% ZrO2	165	162	163.5	0.0001635	
10% ZrO2	192	186	189	0.000189	
10% ZrO2	202	130	166	0.000166	
Average 10% ZrO2			172.8333333	0.000172833	8.867226997
20% ZrO2	205	235	220	0.00022	
20% ZrO2	235	258	246.5	0.0002465	
20% ZrO2	217	231	224	0.000224	
20% ZrO2	233	243	238	0.000238	
20% ZrO2	211	242	226.5	0.0002265	
Average 20% ZrO2			231	0.000231	5.738668203
5% ZrO2 C/P	234	243	238.5	0.0002385	
5% ZrO2 C/P	213	246	229.5	0.0002295	
5% ZrO2 C/P	246	261	253.5	0.0002535	
5% ZrO2 C/P	241	261	251	0.000251	
5% ZrO2 C/P	202	278	240	0.00024	
5% ZrO2 C/P	242	212	227	0.000227	
Average 5% ZrO2 C/P			239.9166667	0.000239917	5.421737129
10% ZrO2 C/P	267	260	263.5	0.0002635	
10% ZrO2 C/P	226	259	242.5	0.0002425	
10% ZrO2 C/P	230	227	228.5	0.0002285	
10% ZrO2 C/P	199	209	204	0.000204	
10% ZrO2 C/P	238	219	228.5	0.0002285	
10% ZrO2 C/P	206	287	246.5	0.0002465	
Average 5% ZrO2 C/P			235.5833333	0.000235583	5.572014549
20% ZrO2 C/P					
20% ZrO2 C/P					
20% ZrO2 C/P	not making any crak				
20% ZrO2 C/P					
20% ZrO2 C/P					
20% ZrO2 C/P					
20% ZrO2 C/P					
Average 20% ZrO2 C/P			#DIV/0!	#DIV/0!	#DIV/0!

2. Lawn and Wilshaw method (load 20kg)

	20kg		Lawn & Wilshaw 1975		
Sample	Crack 1	Crack 2	Avg/2Co mm	2Co/m	Kc,Idt/MPa.m2
Al2O3	459	578	518.5	0.0005185	
Al2O3	439	552	495.5	0.0004955	
Al2O3	446	479	462.5	0.0004625	
Al2O3	483	500	491.5	0.0004915	
Al2O3	474	423	448.5	0.0004485	
Al2O3	440	508	474	0.000474	
Al2O3	425	480	452.5	0.0004525	
Al2O3	405	409	407	0.000407	
Average Al2O3			**468.75**	**0.00046875**	**3.96916203**
5% ZrO2	445	317	381	0.000381	
5% ZrO2	432	302	367	0.000367	
5% ZrO2	336	333	334.5	0.0003345	
5% ZrO2	403	393	398	0.000398	
5% ZrO2	367	322	344.5	0.0003445	
5% ZrO2	332	**420**	376	0.000376	
5% ZrO2	311	353	332	0.000332	
5% ZrO2	347	407	377	0.000377	
5% ZrO2	335	374	354.5	0.0003545	
5% ZrO2	355	344	349.5	0.0003495	
Average 5% ZrO2			**358.25**	**0.00035825**	**5.94061659**
10% ZrO2	268	276	272	0.000272	
10% ZrO2	251	255	253	0.000253	
10% ZrO2	302	263	282.5	0.0002825	
10% ZrO2	315	284	299.5	0.0002995	
10% ZrO2	323	348	335.5	0.0003355	
10% ZrO2	320	302	311	0.000311	
10% ZrO2	305	299	302	0.000302	
10% ZrO2	305	296	300.5	0.0003005	
10% ZrO2	270	314	292	0.000292	
10% ZrO2	352	300	326	0.000326	
10% ZrO2	300	289	294.5	0.0002945	
Average 10% ZrO2			**297.1363636**	**0.000297136**	**7.864607317**
20% ZrO2	318	392	355	0.000355	
20% ZrO2	344	358	351	0.000351	
20% ZrO2	311	331	321	0.000321	
20% ZrO2	358	372	365	0.000365	
20% ZrO2	336	336	336	0.000336	
20% ZrO2	358	355	356.5	0.0003565	
20% ZrO2	356	377	366.5	0.0003665	
20% ZrO2	328	354	341	0.000341	
Average 20% ZrO2			**349**	**0.000349**	**6.178351445**
5% ZrO2 C/P	323	371	347	0.000347	
5% ZrO2 C/P	404	407	405.5	0.0004055	
5% ZrO2 C/P	382	430	406	0.000406	
5% ZrO2 C/P	390	382	386	0.000386	
5% ZrO2 C/P	411	348	379.5	0.0003795	
5% ZrO2 C/P	457	380	418.5	0.0004185	
5% ZrO2 C/P	358	423	390.5	0.0003905	
5% ZrO2 C/P	403	393	398	0.000398	
5% ZrO2 C/P	344	417	380.5	0.0003805	
Average 5% ZrO2 C/P			**390.1666667**	**0.000390167**	**5.226795449**
10% ZrO2 C/P	357	366	361.5	0.0003615	
10% ZrO2 C/P	389	368	378.5	0.0003785	
10% ZrO2 C/P	334	339	336.5	0.0003365	
10% ZrO2 C/P	388	352	370	0.00037	
10% ZrO2 C/P	376	386	381	0.000381	
10% ZrO2 C/P	366	356	361	0.000361	
Average 10% ZrO2 C/P			**364.75**	**0.00036475**	**5.782528719**
20% ZrO2 C/P	338	314	326	0.000326	
20% ZrO2 C/P	325	318	321.5	0.0003215	
20% ZrO2 C/P	392	339	365.5	0.0003655	
20% ZrO2 C/P	407	291	349	0.000349	
20% ZrO2 C/P	430	299	364.5	0.0003645	
20% ZrO2 C/P	306	313	309.5	0.0003095	
20% ZrO2 C/P	352	248	300	0.0003	
20% ZrO2 C/P	405	297	351	0.000351	
20% ZrO2 C/P	310	277	293.5	0.0002935	
Average 20% ZrO2 C/P			**334.8**	**0.0003348**	**6.575557431**

3. Anthis method (load 10kg)

		10kg					
Sample	**Crack 1**	**Crack 2**	**Avg/2Co mm**	**2Co/m**	**E (GPa)**	**H (GPa)**	**Kc,idt/MPa.m2**
Al2O3 (1)	235	285	260	0.0003	363	16.891	
Al2O3 (2)	238	243	240.5	0.0002	363	16.891	
Al2O3 (3)	249	294	271.5	0.0003	363	16.891	
Al2O3 (4)	262	296	279	0.0003	363	16.891	
Al2O3 (5)	250	258	254	0.0003	363	16.891	
Average Al2O3			**261**	**0.0003**	**363**	**16.891**	4.880888134
		Mech.	**Method**	**10kg**			
Sample	**Crack 1**	**Crack 2**	**Avg/2Co mm**	**2Co/m**	**E (GPa)**	**H (GPa)**	**Kc,idt/MPa.m2**
5wt%	284	298	291	0.0003	340	17.205	
5wt%	265	304	284.5	0.0003	340	17.205	
5wt%	268	330	299	0.0003	340	17.205	
5wt%	285	293	289	0.0003	340	17.205	
5wt%	241	282	261.5	0.0003	340	17.205	
Average Al2O3			**285**	**0.0003**	**340**	**17.205**	4.101840923
Sample	**Crack 1**	**Crack 2**	**Avg/2Co mm**	**2Co/m**	**E (GPa)**	**H (GPa)**	**Kc,idt/MPa.m2**
10wt%	165	162	163.5	0.0002	338	16.891	
10wt%	192	186	189	0.0002	338	16.891	
10wt%	202	130	166	0.0002	338	16.891	
Average Al2O3			172.8333333	**0.0002**	338	**16.891**	8.740240715
Sample	**Crack 1**	**Crack 2**	**Avg/2Co mm**	**2Co/m**	**E (GPa)**	**H (GPa)**	**Kc,idt/MPa.m2**
20wt%	205	235	220	0.0002	276	14.972	
20wt%	235	258	246.5	0.0002	276	14.972	
20wt%	217	231	224	0.0002	276	14.972	
20wt%	233	243	238	0.0002	276	14.972	
20wt%	211	242	226.5	0.0002	276	14.972	
Average Al2O3			**231**	**0.0002**	**276**	**14.972**	5.429135058
		Colloidal	**process**			**10kg**	
Sample	**Crack 1**	**Crack 2**	**Avg/2Co mm**	**2Co/m**	**E (GPa)**	**H (GPa)**	**Kc,idt/MPa.m2**
5wt%	234	243	238.5	0.0002	350	15.851	
5wt%	213	246	229.5	0.0002	350	15.851	
5wt%	246	261	253.5	0.0003	350	15.851	
5wt%	241	261	251	0.0003	350	15.851	
5wt%	202	278	240	0.0002	350	15.851	
Average 5 wt%			242.5	**0.0002**	350	**15.851**	5.524233896
Sample	**Crack 1**	**Crack 2**	**Avg/2Co mm**	**2Co/m**	**E (GPa)**	**H (GPa)**	**Kc,idt/MPa.m2**
10wt%	267	260	263.5	0.0003	333	15.709	
10wt%	226	259	242.5	0.0002	333	15.709	
10wt%	230	227	228.5	0.0002	333	15.709	
10wt%	199	209	204	0.0002	333	15.709	
10wt%	238	219	228.5	0.0002	333	15.709	
Average 10 wt%			233.4	**0.0002**	**333**	**15.709**	5.73232167
Sample	**Crack 1**	**Crack 2**	**Avg/2Co mm**	**2Co/m**	**E (GPa)**	**H (GPa)**	**Kc,idt/MPa.m2**
20wt%			#DIV/0!	#DIV/0!	326		
20wt%			#DIV/0!	#DIV/0!	326		
20wt%	NOT MAKING ANY CRAK		#REF!	#REF!	326		
20wt%			#DIV/0!	#DIV/0!	326		
20wt%			#DIV/0!	#DIV/0!	326		
Average 20 wt%			#DIV/0!	**#DIV/0!**	326		#DIV/0!

4. Fracture toughness test by Anthis method (load 20kg)

			20kg				
Sample	**Crack 1**	**Crack 2**	**Avg/2Co mm**	**2Co/m**	**E (GPa)**	**H (GPa)**	**Kc,idt/MPa.m2**
Al2O3 (1)	459	578	518.5	0.0005	363	18.29	
Al2O3 (2)	439	552	495.5	0.0005	363	18.29	
Al2O3 (3)	446	479	462.5	0.0005	363	18.29	
Al2O3 (4)	483	500	491.5	0.0005	363	18.29	
Al2O3 (5)	474	423	448.5	0.0004	363	18.29	
Average Al2O3			**483.3**	**0.0005**	363	**18.29**	3.721661883
		Mech. Method					
Sample	**Crack 1**	**Crack 2**	**Avg/2Co mm**	**2Co/m**	**E (GPa)**	**H (GPa)**	**Kc,idt/MPa.m2**
5wt%	445	317	381	0.0004	340	17.343	
5wt%	432	302	367	0.0004	340	17.343	
5wt%	336	333	334.5	0.0003	340	17.343	
5wt%	403	393	398	0.0004	340	17.343	
5wt%	367	322	344.5	0.0003	340	17.343	
Average 5wt%			**365**	**0.0004**	**340**	**17.343**	5.635775661
Sample	**Crack 1**	**Crack 2**	**Avg/2Co mm**	**2Co/m**	**E (GPa)**	**H (GPa)**	**Kc,idt/MPa.m2**
10wt%	268	276	272	0.0003	338	15.665	
10wt%	251	255	253	0.0003	338	15.665	
10wt%	308	263	285.5	0.0003	338	15.665	
10wt%	315	284	299.5	0.0003	338	15.665	
10wt%	323	348	335.5	0.0003	338	15.665	
Average10wt%			**289.1**	**0.0003**	**338**	**15.665**	8.387579709
Sample	**Crack 1**	**Crack 2**	**Avg/2Co mm**	**2Co/m**	**E (GPa)**	**H (GPa)**	**Kc,idt/MPa.m2**
20wt%	318	392	355	0.0004	276	15.413	
20wt%	344	358	351	0.0004	276	15.413	
20wt%	311	331	321	0.0003	276	15.413	
20wt%	358	372	365	0.0004	276	15.413	
20wt%	336	336	336	0.0003	276	15.413	
Average 20wt%			**345.6**	**0.0003**	**276**	**15.413**	5.846096751
		Anthis_FT Colloidal pro		20kg			
Sample	**Crack 1**	**Crack 2**	**Avg/2Co mm**	**2Co/m**	**E (GPa)**	**H (GPa)**	**Kc,idt/MPa.m2**
5wt%	323	371	347	0.0003	350	16.183	
5wt%	404	407	405.5	0.0004	350	16.183	
5wt%	382	430	406	0.0004	350	16.183	
5wt%	390	382	386	0.0004	350	16.183	
5wt%	411	348	379.5	0.0004	350	16.183	
Average 5wt%			**384.8**	**0.0004**	**350**	**16.183**	5.468491702
Sample	**Crack 1**	**Crack 2**	**Avg/2Co mm**	**2Co/m**	**E (GPa)**	**H (GPa)**	**Kc,idt/MPa.m2**
10wt%	357	366	361.5	0.0004	333	16.209	
10wt%	389	368	378.5	0.0004	333	16.209	
10wt%	334	339	336.5	0.0003	333	16.209	
10wt%	388	352	370	0.0004	333	16.209	
10wt%	376	386	381	0.0004	333	16.209	
Average 10wt%			**365.5**	**0.0004**	333	**16.209**	5.757428868
Sample	**Crack 1**	**Crack 2**	**Avg/2Co mm**	**2Co/m**	**E (GPa)**	**H (GPa)**	**Kc,idt/MPa.m2**
20wt%	338	314	326	0.0003	326	16.357	
20wt%	325	318	321.5	0.0003	326	16.357	
20wt%	392	339	365.5	0.0004	326	16.357	
20wt%	407	291	349	0.0003	326	16.357	
20wt%	430	299	364.5	0.0004	326	16.357	
Average 20wt%			**345.3**	**0.0003**	326	**16.357**	6.175580014

APPENDIX D

Excel sheet of Young's modulus measurements

1. Pure Alumina

	pure Al2O3 mm/g/GHz	m/kg/Hz		R shape factor
Length	63.56	0.06356		
Thick (a)	3.18	0.00318		10.92245504
Width (b)	19.94	0.01994		
Mass	14.86	0.01486		
Dens	0.003687081	3687.080732		
Res freq		7860		
Tor R freq		14940		
E no corr	3.479E+11			Shear Mod G 1.453E+11
Poissons	0.197653233			
New Poissons	0.218237513			
Correction Factor T		1.017187179		
Corr new Poisson		1.017325965		
E with Corr		3.539E+11		
E with 2nd Corr		3.540E+11		

2. Alumina-5wt% zirconia powder mixing and

	Al2O3+5%ZrO2		
	mm/g/GHz	m/kg/Hz	R shape factor
Length	*41.194*	0.041194	
Thick (a)	*2.852*	0.002852	**10.75634118**
Width (b)	*17.892*	0.017892	
Mass	*8.076*	0.008076	
Dens	*0.00384197*	3841.969696	
Res freq		*16000*	
Tor R freq		22700	
E no corr	**3.295E+11**		**Shear Mod G**
			1.445E+11
Poissons	0.139951806		
New Poissons	0.176633555		
Correction Factor T		**1.032178334**	
Corr new Poisson		**1.032556707**	
E with Corr		**3.401E+11**	
E with 2nd Corr		**3.403E+11**	

3. Alumina-5wt% zirconia colloidal processing

	Al2O3+5%ZrO2 C/P		
	mm/g/GHz	m/kg/Hz	R shape factor
Length	*40.052*	0.040052	
Thick (a)	*2.722*	0.002722	**11.64423744**
Width (b)	*17.854*	0.017854	
Mass	*7.4758*	0.0074758	
Dens	*0.003840695*	3840.694959	
Res freq		*16400*	
Tor R freq		22600	
E no corr	**3.395E+11**		**Shear Mod G**
			1.466E+11
Poissons	0.158312814		
New Poissons	0.194439349		
Correction Factor T		**1.031188928**	
Corr new Poisson		**1.031579954**	
E with Corr		**3.501E+11**	
E with 2nd Corr		**3.503E+11**	

4. Alumina-10wt% zirconia powder mixing

	Al2O3+10%ZrO2 P/P		
	mm/g/GHz	m/kg/Hz	R shape factor
Length	40	0.04	
Thick (a)	2.558	0.002558	**15.19423744**
Width (b)	19.462	0.019462	
Mass	7.662	0.007662	
Dens	0.003847637	3847.637492	
Res freq		15200	
Tor R freq		20200	
E no corr	**3.292E+11**		Shear Mod G
			1.527E+11
Poissons	0.077998987		
New Poissons	0.107176645		
Correction Factor T		**1.027066498**	
Corr new Poisson		**1.027241222**	
E with Corr		**3.381E+11**	
E with 2nd Corr		**3.381E+11**	

5. Alumina-10wt% zirconia colloidal processing

	Al2O3+10%ZrO2 C/P		
	mm/g/GHz	m/kg/Hz	R shape factor
Length	41.294	0.041294	
Thick (a)	2.688	0.002688	**12.73291333**
Width (b)	18.518	0.018518	
Mass	7.7808	0.0077808	
Dens	0.003785419	3785.418974	
Res freq		15000	
Tor R freq		21200	
E no corr	**3.244E+11**		**Shear Mod G**
			1.478E+11
Poissons	0.097721863		
New Poissons	0.128629579		
Correction Factor T		**1.028156236**	
Corr new Poisson		**1.028376314**	
E with Corr		**3.335E+11**	
E with 2nd Corr		**3.336E+11**	

6. Alumina-20wt% zirconia powder mixing

	Al2O3+20%ZrO2		
	mm/g/GHz	m/kg/Hz	R shape factor
Length	41.532	0.041532	
Thick (a)	2.42	0.00242	**12.76702312**
Width (b)	16.63	0.01663	
Mass	6.3015	0.0063015	
Dens	0.003770105	3770.105298	
Res freq		12200	
Tor R freq		18600	
E no corr	**2.698E+11**		**Shear Mod G**
			1.149E+11
Poissons	0.174175486		
New Poissons	0.201283356		
Correction Factor T		**1.023086728**	
Corr new Poisson		**1.023314274**	
E with Corr		**2.760E+11**	
E with 2nd Corr		**2.761E+11**	

7. Alumina-20wt% zirconia colloidal processing

	Al2O3+20%ZrO2 C/P		
	mm/g/GHz	m/kg/Hz	R shape factor
Length	40.374	0.040374	
Thick (a)	2.798	0.002798	**11.96579787**
Width (b)	18.654	0.018654	
Mass	7.7197	0.0077197	
Dens	0.003663355	3663.354626	
Res freq		16400	
Tor R freq		22200	
E no corr	**3.165E+11**		**Shear Mod G**
			1.409E+11
Poissons	0.123419982		
New Poissons	0.159474018		
Correction Factor T		**1.032093105**	
Corr new Poisson		**1.032435057**	
E with Corr		**3.266E+11**	
E with 2nd Corr		**3.268E+11**	

APPENDX E

Die component for Young's modulus measurements

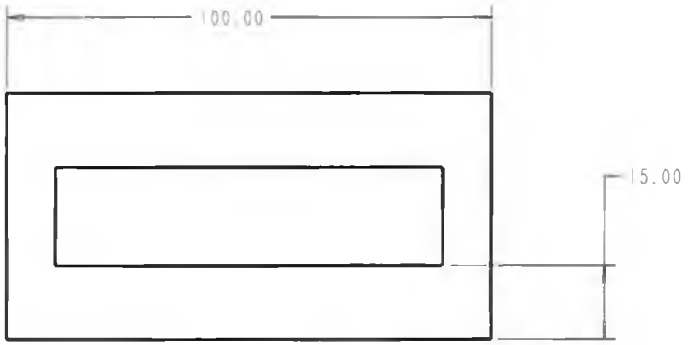

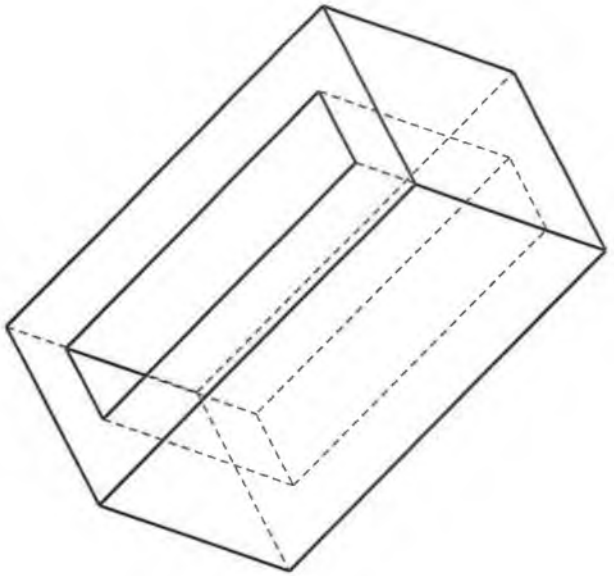

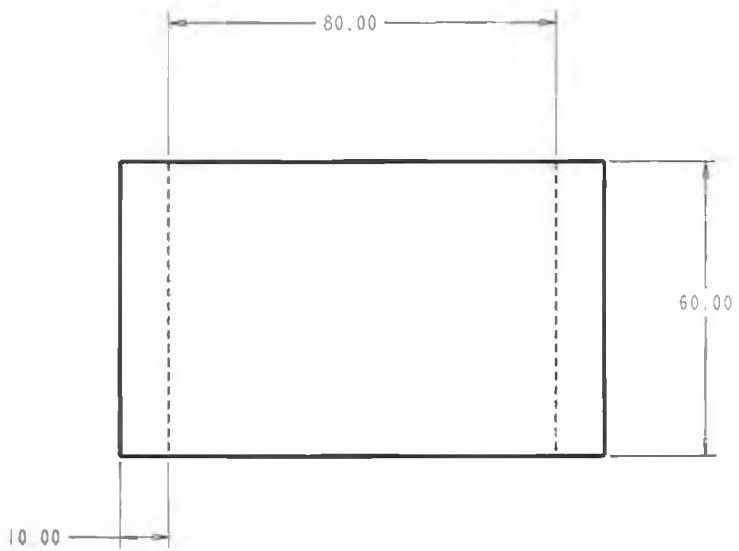

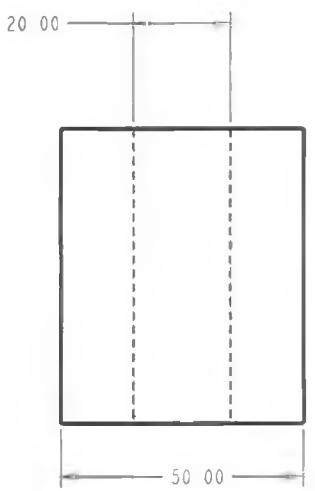

Scale	0.055	Designer	Abdelmuniem Alsebaie	Date	18-05-2005
Materile	Steel	Note	young's modulus Measurement		
Part Name		Project	Materials processing	Control	
Die body		Type	Die	Dublin City University School of Mechanical & Manufacturing Eng.	
		Part No	1		

E-2

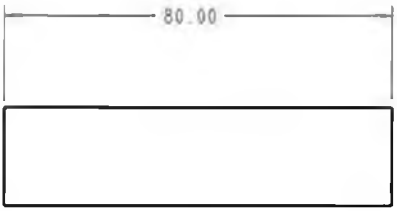
80.00


30.00

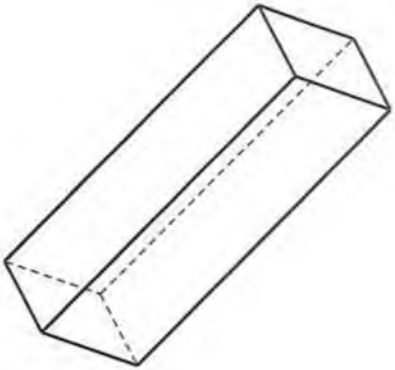

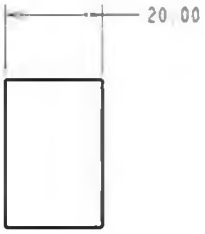

Scale	0.055	Designer	Abdelmuniem Alsebaie	Date	18-052005
Materile	Steel	Note	Young's modulus measurement		
Part Name		Project	Materials processing	Control	
upper punch		Type	Punch	Dublin City University School of Mechanical & Manufacturing Eng.	
		Part No.	2		

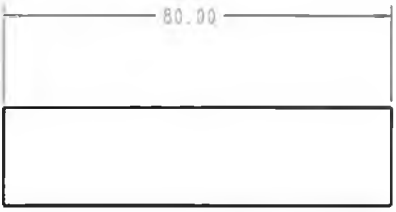
80.00


30.00

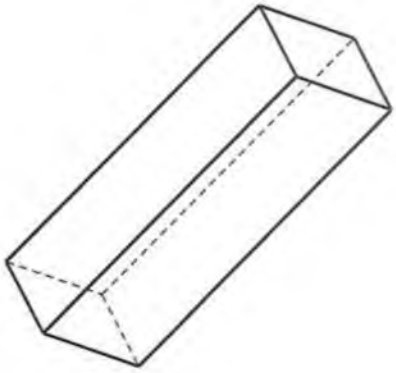

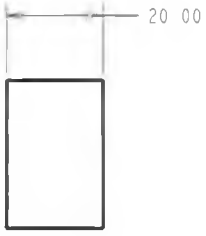

Scale	0.055	Designer	Abdelmuniem Alsebaie	Date	18-052005
Materile	Steel	Note	Young's modulus measurement		
Part Name		Project	Materials processing	Control	
Down punch		Type	Punch	Dublin City University School of Mechanical & Manufacturing Eng	
		Part No	2		

PUBLICATIONS

[1] A. Alsebaie, A. G. Olabi, A. Rafferty, T. Prescott, Preparation, characterization and mechanical testing of alumina-zirconia composites, 8th Annual Sir Bernard crossland symposium and postgraduate research workshop, current R&D in mechanical engineering April 6th & 7th-2005 at Queen's university Belfast, poster, p 171

[2] A. Alsebaie, A. G. Olabi, A. Rafferty, T. Prescott, CHARACTERIZATION OF Al_2O_3-ZrO_2 COMPOSITES PREPARED BY TRADITIONAL AND COLLOIDAL PROCESS, the fourth Arabic congress in material science, Al.fath university Tripoli-Libya, (2) pp390-400